UC San Diego

UC San Diego Electronic Theses and Dissertations

Title

Long-term performance of epoxy-bonded rebar-couplers

Permalink

https://escholarship.org/uc/item/6tj707t8

Author

Brungraber, Griffin Rupp

Publication Date

2009

Peer reviewed|Thesis/dissertation

eScholarship.org Powered by the California Digital Library
University of California

UNIVERSITY OF CALIFORNIA, SAN DIEGO

Long-Term Performance of Epoxy-Bonded Rebar-Couplers

A dissertation submitted in partial satisfaction of the
requirements for the degree Doctor of Philosophy

in

Structural Engineering

By

Griffin Rupp Brungraber

Committee in charge:

Professor Vistasp Karbhari, Chair
Professor Gilbert Hegemier, Co Chair
Professor Neal Driscoll
Professor Hyonny Kim
Professor Yu Qiao
Professor Mohan Trivedi

2009

Copyright

Griffin Rupp Brungraber, 2009

All rights reserved.

The Dissertation of Griffin Rupp Brungraber is approved, and is acceptable in quality and form for publication on microfilm and electronically:

_____

_____

_____

_____

_____
Co-Chair

_____
Chair

University of California, San Diego

2009

DEDICATION

This work is dedicated to my parents for their support and patience, and my wife for her ceaseless motivation.

EPIGRAPH

There's a right tool for every job; and the right tool is Visegrips®.
Robert Brungraber, Ph.D., P.E.

Everyone believes the results of the test except the man who performed it, and no one believes the results of the model except the man who built it.

TABLE OF CONTENTS

LIST OF ABBREVIATIONS

ACI – American Concrete Institute

ASTM – American Society for Testing and Materials

DMA – Dynamic Mechanical Analysis

DMTA – Dynamic Mechanical Thermal Analysis

ES – Evaluation Services

FEA – Finite Element Analysis

ICBO – International Congress of Building Officials

ICC – International Code Committee

LWMS – Low-Weight Molecular Solids

LIST OF SYMBOLS

A - constant
B - constant
b -constant
C - concentration of sorbate per unit sorbent
c –constant
C_1 - constant
C_2 – constant
d - concrete hole diameter
D - diffusion coefficient
d_b - nominal anchor diameter
Do - ambient temperature diffusion coefficient
E_a - activation energy
F – constant
h - thickness of a theoretically infinite sorbent plate
h_{ef} - effective embedment depth of the anchor
h_{ef} - effective embedment depth.
l - total embedment depth
l_c - depth of the upper concrete breakout cone
M_∞ - maximum moisture content at time infinity
M_t - cumulative gravimetric weight gain due to moisture uptake
N_T - adhesive pullout strength of a single anchor in tension
N_τ - failure strength at the steel/adhesive surface
$N_{\tau O}$ - failure strength at the adhesive/concrete surface
P - material property undergoing degradation
P - temperature-dependent material property at temperature T
$P0$ - the material property, of interest, at initial time zero
P_O - material property at reference temperature T_O
R - Universal gas constant
T - absolute temperature
t - time
T_g - glass transition temperature of the material
T_n - load capacity of a single anchor, in tension, due to adhesive failure limit
T_S - and arbitrary reference temperature
y - displacement
α_T - ratio of a mechanical relaxation time at temperature T to its value at a reference temperature T_0
ε - strain
λ' - elastic parameter combining material moduli and dimensional approximations
μ_{max} - maximum adhesive shear stress at the base of the upper concrete breakout cone
σ_E - engineering stress
σ_T - true stress
τ - average adhesive shear stress
τ' - shear strength at the steel/adhesive interface

τ'_O - shear strength at the adhesive/concrete interface
Φ - statistical reduction factor,

LIST OF FIGURES

LIST OF TABLES

ACKNOWLEDGEMENTS

My adviser, Professor Vistasp Karbhari, has been the primary force behind this research. He had the foresight to request funding for this research before the 2006 collapse of the Interstate 90 tunnel ceiling, in Boston, brought the long-term performance of epoxy anchorage to the forefront of the civil engineering consciousness. Without his encouragement, knowledge and patience, this study would never have been completed.

My committee must be credited as well for their patience and guidance.

The rest of the Dr. Karbhari research group, particularly Dr. Stephanie Svetlik-Haley, was a consistent source of motivation and wisdom.

The California Department of Transportation, the sponsor of this research, and their arbiter, Dr. Charles Sikorsky, must also be credited for their contribution to this work.

The staff of the UCSD Structural Engineering Laboratories, Powell Labs and SRMD, were eminently supportive, understanding and adaptable, to all the logistics of testing.

VITA

Born, to Robert Brungraber and Joel Feldmann	1983
Keene High School, Keene, New Hampshire	2001
Bucknell University, Bachelor of Science, Civil Engineering	2005
UCSD, Master of Science, Structural Engineering	2007
UCSD, Doctor of Philosophy, Structural Engineering	2009

THE ABSTRACT OF THE DISSERTATION

Long-Term Performance of Epoxy-Bonded Rebar-Couplers

By

Griffin Rupp Brungraber

Doctor of Philosophy in Structural Engineering

University of California, San Diego, 2009

Professor Vistasp Karbhari, Chair
Professor Gilbert Hegemier, Co-Chair

Rebar-couplers mechanically splice pairs of steel reinforcing bars, end-to-end; they are used regularly in reinforced concrete construction. Epoxy-bonded couplers are one available type, but have unique long-term performance considerations. The adhesive material used in these couplers is a two-part, field-mixed, ambient-cure epoxy system, originally designed for adhesive anchorage to concrete. Many of the adhesive systems used for anchorage to concrete, including the system used with adhesive-bonded couplers, are epoxy systems. The mechanical properties of these types of epoxies have been shown to degrade over time, in the presence of moisture. A variety of commercially available adhesive systems, for anchorage to concrete, were

studied to assess their relative resistance to moisture-based degradation. The material properties of two of the adhesive systems, both epoxies, and the performance of the rebar-couplers were then measured over a fourteen-and-a-half-month period of exposure to a variety of environmental conditions, including water immersion at a range of temperatures. From these results, material degradation models were used to predict the properties of the adhesive over the service life of the rebar-coupler. A Finite Element Analysis (FEA) model was developed to simulate the tensile failure of the epoxy-bonded rebar-coupler system and correlate degrading adhesive material properties to changes in the coupler system's behavior throughout its service life.

1 Introduction

1.1 General Problems

Reinforced concrete is a composite material system consisting of two components: concrete, and reinforcement. The concrete component is itself a composite of Portland cement and aggregates. The Portland cement, through the process of hydration, cures and solidifies the material; the aggregates, usually a combination of sand and gravel, add strength and volume to the concrete. Reinforcement is generally in the form of deformed steel reinforcing bars (rebars). In practice, the rebars are placed and temporarily fixed into their final configuration, and then the fluid concrete is poured around them; the concrete then cures, forming the composite system. The reinforced concrete composite system is successful because the concrete takes the majority of compression forces and is easy to place and form; the rebars carry the tensile forces efficiently. However, it is often necessary to splice rebars together to allow for continuity of tensile forces from one rebar to the next. The most common method of splicing rebars together is to overlap them, creating what is called a "lap splice". However, lap splicing is not always desirable and so a variety of mechanical rebar-couplers have been developed.

Epoxy-bonded rebar couplers are a type of mechanical rebar-coupler used in reinforced concrete construction; they use an epoxy adhesive system to transfer load between reinforcing bars. However, the introduction of the epoxy material into reinforced concrete structures adds additional long-term performance considerations. Although not all adhesives are epoxies, only epoxy has been used in bonded rebar-

couplers, and so the term “epoxy-bonded rebar-coupler” is used to describe a class of construction products, though the mechanisms it refers to would be applicable to any adhesively-bonded rebar-coupler. The long-term performance concerns for typical reinforced concrete structures are generally understood [Mather 1979], both by scientists, and by the engineers responsible for their design. Concrete is vulnerable to long-term degradation from carbonation, alkali-aggregate reaction and freeze-thaw cycles. Steel reinforcing bars are vulnerable to fatigue, and corrosion from chloride infiltration [Mather 1979]. However, the long-term performance concerns for the epoxy adhesive system used inside epoxy-bonded rebar-couplers, and for adhesives in general, are not as well understood by the engineers responsible for their design.

Adhesives, including epoxy, have their own range of long-term degradation mechanisms which could potentially impact performance at the structural system level. Epoxies are typically vulnerable to moisture and elevated temperature, two environmental conditions which are commonly found inside reinforced concrete structures, such as bridge decks [Kaw 1997].

Epoxy-bonded couplers meet all requirements of AC-133 and ACI 318 , to allow their use. However, their long-term performance, specifically due to the reliance on an adhesive, is unknown. Unlike concrete and steel, the impacts on the long-term performance of the system, from the degrading adhesive properties, is not fundamentally understood. Since structure design service-lives are much longer than a reasonable long-term test could be, a fundamental understanding is critical to allow the long-term predictions of system performance.

This research, into the long-term performance of epoxy-bonded rebar couplers, had already been initiated when a major long-term adhesive failure occurred. Although not a failure of epoxy-bonded rebar-couplers, the collapse of the ceiling panels in an Interstate 90, central artery project, tunnel in Boston, Massachusetts on July 10th, 2006, provides additional motivation for the investigation of the long-term performance of adhesive-dependant structural systems. In the Boston collapse post-installed adhesive bonded anchors pulled out of the concrete tunnel ceiling. The anchors were installed with the same class of adhesives which are specified with adhesive-bonded rebar couplers.

1.2 Rebar Couplers

Mechanically coupling reinforcing bars (rebars) together is one way to transfer forces between bars in reinforced concrete structures. Typically, lap splices transfer forces between rebars. However, the use of lap splices in certain sections of reinforced concrete is sometimes impractical, undesirable, or discouraged by building code [ACI 439.3R-2]. Alternatives to lap splicing are welding, and mechanically coupling. Many types of mechanical couplers are commercially available; most rely on some type of bar threading, bar swaging, swaged sleeve, or grouted sleeve mechanism. The grouted sleeve systems rely on either a metallic, cementitious or adhesive compound to fill a gap between a rebar and a sleeve. Cementitiously-grouted rebar-couplers function by the same principles as developing a length of rebar embedded in confined concrete. Adhesively-grouted rebar-couplers, including epoxy-bonded rebar-couplers couplers,

function as a combination of the mechanisms of grouted rebar-couplers and adhesive anchorage to concrete. A bar development length situation, inside a confining sleeve, is similar to other grouted rebar couplers. The adhesive-to-rebar bonding mechanism is similar to adhesive anchorage to concrete; indeed, the same class of adhesives is specified for both adhesively-grouted rebar couplers and adhesive anchorage to concrete.

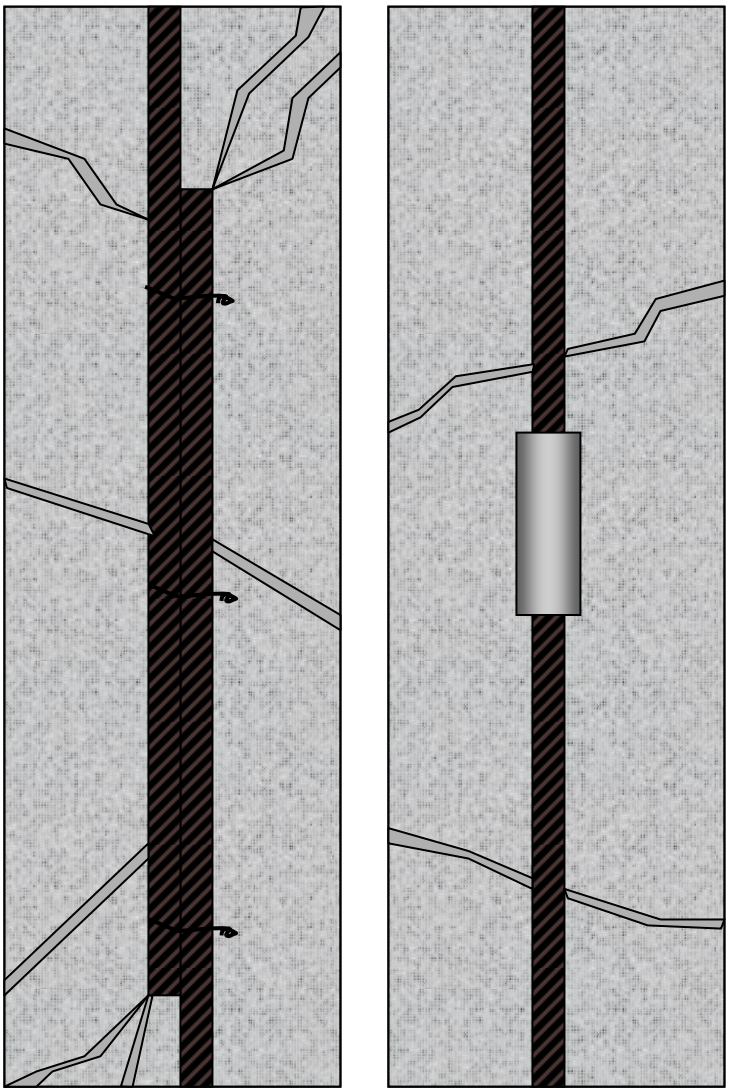

Figure 1: Typical reinforcing bar lap splice, on left, and generic reinforcing bar rebar coupler, on right. Both are shown in cracked concrete.

1.2.1 Types of Rebar-Coupler

1.2.1.1 Incised-Bar Threaded

Threads are incised into the rebar, and then rebar and coupler are screwed together, as shown in Figure 2. Depending on the rebar coupler system and manufacturer the threads can be male or female, straight or tapered, and the rebar may or may not be swaged before the threads are cut. Although these systems have the advantage of using the rebar as the thread material, they require either the rebar or coupler to be rotated during installation. Additionally, incising threads into a rebar introduces stress concentrations which may weaken the bar's fatigue resistance [Manning 1994].

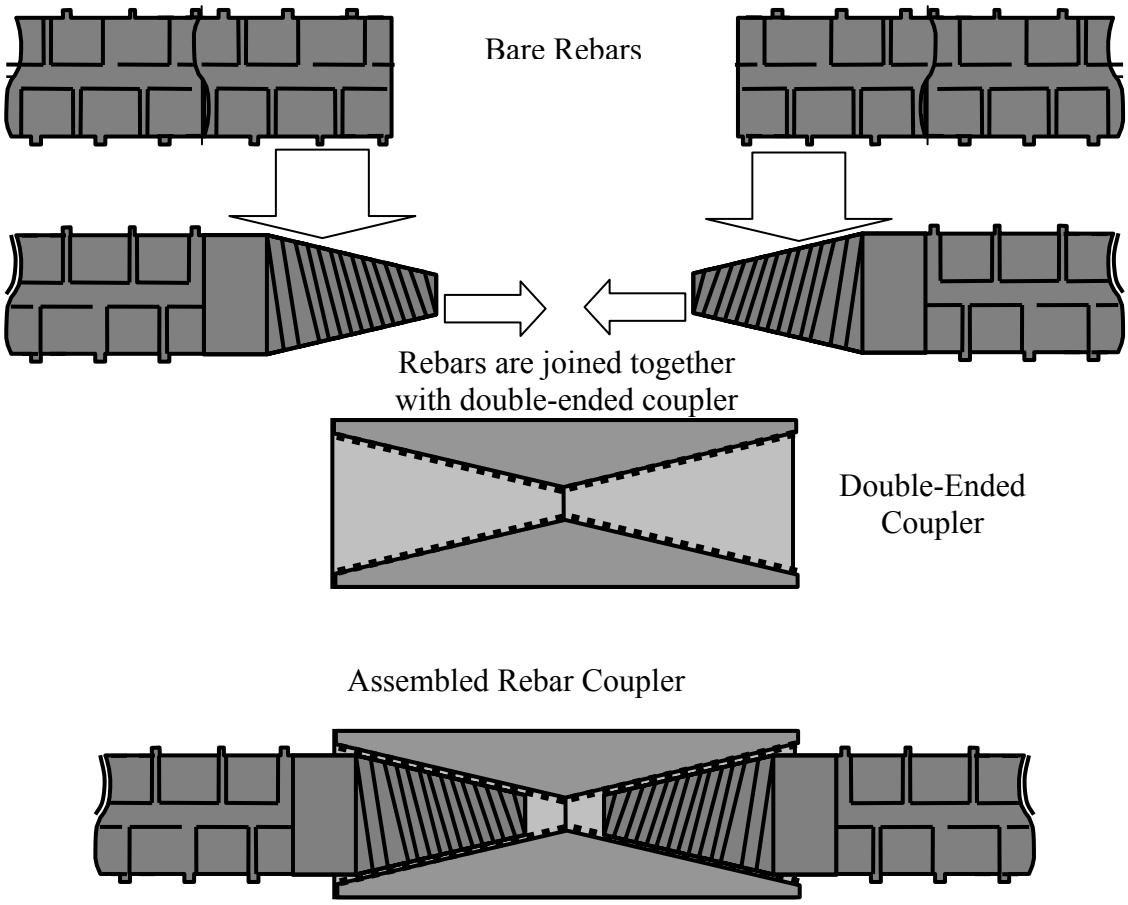

Figure 2: Diagram of assembly procedure for incised-bar threaded rebar-couplers.

1.2.1.2 Bar-Swaged

Rebar swaging, or rebar-end-upsetting, can be used alone or with other methods to couple rebars. By deforming, upsetting, or swaging, a rebar end, the diameter is increased. This increase can either prevent the end of the bar from passing through hole in a coupler, as shown in Figure 3, or provide a larger diameter section upon which to incise threads.

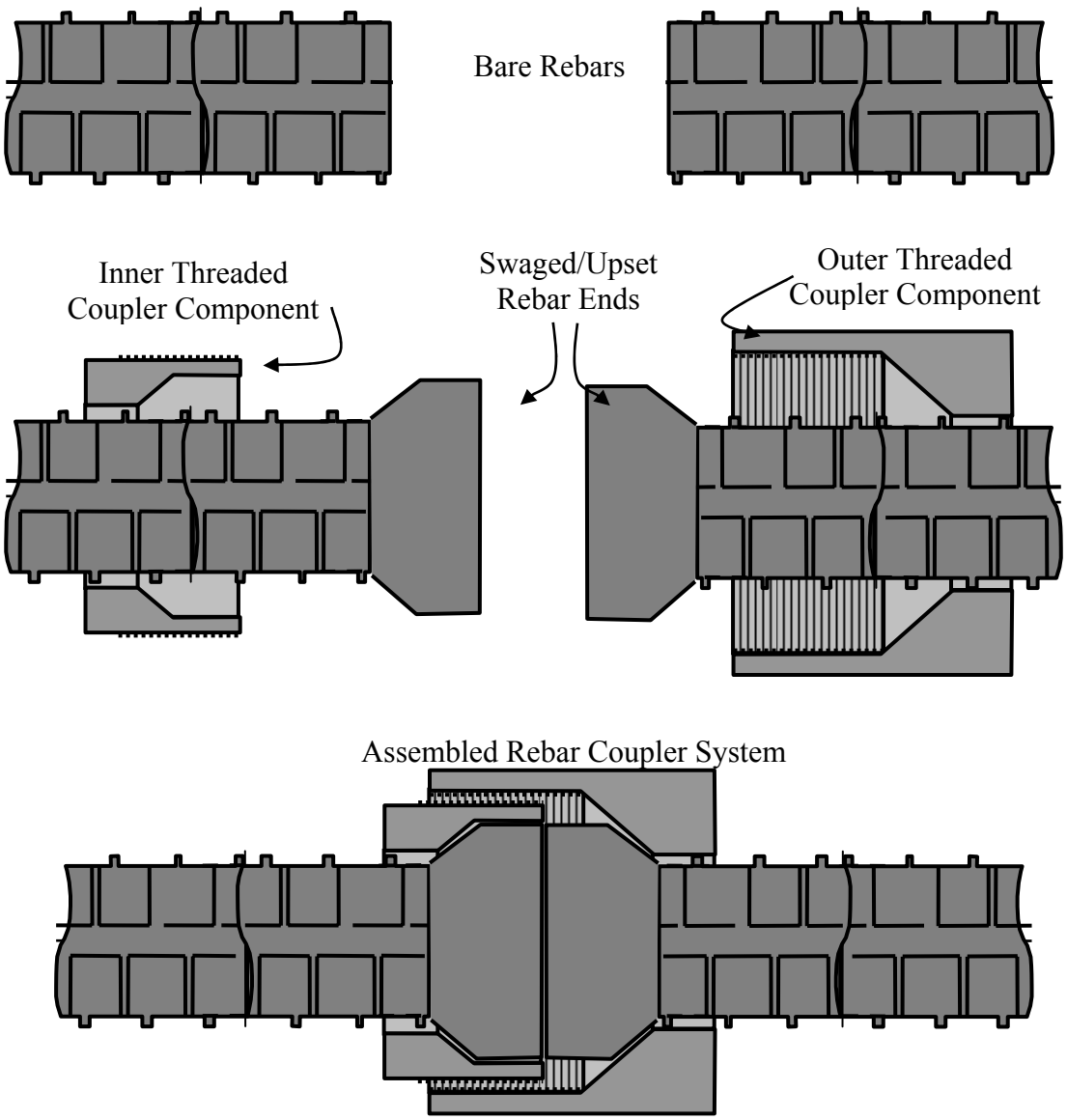

Figure 3: Diagram of assembly procedure for bar-swaged rebar-coupler.

1.2.1.3 Swaged-Sleeve

A metallic sleeve can be plastically deformed, swaged, onto the outside of a rebar, engaging the rebar's deformations and enabling load transfer. Swaged sleeve couplers can either be double-ended, as shown in Figure 4, or single-ended and combined with a number of threaded coupler options.

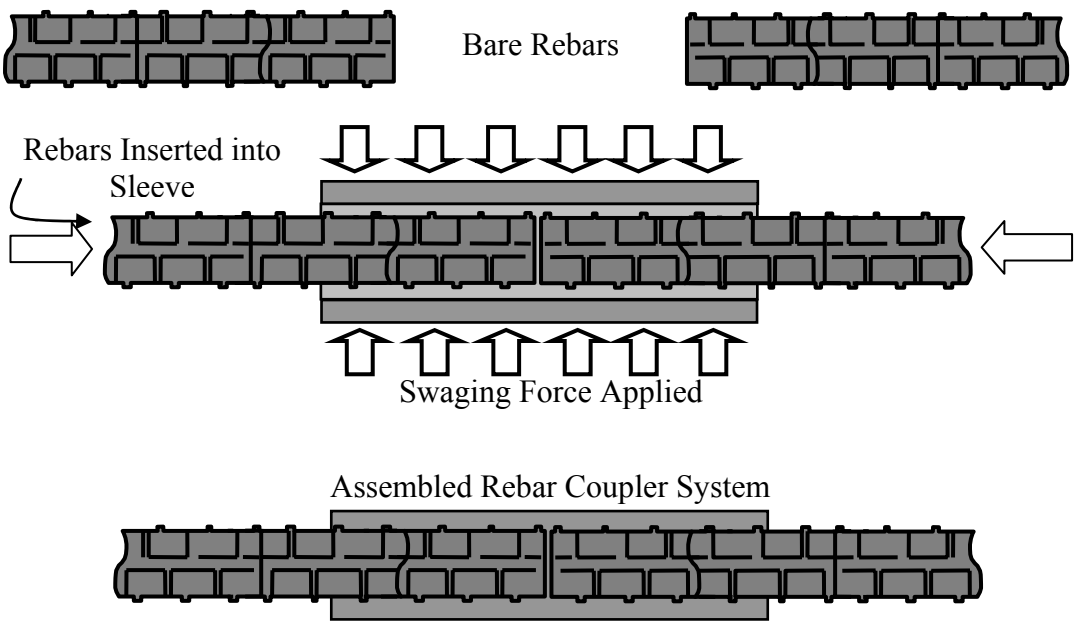

Figure 4: Assembly procedure for swaged-sleeve rebar-couplers.

1.2.1.4 Grouted Sleeve

Grouted sleeve rebar-couplers use the mechanism of development length, to transfer forces from the rebar to the grout, and then to the coupler sleeve. The sleeve provides confinement to the grout, ensuring mechanical interlock between the grout and the deformations of the rebar. Grouted sleeve rebar-couplers can use cementitious, metallic, or adhesive grouts. The grout can be pumped into the sleeve after the rebars are already inserted, or the sleeve can be filled with grout before the rebars are inserted. Grouted sleeve rebar-couplers can also be double-ended, grouting two rebars into the sleeve, or single-ended, using some other mechanism to make the second rebar connection. Figure 5 shows an example of a double-ended cementitiously-grouted sleeve coupler, and Figure 6 shows an example of a single-

ended adhesively-grouted sleeve coupler. The rebar-coupler shown in Figure 6 is of the type studied in this research.

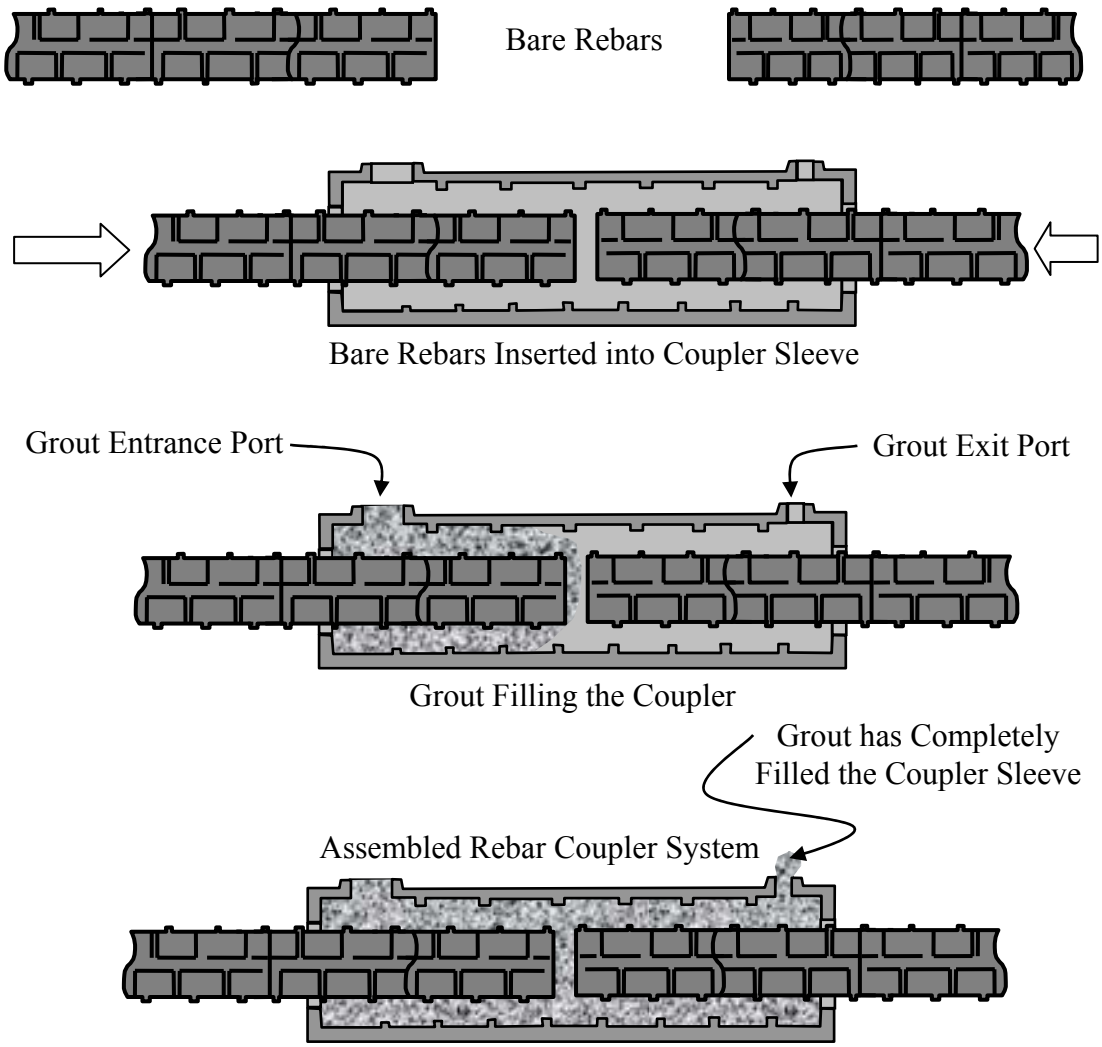

Figure 5: Assembly procedure for cementitiously-grouted sleeve rebar-couplers. Double-ended version shown.

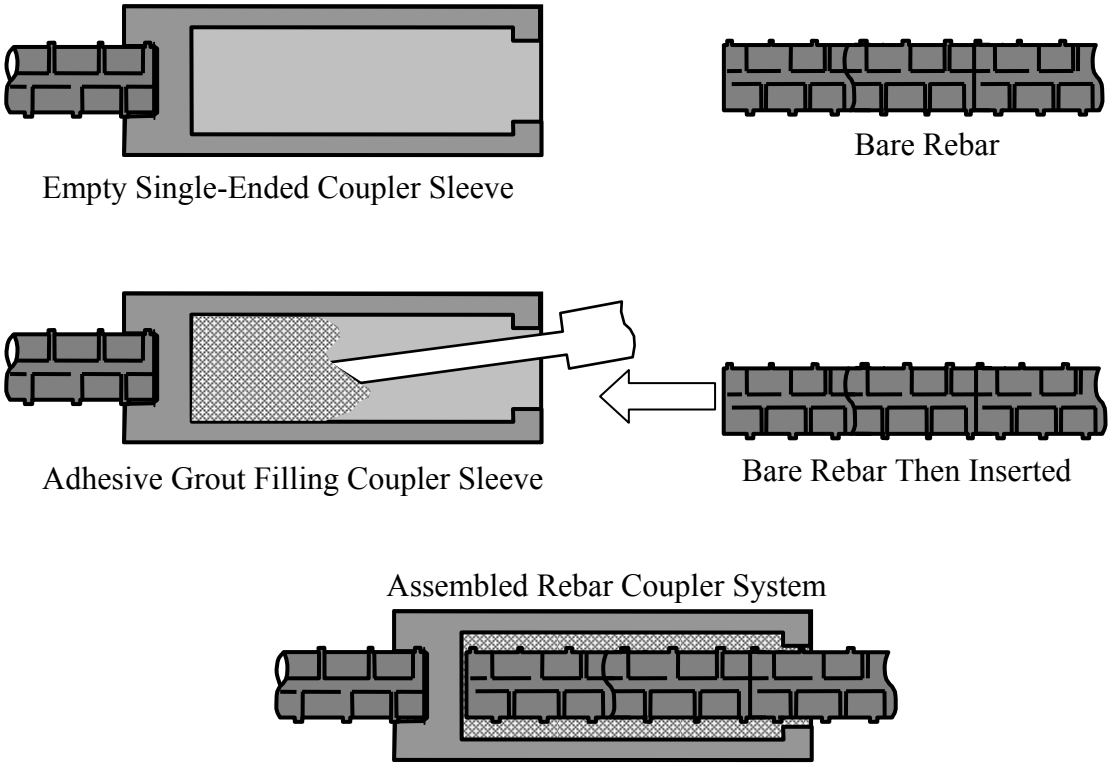

Figure 6: Assembly procedure for adhesively-bonded rebar-couplers. Single-ended version shown.

1.2.2 Applications

Lap splicing of reinforcing bars is the most common and economical methods of transferring loads between rebars. However, alternatives to lap splicing are desirable or required for certain reinforced concrete construction details. Lap splicing is not permitted, by ACI code, for the largest bar sizes, it can lead to rebar congestion in heavily reinforced areas, and it may not be reliable if the rebars are expected to be loaded cyclically in their inelastic range, as during a seismic event [ACI 439.3R-2]. Rebar-couplers are also used extensively in renovation and retrofit construction, and to create structural continuity across construction joints, such as those found in precast construction. Many types of rebar-couplers are designed to interface with the concrete

formwork. After the poured concrete has hardened and formwork is removed, the rebar-couplers are revealed, providing an easy way to create continuity of reinforcing across construction joints [Tolson 2001], as shown in Figure 7.

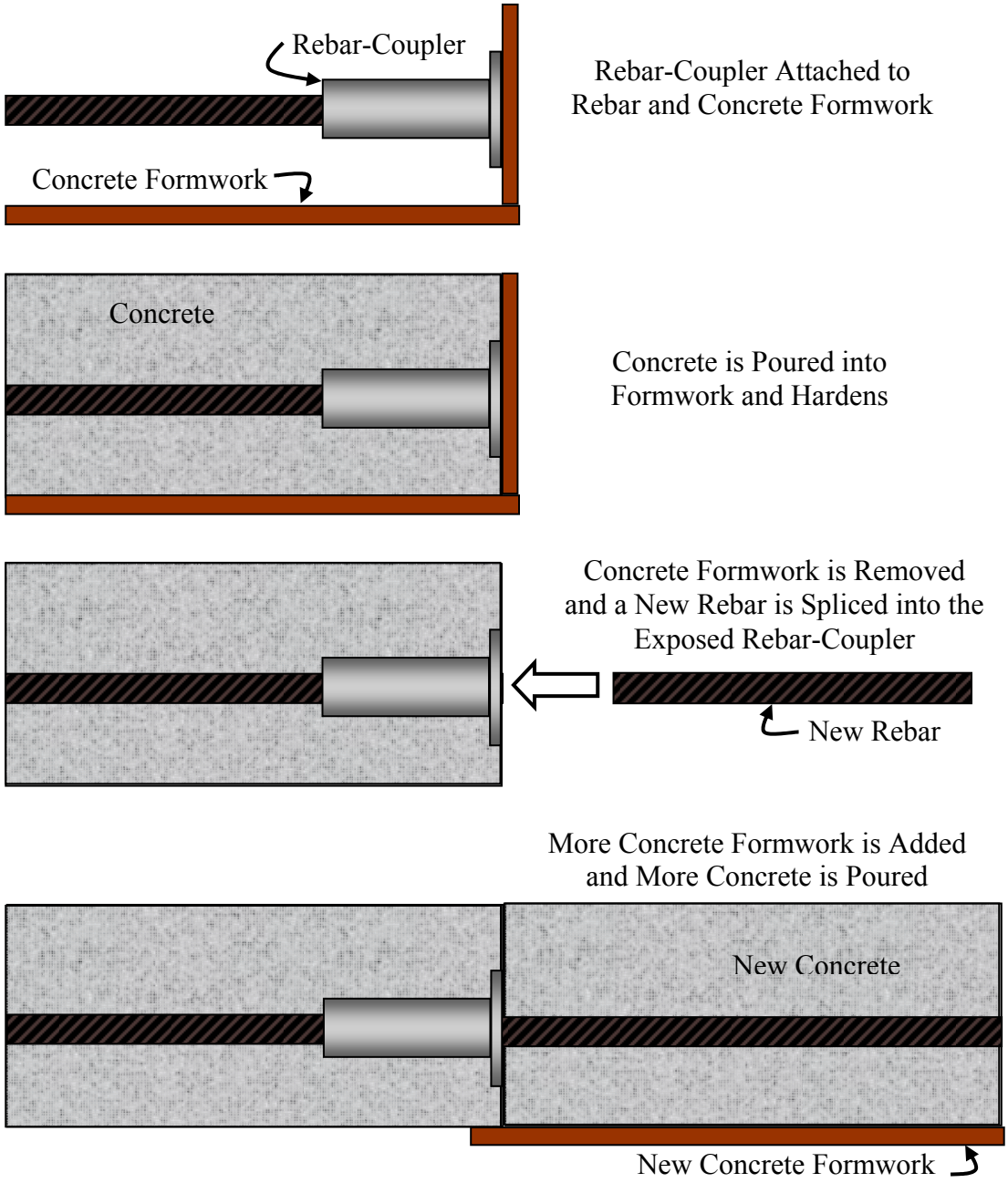

Figure 7: The construction sequence of a rebar-coupler creating continuity of reinforcing across a construction joint.

1.3 Adhesive System

In an epoxy-bonded rebar-coupler, the epoxy adhesive system is used to fill the space between the rebar and the coupler sleeve, locking the two together. The epoxy adhesive system is specified together with the coupler, and cures at ambient temperature and moisture conditions. Like concrete, adhesives, including epoxy, have a range of recommended levels of temperature and moisture for installation. However, adhesives, including epoxy, continue to degrade, in the presence of temperature and moisture, for a much longer time after installation than concrete.

1.4 Objectives and Goals of the Research

1.4.1 Research Objectives

The objectives for this research are four-fold. First, develop a fundamental understanding of time-dependent behavior of epoxies in anchor/coupler configurations. Second, develop a correlation between material and structural behavior for epoxy-bonded couplers. Third, use materials data to model long-term response. Last, develop a draft specification for use of epoxy-bonded mechanical couplers, to later be adopted by Caltrans, as a supplement to its existing test: Method of Tests for Mechanical and Welded Reinforcing Steel Splices [Caltrans 2004].

1.4.2 Research Goals

The goals for this research are four-fold. First, identify critical material characteristics for long-term performance and assessment of commercially available adhesive systems. Second, test for material characterization as well as coupler system response. Third, develop a model to relate material-level and system-level behavior. Last, to evaluate and predict system-level response, over the design service-life of the epoxy-bonded rebar-coupler.

2 Literature Review

Although rebar-couplers have been used in reinforced concrete construction for many years, epoxy-bonded rebar-couplers have been used for a relatively short time. Most rebar-couplers are constructed of steel, and possibly cement grout; the long-term behavior of these materials is relatively well understood, both in academia and industry. Conversely, the long-term behavior of polymers, including the epoxy systems used in epoxy-bonded rebar-couplers, is not as well understood and civil engineers are not trained to consider it in design.

Because epoxy-bonded rebar-couplers and adhesive anchorage to concrete use the same class of adhesive systems, and because the later is more commonly used in industry and better researched in academia, it is important to look for similarities between the two. The two structural systems have important material and geometric differences but research on the long-term performance of the epoxy materials should be equally applicable to both.

The process of moisture diffusion into, and the effects of moisture on, polymers is well understood. This research employs many known techniques for analyzing diffusion of moisture into, and moisture-based degradation of, the epoxy systems in the epoxy-bonded rebar-couplers.

2.1 Adhesive Anchorage to Concrete

Epoxy-bonded rebar-couplers and adhesive anchorage to concrete, shown in Figure 8, have geometric and behavioral similarities. Both consist of a rebar

embedded in a bulk of adhesive. Their primary geometric difference is that in the epoxy-bonded rebar-coupler the bulk of adhesive is encased in the steel sleeve of the coupler; the adhesive in adhesive anchorage is bonded into a drilled concrete hole.

Some of the earliest research into the topic of adhesive anchorage to concrete was done by [Moss 1982]. Through an extensive testing program adhesive anchor pullout was studied and some of the earliest understanding was developed. The ratio of anchor diameter to concrete hole diameter was correlated to increased anchor displacement during tensile tests. Moss surmised that the long-term failure mechanisms of adhesive anchors would be related to the moisture-based degradation of the adhesive, and recommended that only adhesive resins which were "insensitive to water" be used.

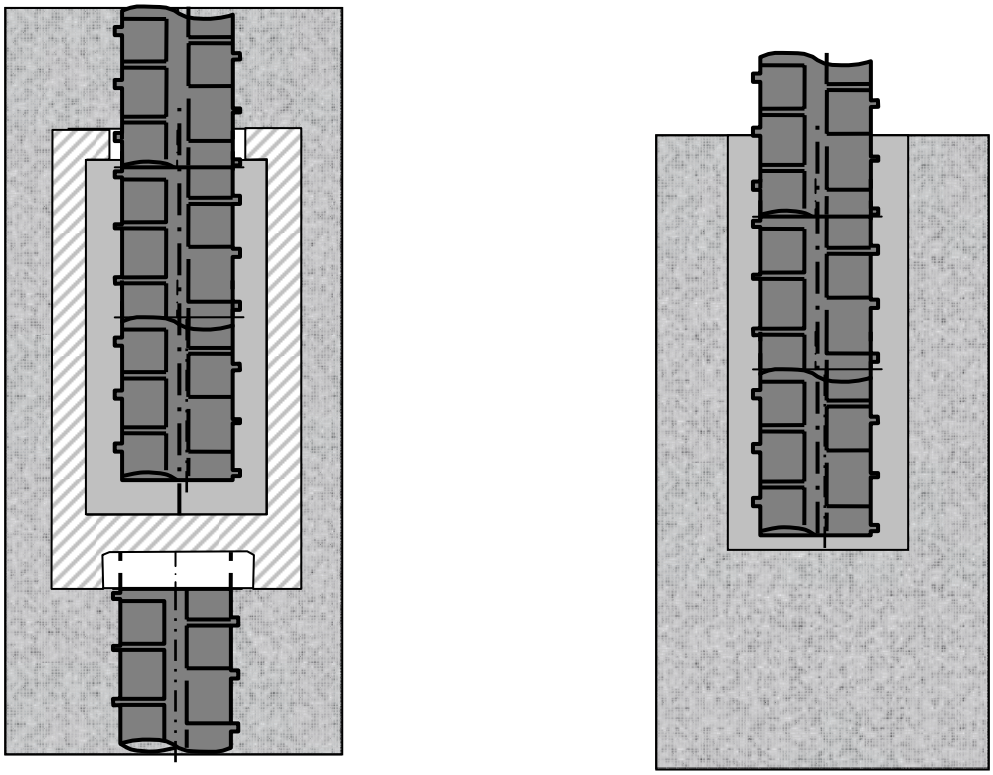

Figure 8: Epoxy-bonded rebar-coupler, on left, and adhesive bonded anchorage to concrete, on right.

2.1.1 Bonded Anchors

The term “bonded anchors” is used to describe a group of concrete anchor types including adhesive and grouted anchors. Many types of mechanical rebar couplers exist, but only filled-sleeve couplers rely on similar load-transfer mechanisms as epoxy-bonded rebar-couplers. Likewise, of the several types of post-installed concrete anchors, only adhesive and grouted anchors are largely similar to epoxy-bonded rebar-couplers.

Bonded anchors consist of either a threaded rod or a deformed reinforcing bar, installed into a hole in hardened concrete with either a polymeric adhesive or a cementitious grout. Grouted anchors can also use an anchor with an enlarged head but this modification makes their mechanisms less similar to that of epoxy-bonded rebar-couplers and so will not be considered.

Adhesive and grouted anchors also differ in the properties and composition of their bonding material. Anchorage adhesives are thermosetting polymer systems; typically epoxies, polyesters, vinylesters, or hybrid systems. [Cook et al. (1998)]. Anchorage grouts are usually cementitious, composed primarily of fine aggregates, Portland cement, and water. The different compositions of the bonding materials also necessitate different installation environments. As will be discussed later in this work, adhesive anchors perform best when installed into dry holes, while the cementitious composition of grouted anchors need wet concrete holes to ensure sufficient hydration of the Portland cement component of the grout. While both adhesive and grouted anchors rely on mechanical interlock between the adhesive or grout and the walls of

the concrete hole, only adhesive anchors also rely on chemical bond of the adhesive to the concrete [Burtz 2003].

Besides the composition of the bonding material, a geometric difference between adhesive and grouted anchors is the ratio of hole diameter to anchor element diameter. Holes for adhesive anchors are typically 10%-25% larger than the anchor element, while the holes for grouted anchors are typically 50% to 200% larger [Burtz 2003].

The five possible failure modes of adhesive anchorage to concrete are shown in Figure 9. Of these modes only steel/adhesive interface failure and steel fracture are possible in epoxy-bonded rebar-couplers. Concrete Cone breakout failures cannot occur since the anchor is embedded in a steel sleeve instead of a concrete block. Full or partial failure at the adhesive/concrete interface, which would actually be the adhesive/steel-sleeve interface in epoxy-bonded rebar-couplers, cannot be responsible for failure because of the decrease in inside-diameter at the sleeve entrance, which prevents pullout of the adhesive. Similarly, many of the large areas of study for adhesive anchors to concrete, such as distances to free slab edges and anchor group interactions, are not relevant to the corollary of epoxy-bonded rebar-couplers.

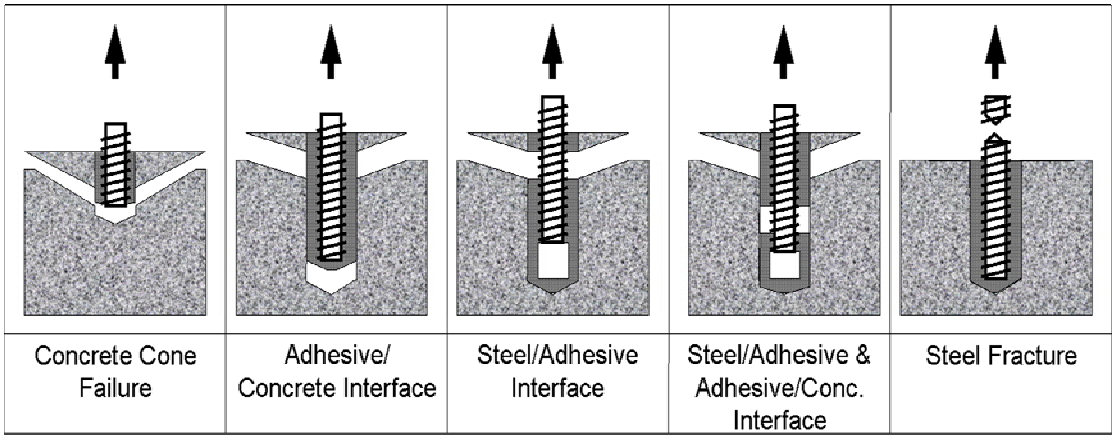

Figure 9: The five possible failure modes of adhesive anchorage to concrete. [Cook et al 1998]

2.1.2 Analytical Models(Uniform Bond Stress)

Although several analytical models for adhesive anchorage to concrete exist, only one is geometrically relevant to epoxy-bonded rebar-couplers. The Concrete Capacity Design Method (CCD), which is used by the American Concrete Institute (ACI) to predict concrete cone breakout strengths, in uncracked concrete, was developed based on extensive research [Fuchs et al (1995]. The model was developed to predict breakout strengths of headed grouted anchors and post-installed mechanical anchors. Unlike adhesive anchors these types of anchors transfer the majority of tensile loads to the concrete at the bottom tip of the anchor. However, adhesive anchors with a large diameter to embedment ratio can generate similar concrete cone breakout failures. However, since concrete cone breakout failures are not possible in epoxy-bonded rebar-couplers this failure model has limited applicability to this research.

[Cook 1993] undertook an experimental program to develop a rational design procedure for adhesive anchors which would predict their adhesive failure loads.

Anchor tensile tests of six different adhesives, of varying embedment and bond length, including an intentionally unbonded length of the anchor close to the concrete surface. An elastic, analytical model was developed which accurately explained the behavior and failure modes of adhesive anchors. Small concrete cones were shown to pull out near the surface of the concrete prior to ultimate anchor failure, by either adhesive failure or steel fracture. Figure 10 shows the formation of a concrete breakout cone and the accompanying physical variables from the uniform bond stress equation. The pullout of these small cones was preventable by debonding the top few inches of anchor embedment. Anchor embedment depth past a certain level was shown to not increase anchor capacity since steel fracture became the failure mode once sufficient embedment was attained. From the elastic model, a design procedure was offered for the load capacity for a single anchor in tension, due to adhesive failure limit

$$T_n = \frac{\pi \mu_{\max} d^{1.5}}{\lambda'} \tanh\left(\frac{\lambda'\left(l - l_c\right)}{\sqrt{d}} \right) \ell \qquad (1)$$

where μ_{max} is the maximum adhesive shear stress at the base of the upper concrete breakout cone, l is the total embedment depth, l_c is the depth of the upper concrete breakout cone, d is concrete hole diameter, λ' is an elastic parameter combining material moduli and dimensional approximations. However, the values of λ' and μ_{max} needed to be determined from multiple anchor tests and μ_{max} is difficult to measure.

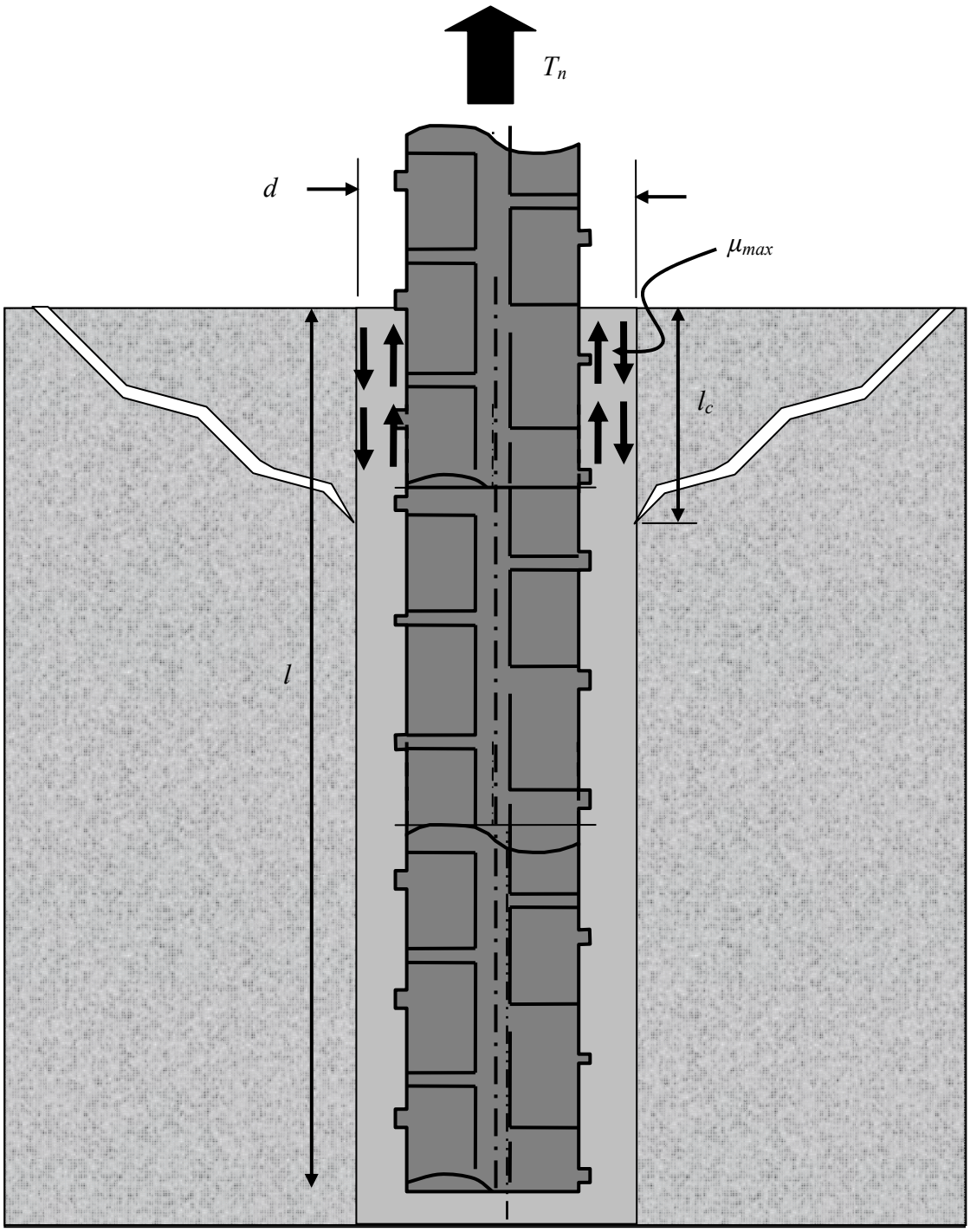

Figure 10: Diagram of physical variables for Equation 1.

To develop a simpler adhesive anchor design method [Cook 1998] followed up his earlier work and produced the Uniform Bond Stress model, shown in Equation 2.

The Uniform Bond Stress model has been shown to accurately fit a database of adhesive anchor test results for anchors where embedment depth does not exceed twenty-five times anchor diameter [Cook et al. (1998)]. All known designs for epoxy-bonded rebar-couplers fall well within this limit. The model assumes uniform bond stress along the entire embedment of the anchor.

$$N_T = \tau \cdot \pi \cdot d_b \cdot h_{ef} \tag{2}$$

where N_T is the adhesive pullout strength of a single anchor in tension, τ is the average adhesive shear stress, d_b is the nominal anchor diameter, and h_{ef} is the effective embedment depth of the anchor. This model is simple, in that it does not make an analytical distinction between which adhesive interfaces at which failure occurs, steel or concrete. Despite its simplicity, this first proposed iteration of the Uniform Bond Stress Model has been used in most adhesive anchorage research and been incorporated into ICC-ES AC308 and is due to be incorporated into ACI 355 in 2011. [Meinheit, et al 2007]

In an effort to bring phenomenological clarity to the Uniform Bond Stress model, [Zamora et al. (2003)] performed 237 tension tests on headed and unheaded adhesive and grouted anchors, focusing not only on failure load, but the interface at which failure occurred. From these results he presented two equations to differentiate between the two possible locations for adhesive failure to form: at the steel/adhesive interface, and the adhesive/concrete interface.

$$\phi N_\tau = \phi \cdot \tau' \cdot d_b \cdot h_{ef} \tag{3}$$

where Φ is a statistical reduction factor, N_τ is the failure strength at the steel/adhesive surface, τ' is the shear strength at the steel/adhesive interface, d_b is the diameter of the anchor bar, and h_{ef} is the effective embedment depth.

$$\phi N_{\tau 0} = \phi \cdot \tau'_O \cdot d \cdot h_{ef} \quad (4)$$

where Φ is a statistical reduction factor, $N_{\tau O}$ is the failure strength at the adhesive/concrete surface, τ'_O is the shear strength at the adhesive/concrete interface, d is the diameter of the concrete hole, and h_{ef} is the effective embedment depth.

2.1.3 Finite Element Models

[James et al. (1987)] developed a non-linear finite element model of a single adhesive anchor loaded in tension. Their results also correlate well with a uniform bond stress model.

[Eligehausen et al 2006] developed a three-dimensional adhesive anchorage model to examine the effects of anchor embedment depth, concrete strength, and anchor diameter on failure behavior of adhesive anchors loaded in tension. The model was also used to examine anchor group and concrete free edge effects, though these results are not relevant to epoxy-bonded rebar-couplers.

2.1.4 Environmental Testing

The effects of moisture on the ultimate strength of adhesive anchors have been included in some research, but only effects on the initial bond formed at the adhesive/concrete interface have been thoroughly studied [Best and McDonald 1990]

[Higgins and Klinger 1998] [Cook and Konz 2001]. Adhesive anchorage has traditionally been researched from the civil/structural engineering prospective, not from a material science perspective. The long-term effects of moisture on the mechanical properties of the adhesive in an anchorage system have not been thoroughly examined. There are no ASTM specifications for environmental exposure of anchors [Higgins, Klinger 1998].

Early work by [Best and McDonald 1990] compared the pullout strength of grouted, and polyester and epoxy adhesive anchors. Anchors were installed in submerged conditions, which was posited to be the worst-case scenario for developing adhesive bond. The anchors were then either submerged, or alternating submerged and dried, for a period of 32 months. No measurable declines in adhesive anchor pullout strengths were found during this test. However, elevated temperature was not used to accelerate the moisture degradation of the adhesive.

The effects of a variety of environmental conditions on several types of anchors, including adhesive anchors, were studied by [Higgins, Klinger 1998]. The couplers were exposed to five different environments and their load/deflection behaviors were compared to untreated anchors. The five exposure conditions were combinations of ultraviolet light, freeze/thaw cycles, salt solution, and wetting/drying cycles with a simulated acid rain solution. The experiment was designed to simulate fifty days of exposure time in these environments. None of these environments, or combination of environments, produced an effect on the performance of the adhesive anchors.

The effects of several factors on the strength of adhesive anchors were studied by [Cook, Konz 2001], among them testing at elevated temperature. Adhesive anchors, of both ester and epoxy formulation, were tested at a temperature of 43C. The variety of commercial adhesive systems studied covered nearly all available systems, on the market at the time of the study. The increased temperature had different effects on each system, some positive and some negative. While not conclusive on the effect of testing adhesive anchors at elevated temperature, the research did prove that the behavior of adhesive anchors is temperature-sensitive.

[Test Florida Method 5-568 (FDOT 2000)] is a test method for the effect of installation and service conditions on adhesive anchor bond strengths. Service conditions covered in this test are elevated temperature tests and long-term loading tests. However, no long-term service condition at elevated temperature is specified.

2.1.5 Historical Long-Term Failures of Adhesive

The class of adhesives used with epoxy-bonded rebar-couplers is the same which so dramatically failed during the collapse of ceiling panels in an Interstate 90, "Big Dig," tunnel in Boston, Massachusetts on July 10th, 2006 (3). In this failure, post-installed adhesive anchors pulled out of a concrete ceiling. Some of these anchor bolts had passed proof-tests after installation but then failed at lower, service loads, over a year later. The adhesive used for the anchors was an ASTM C881 certified product, and is System F, studied in this research.

2.1.6 Epoxy-Bonded Rebar-Couplers vs. Post-Installed Adhesive Anchors

Adhesive joints can be modeled to obtain closed-form analytical solutions but several complexities of the rebar coupler system do not make it an acceptable candidate. The closest adhesive joint to the rebar coupler is a post-installed, adhesive anchorage to concrete; the application for which the studied class of adhesives was designed. Closed-form solutions have been shown to accurately model such joints, but important differences prevent adhesive rebar couplers from being modeled in the same way.

The adhesive does not rely on bond strength, but rather mechanical interlock, to transfer forces between rebar and coupler. The adhesive actually behaves more like a compressional grout. The rebar coupler system still passes initial testing requirements, and has simpler long-term durability issues, if the adhesive is replaced with a cementitious grout. The adhesive is used for its faster cure time and ease of field application.

Unlike the sides of concrete anchorage holes, the inside of the rebar coupler sleeve does not allow for a good mechanical bond with the adhesive. Instead, the choked-down, smaller inside-diameter, mouth of the coupler prevents the block of adhesive from pulling out of the sleeve. This mechanical interlock also moves the majority of the stresses in the adhesive towards the mouth of the coupler, and makes any sort of average shear stress approximation invalid.

2.2 Moisture Diffusion in Polymers

Diffusion is the process by which the movement of a diffusing substance, a sorbate, moves into a diffusion media, a sorbent. A non-steady state diffusion process continues until the concentration of sorbate reaches a maximum, equilibrium value. The presence of a sorbate is described by its local concentrations [Crank 1968]. Since actual sorbate concentration is difficult to measure, gravimetric weight gain, normalized to original sample weight, is often used to calculate sorbate uptake concentration. Moisture uptake specimens are often in the form of thin plates so that diffusion from the large faces, though the small dimension of the geometry outpaces diffusion in the other two dimensions. In this way, diffusion can be described in simpler, one dimensional terms [Shen and Springer 1976].

2.2.1 Plasticization and Moisture Effects

The physical properties of polymers are known to degrade, over time, in the presence of moisture [Lee, Peppas 1993]. This degradation is due to a combination of physical and chemical processes. Physical processes include plasticization, relaxation and swelling of the polymer. The primary chemical degradation process is the hydrolysis of the polymer matrix [Antoon 1980].

Hydrolysis is the process in which water molecules hydrogen bond to the polymer chains. [Kwei 1966].While the hydrolysis does not weaken the actual polymer chains it does interrupt hydrogen bonding between chains, which allows

greater inter-chain mobility in the polymer; this process is known as plasticization. [Nissan 1976] The effect increases with increased moisture content.

The strength of hydrogen bonds between water molecules are slightly stronger than hydrogen bonds between water and polymer chains. This slight difference can lead to pockets, or clusters, of water forming inside a polymer, over time. [Starkweather 1963, Zhou and Lucas, Part I 1999].

Along with this plasticization due to hydrolysis, small segments of polymer chain, low molecular weight solids (LMWS), may diffuse out of the polymer matrix. If this effect is pronounced, as it may be at elevated temperature, it can result in an overall weight loss for the bulk polymer. [Lee, Rockett and Hoffman 1992]. The average polymer chain length is increased by the departure of the LMWS, and an increase in some physical properties, such as glass transition temperature, T_g, has resulted. [Karbhari 1996]. However, this potential gain from leaching LMWS is over overwhelmed by the effects of plasticization, which decreases glass transition temperature, T_g. Since the plasticization process can largely be reversed with drying, the permanent effect of the LMWS leaching becomes more salient if the polymer is dried. [Zhou and Lucas, Part II 1999].

Several assumptions are made to simplify the considerations of moisture uptake. It is assumed that gravimetric weight gain represents only an increase of moisture in the polymer. This assumption neglects the possible weight loss due to leaching of LMWS. It is also assumed that ions in solution do not diffuse into the polymer. This assumption is most significant for environments other than de-ionized water, in which ionic concentrations are significant.

2.2.2 Fickian Diffusion Model

Fick's laws, which use a diffusion coefficient to modify a logarithmic moisture uptake model, constitute the simplest diffusion model.

$$\frac{\partial C}{\partial t} = \nabla \bullet \left[D \cdot \left(\vec{\nabla} C \right) \right] \tag{5}$$

where C is the sorbate concentration, t is time, D is the diffusion coefficient. The simplicity of the model also leads to diffusion into, and out of, of a sorbent being treated equally, although this theoretical assumption has been proven to be experimentally unfounded. [Cotugno et al 2001, van Amerongen et al 1964,Whitney and Browning 1978].The Fickian diffusion coefficient relates to the speed at which a diffusion process occurs. A higher diffusion coefficient equates to a higher diffusion process; the diffusion coefficient of a process is not only inherent to a sorbent/sorbate combination, but can also be affected by the geometry of the sorbent and environmental conditions, such as temperature.

The general equation for Fickian diffusion can be reduced if diffusion is considered in only a single sorbate in a single dimension

$$\frac{\partial C}{\partial t} = D \frac{\partial^2 C}{\partial x^2} \tag{6}$$

where C is the concentration of sorbate per unit sorbent, t is time, D is the Fickian diffusion coefficient, and x is the length of the diffusion path through the sorbent.

For the simple case of the initial concentration of sorbate at the surface of a one-dimensional sorbent path, such as an infinite plate or sheet, the solution to the

equation is known. [Crank 1970, Carslaw 1959]. The solution can be expressed in terms of gravimetric moisture weight gain of an infinite plate with diffusion occurring from both surfaces of the plate, so that the thickness of the plate is *h* and the lengths of the diffusion paths are *h*/2, with an initial concentration of zero throughout the plate.

$$M_t = M_\infty \left[1 - \frac{8}{\pi^2} \sum_{n=0}^{\infty} \frac{1}{(2n+1)} e^{\left(\frac{-D \cdot t}{h^2} \pi^2 (2n+1)^2 \right)} \right] \tag{7}$$

where M_t is the cumulative gravimetric weight gain due to moisture uptake at a given time, M_∞ is the maximum moisture content at time infinity, D is the Fickian diffusion coefficient, and h is the thickness of the theoretically infinite sorbent plate.

Shen and Springer [1976] developed a simplified approximation of the equation which can be used for curve fitting to obtain diffusion coefficients.

$$M_t \approx M_\infty \left(1 - e^{-7.3 \frac{D \cdot t}{h^2}} \right) \tag{8}$$

2.2.2.1 Equilibrium Moisture Content

One of the implications of the Fickian Diffusion Model is that moisture content increases towards an asymptotic maximum, or equilibrium, moisture content, which would theoretically be reached at time infinity.

2.2.2.2 Diffusion Coefficient

Diffusion coefficients are known to be inherent to a specific polymer, buy also vary with temperature. [Abeysinghe et al 1982][Lee, Rockett, and Hoffman, 1992] Equation 8 can be simplified if the diffusion coefficient is assumed to be independent

of time or sorbate concentration. This simplified equation is known as the Arrhenius relationship. The Arrhenius relation can be used to represent the thermal dependence of the diffusion coefficient.

$$D = D_o e^{\left(\frac{-E_a}{R \cdot T}\right)} \tag{9}$$

where D *is* the diffusion coefficient, D_o is the ambient temperature diffusion coefficient, E_a is the activation energy, R is the universal gas constant and T is absolute temperature.

2.3 Moisture-based Degradation of Polymers

Predictive degradation models allow the prediction of material properties as a function of time. For instance, a property, such as the elastic modulus of a material, is measured periodically during a period of environmental exposure. For reasons of practicality, materials cannot be tested for time periods equal to its service life, so increased temperature environments are used to accelerate the degradation processes and give further insight into a material's long-term behavior. By treating materials at a range of temperatures, including ambient temperature, degradation rate and temperature can be correlated.

2.3.1 Arrhenius Degradation Model

The Arrhenius Rate Model can also describe the rate of degradation of a material property P as a function of time. This model assumes that the rate of the

material property change is proportional to the rate of the chemical process or reaction which is causing it. [145].

$$\frac{\partial P}{\partial t} = A \cdot e^{\left(\frac{-E_a}{R \cdot T}\right)} \tag{10}$$

where P a material property undergoing degradation, t is time, A is a constant, E_a is the activation energy for the degradation process, R is the gas constant, and T is absolute temperature.

Although the rate of degradation, in terms of time, is useful for understanding the relationship between a degradation process and increasing temperatures, it is also useful to predict the cumulative moisture uptake percentage with respect to time.

By measuring mechanical property degradation of glass fiber composites at a range of temperatures, the proportionality of moisture content to the natural logarithm of time, *ln(t)*, was established[Litherland et al 1981]. This relationship is described in Equation 11.

$$\ln[t] \propto \frac{1}{T} \tag{11}$$

By combining Equations 10 and 11, yields Equation 12, the Arrhenius Degradation model.

$$P(t) = B \cdot e^{\left[\frac{-E_d}{R \cdot T}\right]} \cdot \ln(t) + P_o \tag{12}$$

where B is constant and P_0 is the material property, of interest, at initial time zero. Equation 12 can be simplified further, at the expense of its transparency. Multiple constants can be combined to yield Equation 13.

$$P(t) = F(1 - A \cdot \ln(t)) \tag{13}$$

where F and A are constants.

2.3.2 Time-Temperature Superposition

Time-Temperature Superposition (TTS) is a theoretical principle relating viscoelastic material properties, usually modulus, to variations of time and temperature. [Williams, M.L., R.F. Landel, and J.D. Ferry 1955].

$$\log \alpha_T = \frac{-C_1(T - T_S)}{(C_2 + T - T_S)} \tag{14}$$

where α_T is the ratio of a mechanical relaxation time at temperature T to its value at a reference temperature T_0, C_1 and C_2 are constants, and T_S is and arbitrary reference temperature. However, T_0, C_1, C_2, and T_S all need to be developed for a particular material system, and make comparisons between materials difficult.

A simplified form of equation 11, normalized to a material's glass transition temperature, T_g, was made available by [C.C. Chamis 1984]

$$\frac{P}{P_O} = \left[\frac{T_g - T}{T_g - T_O}\right]^{-0.5} \tag{15}$$

where P is a temperature-dependent material property at temperature T, P_O is the material property at reference temperature T_O, and T_g is the glass transition temperature of the material.

By testing for a material property across a range of temperatures and rates, a spectrum of test data is obtained. Since test rates are essentially the inverses of test

times, a series of curves of the material property in relation to time can be shifted, using TTS, and combined into a master curve for the material.

Master curves are inherent to a given material system; however, they do change when a material undergoes degradation. The changes to the parameters of a material's master curves, due to degradation, can be modeled, as functions of time, by the Arrhenius degradation model. [Nakada et al 2002].

2.4 Creep of Polymers

[Moss 1982] conducted material-level creep tests on adhesive-anchorage-type epoxies. Tests were performed in flexural, tensile and compressive loading fixtures. The flexural test setup controlled load and the tensile and compressive test setups controlled deflection. The load-controlled, flexural test produced the clearest results, which indicated that creep rate increased with decreasing elastic modulus.

2.5 Dynamic Mechanical Thermal Analysis (DMTA) of Polymers

Dynamic Mechanical Thermal Analysis (DMTA) is a procedure which consists of the sinusoidally-oscillating mechanical loading, of a material specimen, in a thermally-controlled environment [Williams, Landel, and Ferry 1955]. DMTA is often referred to as Dynamic Mechanical Analysis (DMA), though the former specifies temperature as a variable in the test procedure. DMTA is well understood to be an effective material characterization tool; particularly for materials which are temperature-sensitive, such as polymers [Menard 1999]. DMTA has also been used to

investigate the effects of moisture upon polymer material properties, helping to correlate micro-structural changes in the material to declining mechanical properties [Xian and Karbhari 2007].

3 Experimental

3.1 Introduction

Experimental testing was performed to develop an understanding of the long-term behavior of the epoxy systems used in rebar-couplers, and how the properties of the epoxy affected the performance of the coupler system. First, a preliminary de-selection test was performed on a variety of commercially available epoxy systems to assess their moisture-based degradation behavior and their relative predicted suitability for application in epoxy-bonded rebar-couplers. Moisture uptake, tension and Dynamic Mechanical Thermal Analysis (DMTA) testing, at a limited variety of environmental conditions, were performed in the preliminary de-selection test. Next, a longer, primary, environmental testing program was performed on two of the epoxy systems selected from the results of the preliminary test. Moisture uptake, material tension, material compression, and DMTA testing, at a large variety of environmental conditions, were included in the primary testing program. Concurrently, epoxy-bonded rebar couplers were tested at periodic time intervals of environmental conditioning. Additionally, tests on modified versions of the rebar-coupler were performed, in an effort to gain insight into the mechanical and moisture-diffusion behavior of the couplers.

3.2 Material Description

3.2.1 Adhesive Classification

ASTM C881 is a standard which specifies numerous properties of epoxy-resin-based bonding systems for concrete. Bond strength to moist surfaces, heat deflection temperatures, linear coefficients of shrinkage, compressive strength and modulus, tensile strength and modulus and minimum elongation at break are all specified. Six commercially available ASTM C881 products were evaluated as part of this research.

ASTM C881 classifies different epoxy adhesive systems in three different classifications: “types”, “grades” and “classes”. “Types” are categories of physical properties, “grades” are ranges of flow characteristics, and “classes” are ranges of suitable application temperatures. The requirements for “types” and “grades” are shown below in table 1 and the ranges for “classes” are shown in table 2.

Table 1: Material property limits for types and grades of ASTM C881 epoxy adhesive systems.

Property	Units	Type I	II	III	IV	V
Viscosity						
- Grade 1, max	Pa-s	2.0	2.0	2.0	2.0	2.0
- Grade 2, min	Pa-s	2.0	2.0	2.0	2.0	2.0
- Grade 2 max	Pa-s	10.0	10.0	10.0	10.0	10.0
- Grade 3, max	Pa-s	6.0	6.0	6.0	6.0	6.0
Gel Time, min	Minutes	30	30	30	30	30
Bond Strength, min						
- 2 Day	MPa	7.0			7.0	
- 14 Day	MPa	10.0	10.0	10.0	10.0	10.0
Absorption, 24hr, max	%	1	1	1	1	1
Heat Deflection Temp, 7 Day, min	°C				50	50
Linear coefficient of shrinkage on cure, max	mm/mm	0.005	0.005		0.005	0.005
Compressive Yield Strength, 7 Day, min	MPa	55.0	35.0		70.0	55.0
Compressive Modulus						
- min	MPa	1000	600		1400	1000
- max	MPa			896		
Tensile Strength, 7 Day, min	MPa	35.0	14.0		50.0	40.0
Elongation at Break, min	%	1	1	30	1	1

Table 2: Ranges of suitable use temperatures for classes of ASTM C881 epoxy adhesive systems.

Class	Suitable Use Temperatures, °C Lower Limit	Upper Limit
A	-	4
B	4	15
C	15	-
D	4	18
E	15	30
F	25	30

3.2.2 Proprietary Adhesive Systems

3.2.2.1 System A

System A is a two-component structural epoxy gel. It is solvent-free with 100% solids. The mixing ratio of the system is 2:1 resin to hardener. The resin and hardener are dispensed from a dual-cartridge system and simultaneous mixed in a static mixing nozzle. The system meets ASTM C881, types I, II, IV, and V, grade 3, classes A, B, and C.

The first component is composed primarily of Bisphenol A, an epoxy resin. The second component is composed primarily of n-aminoethylpiperazine and Nonyl-phenol. Both components contain small portions of ethylene-glycol and quartz silica sand.

3.2.2.2 System B

System B is a two-component injectable epoxy adhesive. The mixing ratio of the system is 3:1 resin to hardener. The resin and hardener are dispensed from a dual-chambered cartridge and simultaneous mixed in a static mixing nozzle. The system meets ASTM C881, type IV, grades 2 and 3, classes A, B, and C except gel times.

The first component of System B is composed primarily of bisphenol A and bisphenol F epoxy resins. The second component is composed primarily of m-xylene diamine and aliphatic polyamine.

3.2.2.3 System C

System C is a two-component structural adhesive. It is a solvent-free, non-shrink, non-sag anchoring compound. The mixing ratio of the system is 1:1 resin to hardener. The resin and hardener are dispensed from a dual-cartridge system and simultaneous mixed in a static mixing nozzle. The system meets ASTM C881, types I, II, IV, and V, grade 3, classes A, B, and C.

The first component is composed primarily of a bisphenol A-epichlorohydrin diepoxy resin and neopentyl glycol diglycidyl ether mixture; together these compounds act as the epoxy resin. The second component is composed primarily of n-aminoethyl piperazine and a nonylphenol mixture; together these compounds act as an amine aduct.

3.2.2.4 System D

System D is a two-component, 100% solids, structural epoxy. When mixed, the resin and hardener combine into a smooth, non-abrasive, paste adhesive. The mixing ratio of the system is 1:1 resin to hardener. The resin and hardener are dispensed from a dual-cartridge system and simultaneous mixed in a static mixing nozzle. The system meets ASTM C881, types I, II, IV, and V, grade 3, classes A, B, and C.

The first component is composed primarily of a proprietary modified epoxy resin mixture; the component also contains small portions of benzyl alcohol, calcium carbonate, and talc. The second component is composed primarily of a proprietary

blend of aliphatic and cycloaliphatic amines and an aromatic hydrocarbon blend; the component also contains benzyl alcohol, calcium carbonate, and talc.

3.2.2.5 System E

System E is a two-component epoxy-based adhesive for use as a non-shrink anchor grouting material. It is low-odor with 100% solids. The mixing ratio of the system is 1:1 resin to hardener. The resin and hardener are dispensed from a dual-cartridge system and simultaneous mixed in a static mixing nozzle. The system meets ASTM C881, types I, II, IV, and V, grade 3, classes B, and C.

The first component is composed primarily of bisphenol A-epichlorohydrin diepoxy resin; the component also contains small portions of n-butyl glycidyl ether and amorphous silica. The second component is composed primarily of n-aminoethyl piperazine and nonylphenol; the component also contains amorphous silica and calcium carbonate.

3.2.2.6 System F

System F is a two-component, 100% solids, structural epoxy. When mixed, the resin and hardener combine into a smooth, non-abrasive, paste adhesive. The mixing ratio of the system is 1:1 resin to hardener. The resin and hardener are dispensed from a dual-cartridge system and simultaneous mixed in a static mixing nozzle. The system meets ASTM C881, types I, II, IV, and V, grade 3, classes A, B,

and C, except gel times. The gel time for the system varies from 30 minutes to 10 minutes, at temperatures from 4°C -32°C, respectively.

The first component is composed primarily of bisphenol A-epichlorohydrin diepoxy resin; the component also contains small portions of methyl toluensulphonate. The second component is composed primarily of piperazom-ylethylamine and nonylphenol; the component also contains a proprietary mixture of fillers.

3.3 Environmental Conditions

3.3.1 Range of Service Conditions

Material and coupler specimens were exposed to a range of environments to simulate service conditions and environments, as well as provide a means of accelerated testing to allow predictions of material and system behavior further into the future.

The seven exposure environments were:

1. 23°C air (ambient conditions) (Abbreviated throughout this report as 23AM)
2. 60°C air, with relative humidity less than 20% (Abbreviated throughout this report as 60AM)
3. 23°C de-ionized water (Abbreviated throughout this report as 23DI)
4. 40°C de-ionized water (Abbreviated throughout this report as 40DI)
5. 60°C de-ionized water (Abbreviated throughout this report as 60DI)
6. 5% salt (NaCl) solution at 23°C. (Abbreviated as 23Na)

7. Concrete leachate solution at 23°C (created by submerging concrete blocks into de-ionized water, with the resulting solution having a pH of 11.5-12.5) (Abbreviated throughout this report as 23OH)

3.3.2 Experimental Rationale for Selection

This research assumed that any degradation of long-term performance of the adhesive systems would be linked to heat and moisture uptake. Adhesives have been shown to be susceptible to moisture-based degradation [Kaw 1997]. Although the adhesive would be inside a steel coupler and embedded in concrete, the humidity level inside concrete bridge decks, in regions of moderate rainfall, has been shown to stay around 80% [Stark et al 1993]. Heat accelerates the moisture uptake process and in warm climates, with intense solar radiation, the temperature inside concrete bridge decks, at depth of reinforcement, has been shown to approach 60°C [Priestly 1976].

3.4 Specimen Fabrication

Specimens for DMTA, moisture uptake and tension testing were cut from plates of the material, as described later in this section. Compression specimens were cut from cured cylinders of the material. Rebar-coupler specimens were assembled according to the manufacturer's recommendations. All adhesive systems were provided from their manufacturers in two-part, nozzle-mixed cartridges. Cure of all adhesive systems occurred at ambient temperature, pressure, and humidity conditions, which were 23°C, 100kPa and 30% relative humidity, respectively.

3.4.1 Plate Specimens(Moisture, Tension, DMTA)

The plates were created by pressing a bulk of the mixed epoxy adhesive between a sheet of polyethylene and an aluminum plate which had been coated with a wax-based mold release. The size of the molds, and formed plates, was 356 mm, square, and the resulting thickness of the cured plates was approximately 3mm. The fabrication process and cure of the plates occurred at ambient temperature and pressure. A schematic of the plate specimen fabrication setup is shown in Figure 11.

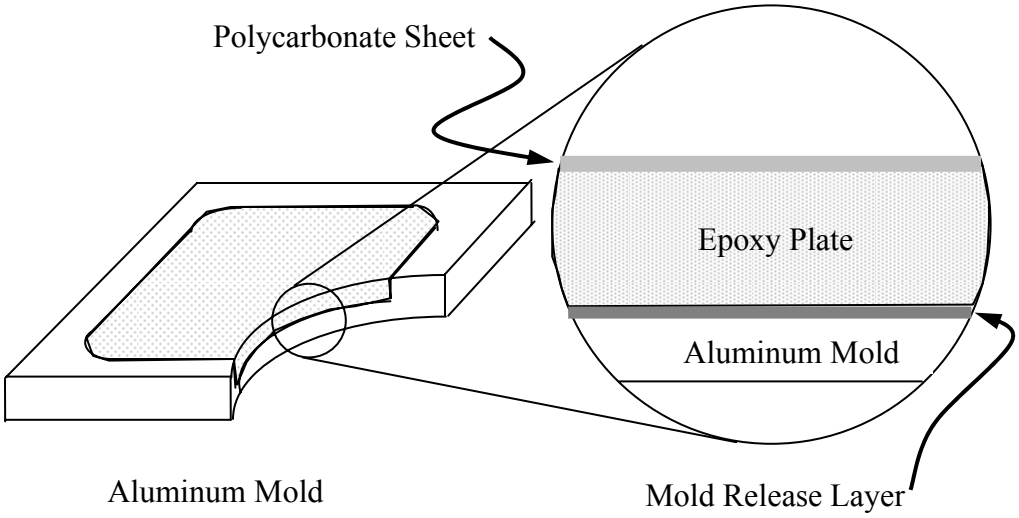

Figure 11: Exploded view of epoxy plate fabrication setup.

3.4.2 Compression Specimens

Cylindrical specimens for compression testing were created by injecting the adhesive into 12.7mm inside-diameter polyethylene tubing. This tubing was cut away and discarded after the adhesive had cured. The resulting adhesive cylinders were then cut to specimen lengths.

3.4.3 Coupler Specimens

The rebar-coupler specimens were fabricated using a factory-produced coupler, a bare rebar and the proprietary adhesive systems. The coupler sleeves were, filled from the bottom, with the adhesive nozzle then the bare rebar was inserted and the specimens were supported, in a horizontal aligned position, and were left to cure for at least one day.

3.4.4 Embedded Coupler Specimens

Assembled, cured, rebar-coupler specimens were embedded in concrete cylinders by casting the cylinders around the couplers. Concrete cylinder molds of 10cm diameter and 20cm height were drilled to allow the assembled rebar couplers to fit inside before concrete was poured. Figure 12 shows a photograph and cutaway views of the rebar-coupler specimens, alone, and embedded in a concrete cylinder.

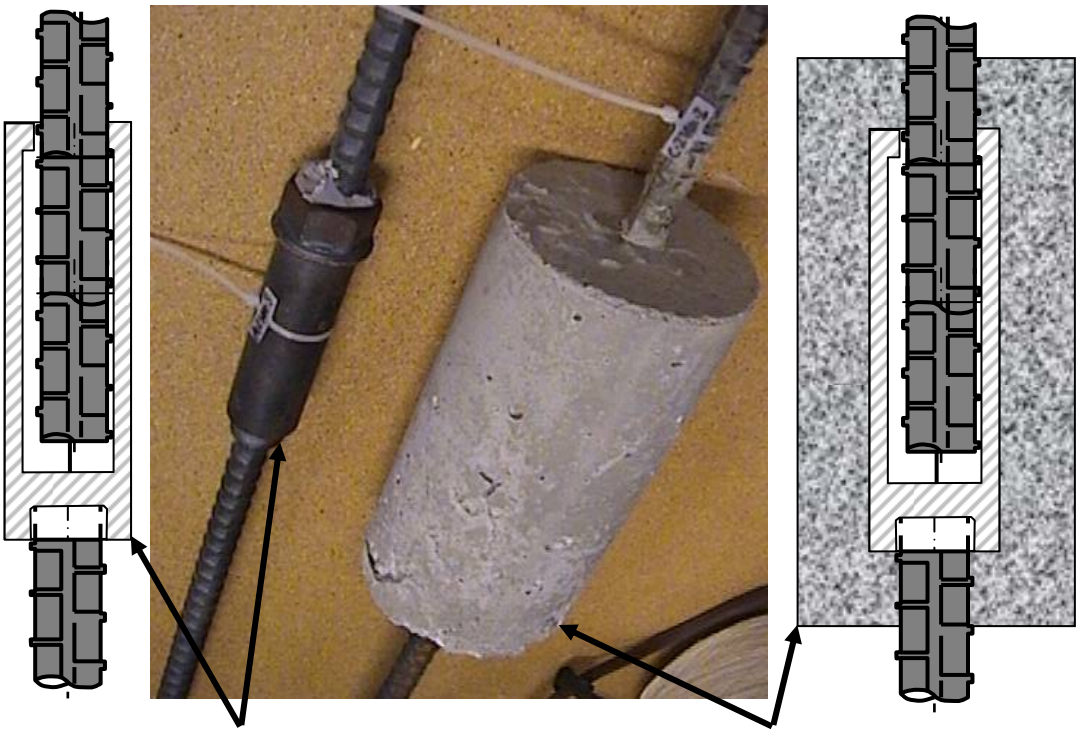

Figure 12: Photograph of assembled epoxy-bonded rebar-coupler, exposed and encased in concrete cylinder. Cutaway diagrams are included for clarification of each.

3.5 Testing Programs

3.5.1 Preliminary De-Selection Test

The purpose of the preliminary de-selection test was to examine a range of commercially-available epoxy systems and select several systems for the primary test program. Systems were evaluated quickly for their resistance to moisture degradation, which was deemed more important than the actual material property values. With this metric in mind, the tests were not of sufficient statistical rigor to perform material characterization.

All six ASTM C881 proprietary systems, A through F, were included in this preliminary testing program. The preliminary de-selection test consisted of three components: gravimetric moisture uptake, tension testing, and DMTA.

3.5.1.1 Moisture

The six systems were tested for moisture uptake properties according to ASTM D570. Moisture uptake testing was conducted in de-ionized water at 40°C and 60°C. Testing was performed at two temperatures to assess the proportionality of moisture uptake at increasing temperature for each material system. These two temperatures were chosen because 60°C was near the upper level of service temperature [Priestly 1976] and 40°C was approximately midway between 60°C and room temperature, 23°C. Moisture uptake was not measured at 23°C because the results of the elevated temperature tests were assumed to accelerate the moisture uptake processes during the four-week-long test. The specimens used were 25.4mm x 25.4mm x 3mm plate specimens.

3.5.1.2 Material Tension

Tension testing of the epoxy material was performed according to ASTM D638. The specimens were cut from plates into 12.7mm-wide strips. Although these strips were not an ASTM D638 supported specimen type and were therefore not appropriate for material characterization testing, they did give a reasonable idea of the materials' strength and stiffness sensitivity to moisture exposure. The strips were

tested in the unexposed condition, and after two and four weeks of immersion in 60°C de-ionized water. This environment was selected to rapidly assess the relative resistance of moisture of each material. Since higher temperatures accelerate the moisture uptake and degradation processes, 60°C was selected because it was at the upper end of temperatures that were expected during the service life of the material, embedded in a concrete bridge deck [Priestly 1976].

3.5.1.3 Dynamic Mechanical Thermal Analysis (DMTA)

DMTA testing of the epoxy material, after environmental exposure, helps to understand the effect of moisture uptake on the material's viscoelastic response. The test determines the glass transition temperature (Tg) of the material, which is the material's transition temperature from glassy to rubbery behavior. Testing was performed in the unexposed condition, and after two and four weeks of immersion in 60°C de-ionized water.

DMTA testing was conducted in three-point bending mode on rectangular plate specimens with dimensions 50mm x 10mm x 3mm. Testing in the preliminary program was at 1 hz frequency, from 20°C to 120°C using a temperature ramp rate of 4°C/min.

3.5.2 Primary Testing

The primary testing program consists of two material systems, seven environments, and five test procedures. The two material systems tested were the two

chosen at the end of the preliminary de-selection test program: systems A and C. The seven environments were: 23°C air, 60°C air with humidity less than 20%, immersion in 23°C, 40°C, and 60°C de-ionized water, a concrete leachate solution at 23°C, and a 5% salt solution at 23°C. The five tests performed were: moisture uptake, material tension, material compression, DMTA and coupler system tension.

The original test plan called for testing to be performed at the following time intervals: zero time/as built, ½, 1, 2, 4, 8, 12, and 16 months. However, due to the changes caused due to the constraints from the research sponsor, the California Department of Transportation, the testing scheduled for 12 months was performed at 11.5 months, and the testing originally planned for 16 months was performed for 14.5 months. This acceleration of schedule appeared reasonable due to the predictability of the results gathered during months 0-8.

3.5.2.1 Moisture

Gravimetric moisture-uptake testing was performed according to ASTM D570. The specimens used were 25.4mm x 25.4mm x 3mm plate specimens.

3.5.2.2 Material Tension

Tension testing of the epoxy material was performed according to ASTM D638; the preliminary tension specimens were 12.7mm-wide strips, the primary tension specimens were Type I dog-bones [ASTM D638]. Tension testing, after environmental exposure, is important because the material is primarily loaded in shear

within the coupler system and when used in adhesive anchorage to concrete. When loaded in shear, to failure, tensile cracks open up in the material at approximately 45° angles to the material surface, so shear behavior off the material appears to be tensile-property-limited. This induced tensile force is depicted in figure 8.

3.5.2.3 Material Compression

Compression testing of the epoxy material was performed according to ASTM D695; the specimens were standard cylinders of 12.7mm diameter and 25.4mm length [ASTM D695]. Compression testing, after environmental exposure, is important because of the unique geometry of the rebar coupler, which differs from the geometry of an adhesive anchor to concrete. The reduced inner-diameter entrance to the coupler sleeve allows the formation of compressive forces in the epoxy material between the decreased diameter region and the deformations of the reinforcing bar. These compressive forces, at the entrance of the coupler sleeve, are depicted in figure 13.

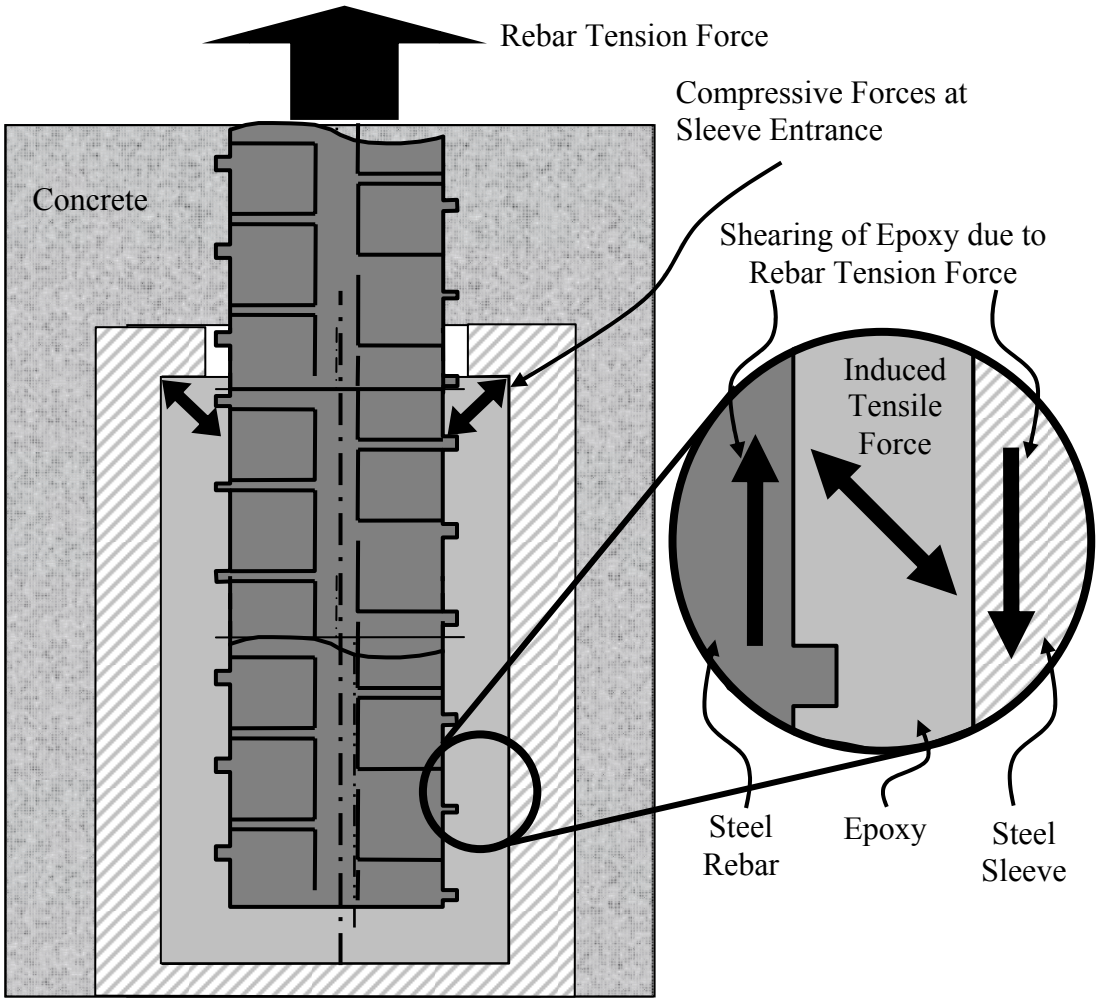

Figure 13: Diagram of forces during tensile loading of epoxy-bonded rebar-coupler.

3.5.2.4 Dynamic Mechanical Thermal Analysis (DMTA)

DMTA testing of the epoxy material, after environmental exposure, helps to understand the effect of moisture uptake on the material's viscoelastic response. The test determines the glass transition temperature (Tg) of the material, which is the material's transition temperature from glassy to rubbery behavior. The Tg of an epoxy-based adhesive can be increased by post-curing, but can be decreased due to

moisture uptake (18). Additionally, multi-frequency DTMA data can be analyzed, using time-temperature superposition to develop master creep curves for a material.

DMTA testing was conducted in three-point bending mode on rectangular plate specimens with dimensions 50mm x 10mm x 3mm. Testing in the primary program was at 0.3, 1, 3, 10 and 30 hz frequencies, from 20°C to 140°C using a temperature ramp rate of 4°C/min.

3.5.2.5 Coupler System

3.5.2.5.1 Slip Testing

Slip Testing was performed according to California test 670 specifications, but with supplementary instrumentation. The loading procedure used was identical to California Test 670 specifications but measurement, over a 200 mm. gauge length, across the coupler area was performed with an extensometer instead of calipers. A special 200 mm. gauge length extensometer allowed continuous measurement over the coupler area, instead of several times throughout the test, as would be allowed with calipers. The rebar coupler specimens were preloaded to 4 MPa of rebar tensile stress and a baseline measurement along the 200 mm gauge length, over the coupler length, was taken. Next the specimen was loaded to 200 MPa and held for 60 seconds. Finally, the load was reduced to 20 MPa and the slip was measured as the change in gauge length over the original 200 mm. length. After slip testing was finished the coupler specimens were loaded to failure.

3.5.2.5.2 Cyclical Testing

Cyclical testing of rebar coupler specimens was performed according to California Test 670 specifications. The couplers were subjected to 100 cycles of 5%-90% of rebar yield load. The cycles were applied at 0.7 cycles per second of haversine waveform. After the cyclical loading was finished the coupler specimens were loaded to failure.

3.5.2.5.3 Fatigue Testing

Fatigue testing of rebar coupler specimens was performed according to California Test 670 specifications. The couplers were subjected to 10,000 cycles of ±173 MPa at 0.35 cycles per second of sine waveform. After the fatigue loading was finished the coupler specimens were loaded to failure.

3.5.2.5.4 Elevated-Temperature Testing

Most rebar-coupler tests specimens were environmentally exposed, but the actual tests were performed post-exposure in dry, ambient temperature conditions. To investigate the rebar-coupler response when tested at elevated temperature, a heating jacket was wrapped around the specimens and the temperature was allowed to reach steady state before testing. Figure 14 shows the elevated-temperature test setup. These tests were performed at 40°C, 60°C and 80°C.

Figure 14: Photograph of epoxy-bonded rebar-coupler elevated-temperature test setup.

3.5.3 Additional Testing

Besides the preliminary and primary test programs, additional experiments were performed to gain insight into both the mechanical and moisture-uptake phenomenon inside the epoxy-bonded rebar-coupler system.

3.5.3.1 Modified Rebar Couplers

Rebar-couplers were fabricated with important geometric changes from the commercially available models. The qualitative observations of testing these

geometrically-altered couplers led to important insight into the mechanics of a complicated system.

3.5.3.1.1 Thin Walled

A rebar-coupler was fabricated with a proportionally thinner sleeve-wall thickness to investigate the level and location of any confinement stresses placed on the epoxy by the sleeve. Any yielding of the coupler sleeve would indicate a concentration of stresses.

3.5.3.1.2 No Choked Mouth

A rebar-coupler specimen was fabricated to investigate the relative load resistance levels of the chocked coupler mouth and bond between the adhesive and the inside rebar-coupler sleeve walls. This specimen had no choked-down entrance section and hence was completely dependent on bond between the epoxy and the inside of the sleeve for tensile load-transfer. Figure 15 shows cutaway views of the standard geometry of rebar-coupler and a rebar-coupler with no choked mouth.

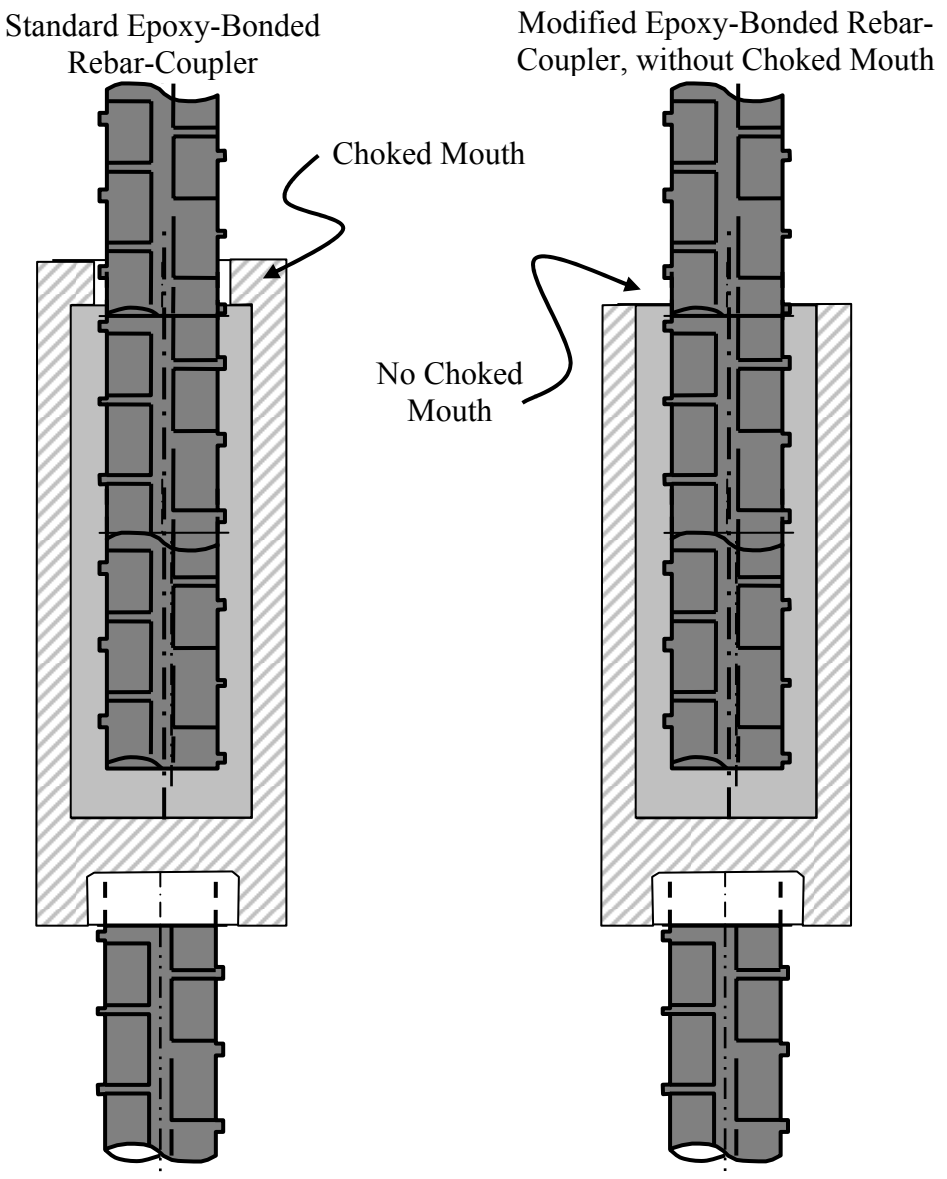

Figure 15: Diagram comparing standard epoxy bonded rebar-coupler, on left, and coupler modified to have the choked mouth removed, on right.

3.5.3.1.3 No Choked Mouth, Ribbed Inner Sleeve Wall

A rebar-coupler specimen was fabricated to investigate the effects of small incised ribs on the inside of the rebar-coupler sleeve on force transfer between the sleeve and epoxy. This specimen also had no choked-down entrance section,

however, the force transfer between epoxy and the inside of the sleeve were able to transfer tensile load by both bond and mechanical-interlock. Figure 16 shows cutaway views of the standard geometry rebar-coupler and a rebar-coupler with no choked mouth and ribbed inner sleeve walls.

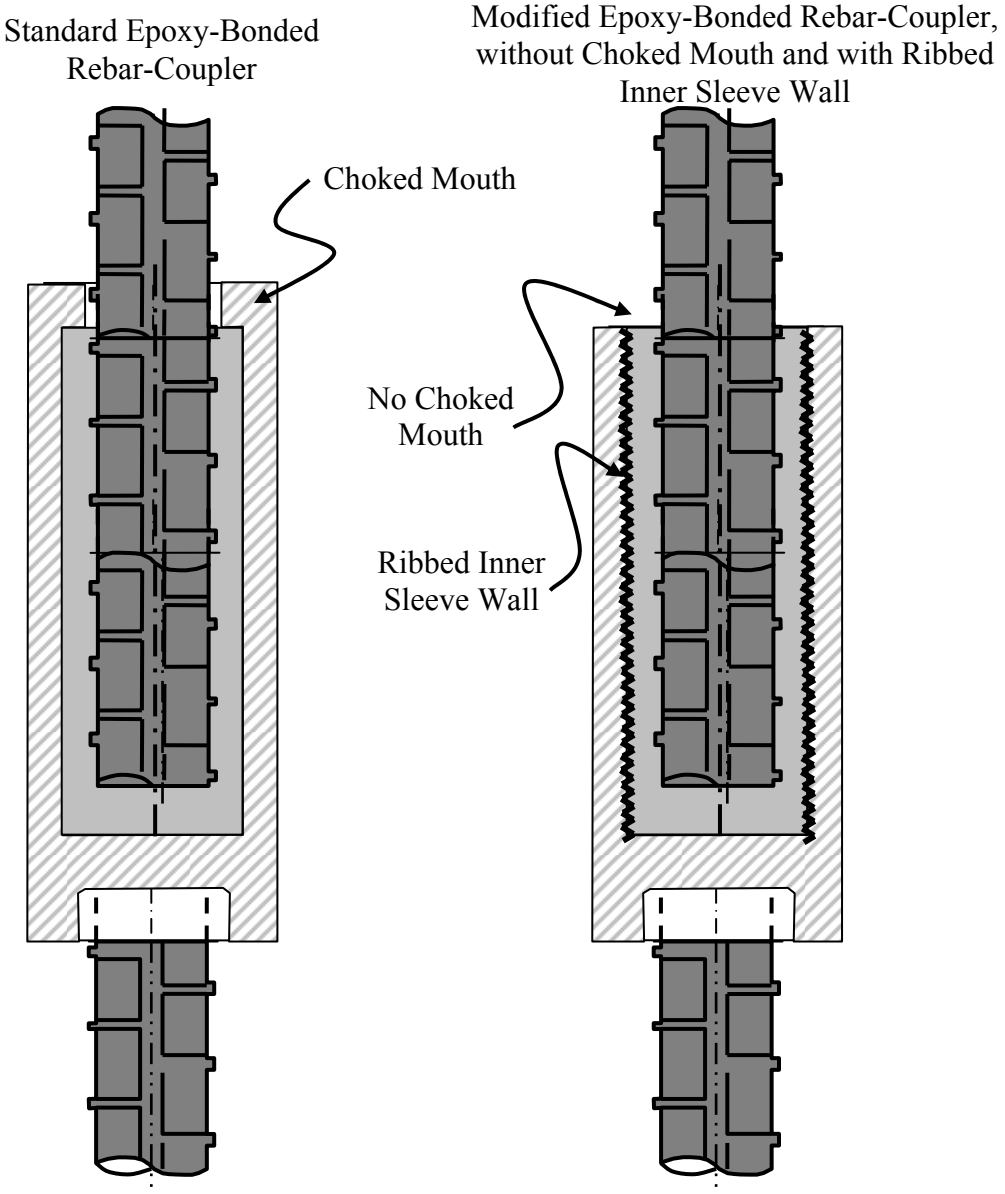

Figure 16: Diagram comparing standard epoxy bonded rebar-coupler, on left, and coupler modified to have the choked mouth removed and ribbing added to the inner sleeve wall, on right.

3.5.3.2 Destructive Testing of Moisture Sleeves

To supplement the free moisture uptake experiments, testing was also performed to examine the moisture uptake of epoxy inside a coupler sleeve-like geometry. Since moisture uptake of the epoxy does produce some expansion, these sleeve specimens were used to compare the maximum moisture uptake levels of epoxy in a free-expansion and confined state. Specimens were fabricated, matching the geometry of an epoxy-bonded rebar coupler, but using stainless steel sleeve and bar, to eliminate corrosion and simplify testing. These specimens were immersed in 60°C de-ionized water for 14.5 months, and then cut into slices, normal to symmetry axis. The epoxy from these slices was monitored for gravimetric weight loss and dried to calculate maximum moisture uptake of the epoxy inside confining, sleeve geometry. A photograph of one of the test sleeves is shown in Figure 17.

Figure 17: Photograph of moisture sleeve test specimen. Notice the stainless steel material, but with identical geometry to a typical epoxy-bonded rebar-coupler.

3.5.3.3 Creep Test Setup

A test setup was performed for epoxy-bonded rebar-coupler creep testing. A diagram of the test setup is shown in Figure 18. The results of the test were used to evaluate the performance of epoxy-bonded rebar-couplers compared to available data for both adhesive anchors and other types of rebar-couplers. Creep of concrete

anchors is typically evaluated using ASTM E 1512, or through ICC-ES Acceptance Criteria 58, which references the ASTM Standard. The creep test setup for the epoxy-bonded rebar-couplers adapted the ASTM E 1512 Standard wherever possible. The length of test, 42 days, and the stress-level of the test, 40%$fu_{,steel}$ were both adapted from this standard. Although no specific standard exists for creep of rebar-couplers, the results of this test were compared to the results of a test on cementitiously-grouted rebar-couplers by the Michigan Department of Transportation [Jansson, 2008]. Systems C and F were both evaluated, using two specimens each, to assess the potential for creep of the system as specified, and with a non-optimal epoxy system, respectively.

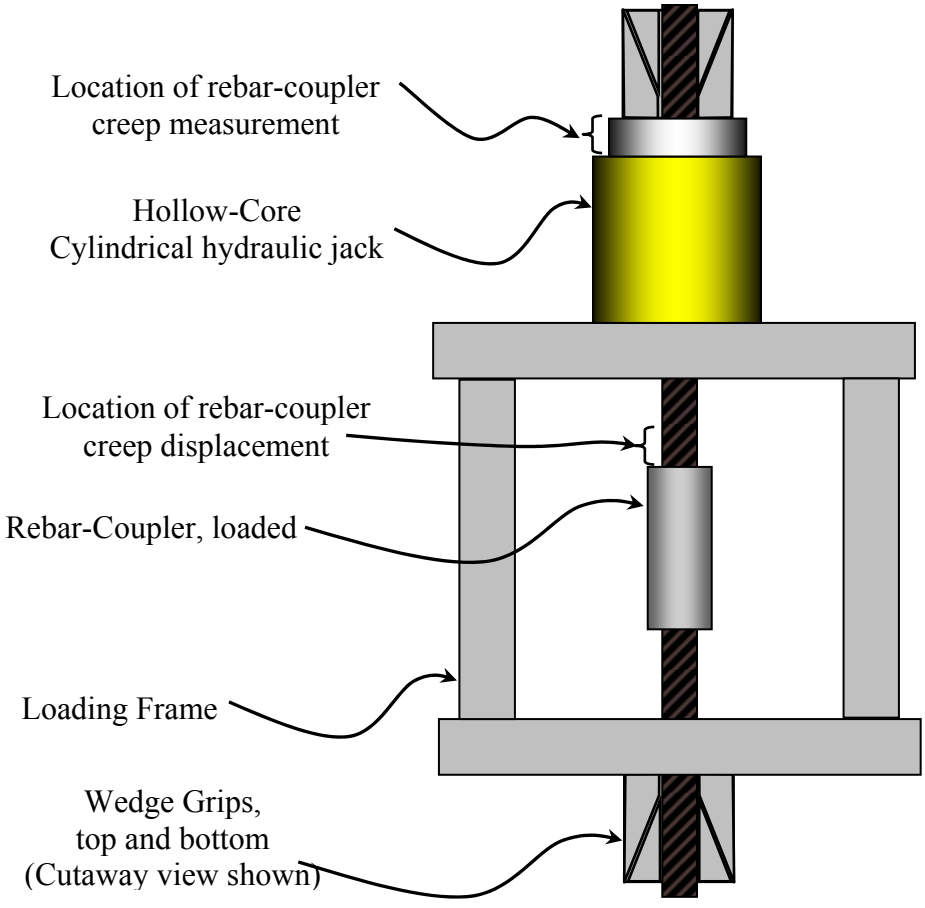

Figure 18: Diagram of rebar-coupler creep test setup.

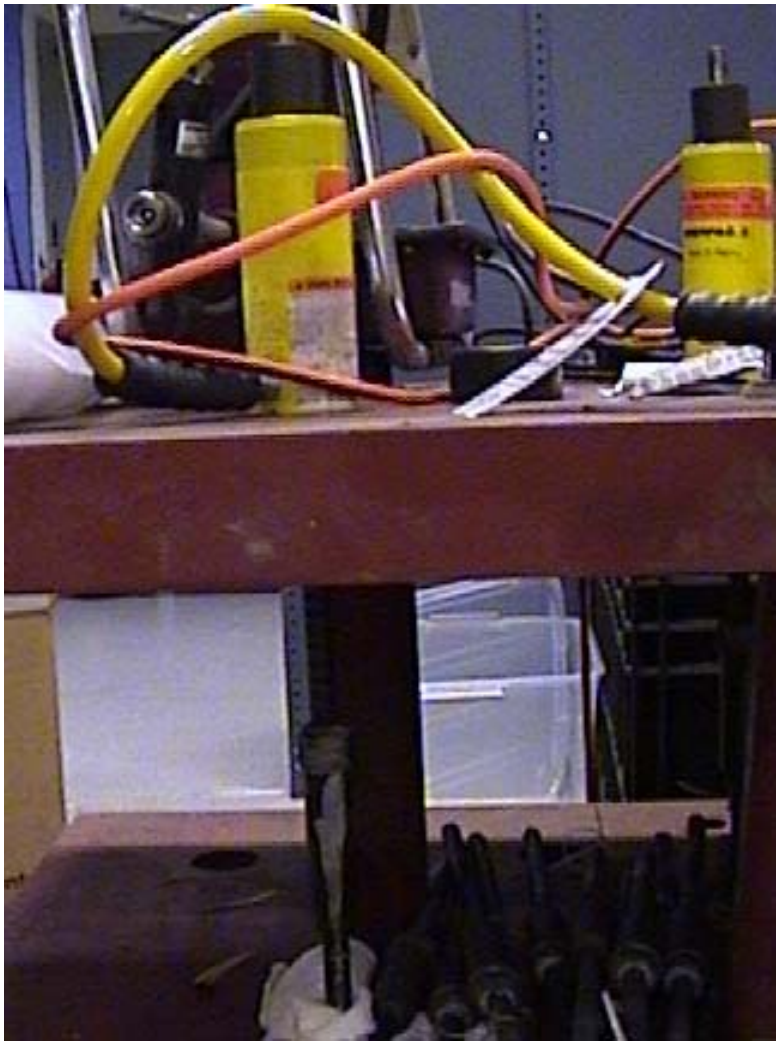

Figure 19: Photograph of rebar-coupler creep test setup.

4 Results

4.1 Introduction

The results of the preliminary de-selection test, primary testing program, modified rebar-coupler tests, and destructive testing of moisture sleeves are presented in this chapter. In an effort to illustrate the results important to this research typical and significant test results are presented, and the results of all tests are summarized in tables. Through the course of this research a large number of tests were performed; all test data is available in appendices.

4.2 Preliminary De-Selection Results

4.2.1 Moisture

Figure 20 shows moisture uptake curves for the six systems in the preliminary de-selection test. These curves are for moisture uptake in the 60°C, de-ionized water environment. A range of behaviors are displayed by the systems. Generally, the Systems gained weight quickly at the beginning of exposure, and the rate of gain decreased with increasing time. Systems A, B, C, appear to follow this trend, and are still gaining weight by the end of the trial time. System E gained weight the quickest of all systems initially, but also appeared to level off at some level of weight gain lower than the other Systems. System D initially gained weight but then quickly started loosing it. The loss of mass, measured as negative moisture uptake, in such an environment, indicates significant degradation of the material, as material mass is

being degraded and lost faster than moisture uptake can replace it. System F showed fairly predictable initial moisture uptake but it quickly became evident, from the visual sagging of the specimens in the environment, that System F was not remaining stable.

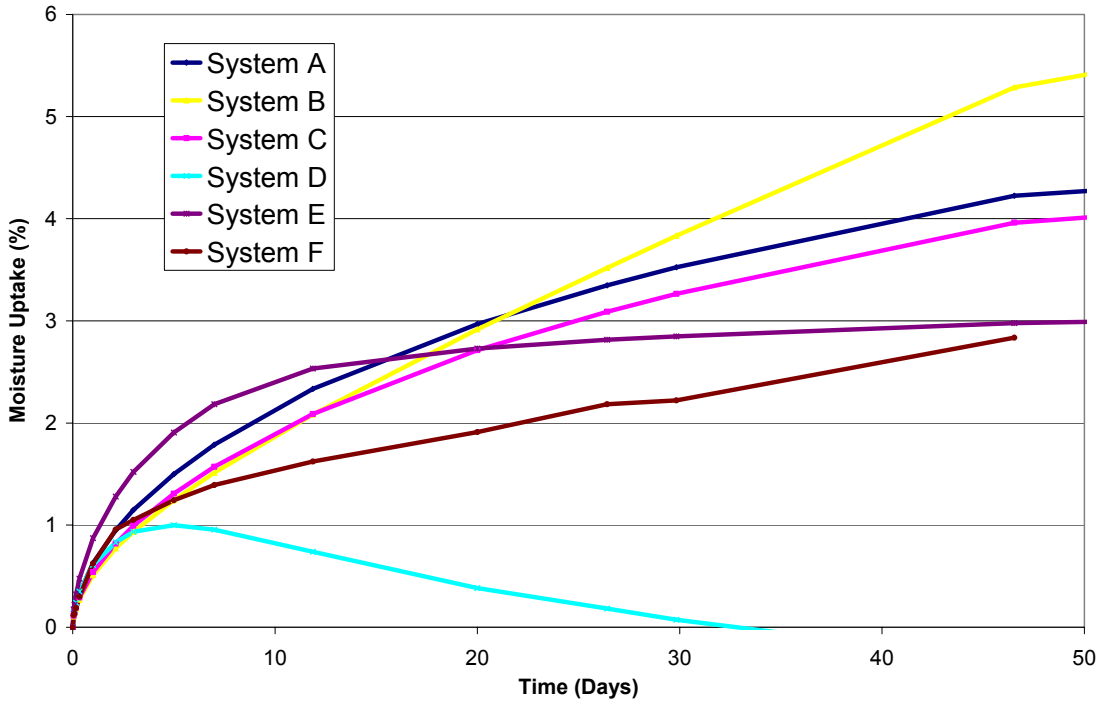

Figure 20: Preliminary De-Selection moisture uptake test results for Systems A-F.

Fickian diffusion curves were fitted to these uptake curves to obtain diffusion properties: maximum moisture uptake at time infinity, and the corresponding diffusion coefficient. Ideally, a system which is stable in moist environments would have a relatively low value for both of these properties. The quantitative results of this test are summarized in Table 3.

4.2.2 Tension

Figure 21 shows a typical plot of stress vs. strain tension results for epoxy System C at three different times of exposure. Each system was tested after cure in the unconditioned state, and again at two weeks, then four weeks, of environmental exposure in 60°C, de-ionized water. The behavior of the unexposed material is approximately linear-elastic; however, the behavior becomes increasingly visco-elastic with increasing exposure time. Elastic modulus and ultimate stress decrease with increasing exposure and strain-to-failure increases with increasing exposure. These are the expected response of an epoxy system plasticizing when exposed to moisture [Mikols 1982], and are typical all the systems studied in the preliminary de-selection test. Systems were evaluated not on absolute test values, but on elastic modulus and tensile strength retention. The rationale for this evaluation was that the ability of System to maintain its mechanical properties, after exposure to moisture and elevated-temperature, was more important for the long-term performance of the coupler than having a slightly higher initial property value. The results for each system are located in Table 3.

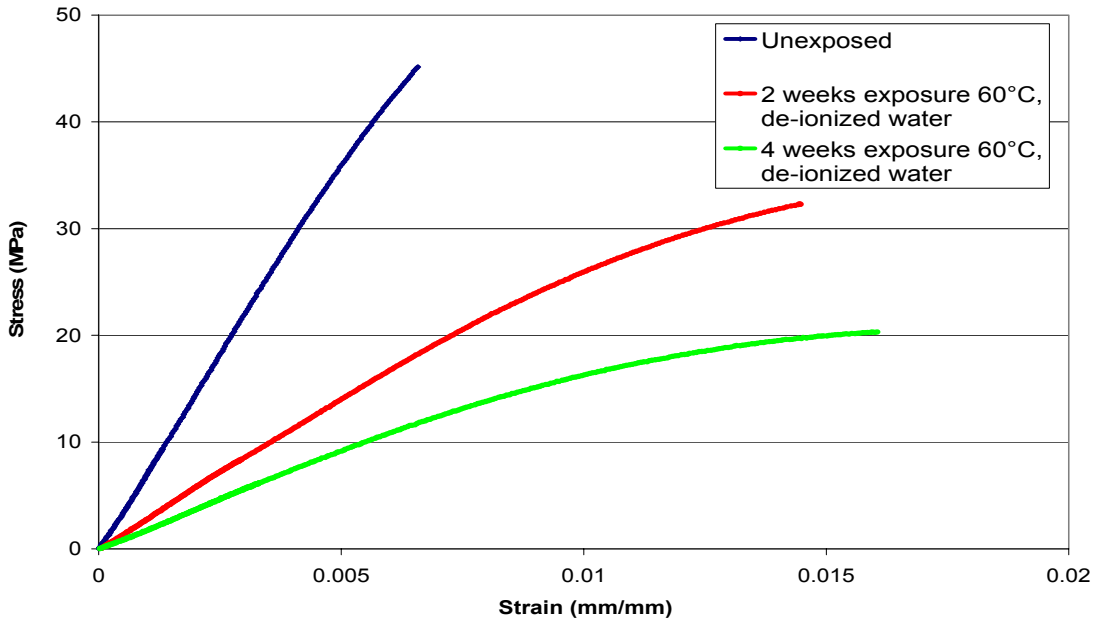

Figure 21: Typical Preliminary De-Selection tension testing results. System C shown.

4.2.3 Dynamic Mechanical Thermal Analysis(DMTA)

Figure 22 shows a typical plot of storage modulus, E', and tan-δ plotted, with respect to temperature, at a single frequency, for a material specimen. The storage modulus can be seen to undergo a significant decline, of over an order of magnitude, across the temperature range. This decline corresponds to the materials transition from a glassy state to a rubbery one. The peak of the tan- δ curve is one way to calculate a temperature to associate with this transition. The temperature at which this transition takes place, *Tg*, is significant.

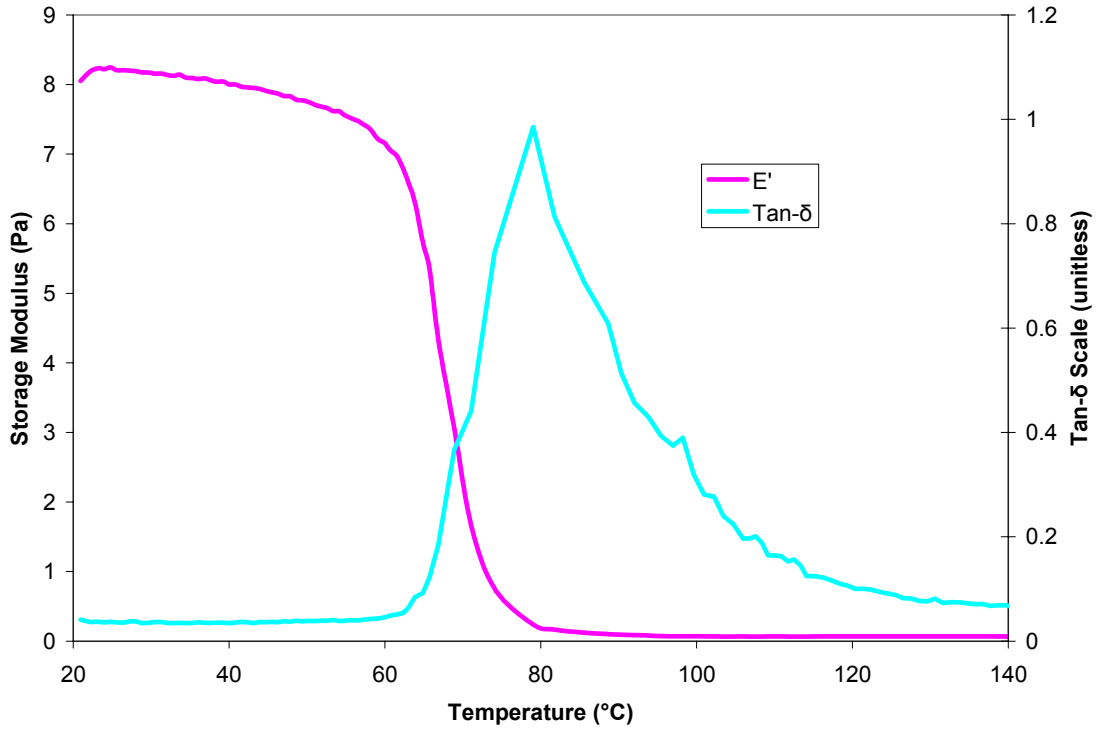

Figure 22: Typical plot of single frequency DMTA test result. System A shown.

Figure 23 shows a typical comparison plot of the tan- δ curves for an unexposed sample and a sample after two weeks of exposure. Each system was tested after cure in the unconditioned state, and again at two weeks, then four weeks, of environmental exposure. The glass transition temperature (*Tg*) is taken as the temperature at the peak of the tan delta curve. By comparing these two curves it can be seen that the *Tg* decreases with increasing exposure. These are the expected response of an epoxy system plasticizing when exposed to moisture, and are typical all the systems studied in the preliminary de-selection test.

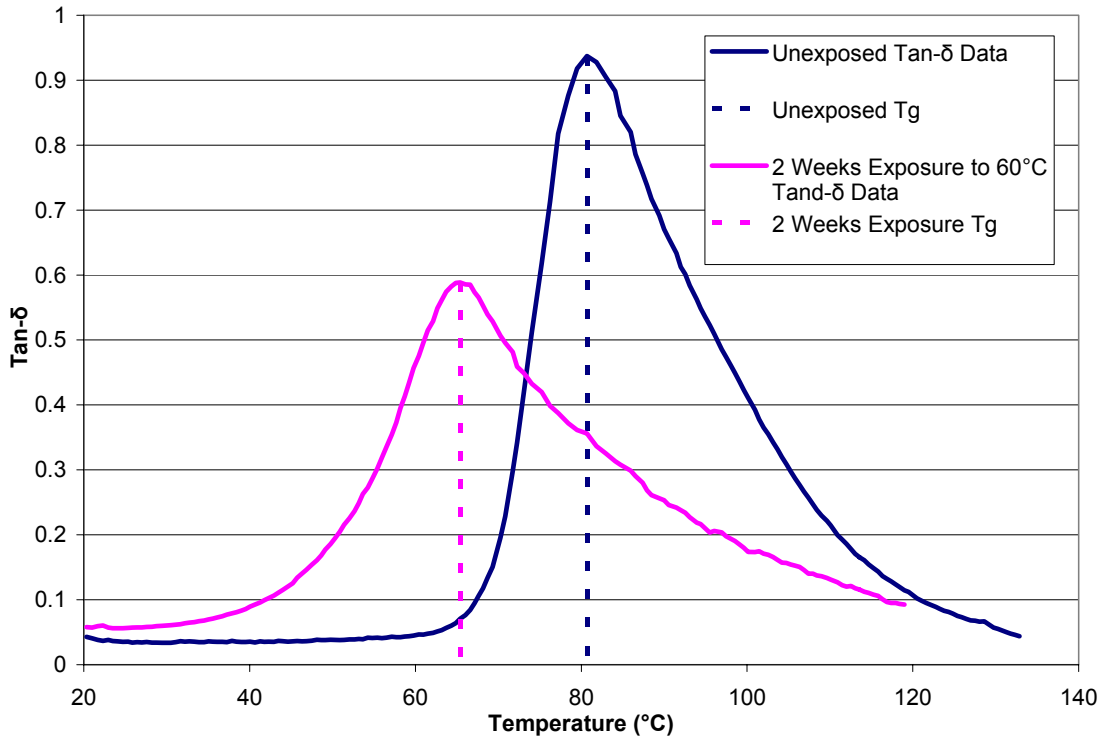

Figure 23: Sample De-Selection DMTA testing results. System B shown.

4.2.4 Summary

Table 3 is the results summary of the preliminary de-selection test. Tension, DMTA and moisture-uptake results are shown for each system. Worst-in-test results are highlighted in red and best-in-test results are highlighted in green.

Table 3: Summary of results for Preliminary De-Selection testing. Best in category results highlighted green. Worst in category results highlighted red.

System	Conditioning Time	Tension		DMTA	Moisture		
		Strength % Retention	Elastic Modulus % Retention	Glass Transition Temperature (by Tan Delta Peak) °C	Predicted Maximum Moisture % increase	Fickian Diffusion Coefficient (10^-7) (mm^2/s)	Mass Loss
A	Zero Time			70	5.0	2.3	NO
	2 Weeks	64	65	60			
	4 Weeks	54	41	58			
B	Zero Time			66	8.2	1.7	NO
	2 Weeks	53	45	65			
	4 Weeks	44	45	66			
C	Zero Time			70	5.8	3.6	NO
	2 Weeks	62	19	55			
	4 Weeks	48	19	58			
D	Zero Time			60	1.3	111.2	YES
	2 Weeks	20	8	41			
	4 Weeks	31	13	45			
E	Zero Time			65	3.4	23.9	NO
	2 Weeks	89	13	50			
	4 Weeks	103	27	47			
F	Zero Time			52	3.5	10.6	YES
	2 Weeks	27	2	46			
	4 Weeks	48	7	41			

Large differences between systems are highlighted in Table 3. Though systems A and C did not excel at all categories they avoided doing poorly in all and exhibited at general predictability in all results. System A had the best elastic modulus retention of any system and one of the lowest Fickian diffusion coefficients of any system; importantly, it avoided placing worst-in-class in any category. Although System B exhibited the best *Tg* retention and lowest Fickian diffusion coefficient of any system tested, it also had the highest predicted moisture uptake level. System C had one of the lowest Fickian diffusion coefficients of any system; importantly, it avoided placing worst-in-class in any category. Although System D had the lowest predicted maximum moisture uptake percentage, this value is misleading because the system quickly started losing mass, indicating a significant vulnerability to moisture-based degradation, and therefore poorly fit the Fickian diffusion regime; the system also had some of the worst performance in categories of tensile strength retention, tensile modulus retention, and Fickian diffusion coefficient. Although System E exhibited the best tensile strength retention of any system tested, its Fickian diffusion coefficient was one of the highest in the test, and an order of magnitude higher than those of many of the other systems tested. Such a high Fickian diffusion coefficient indicates a lack of resistance to moisture uptake, which is not ideal for a product with a long service life in moist conditions. System F had some of the worst performance in categories of tensile strength retention, tensile modulus retention, *Tg* and *Tg* retention, and Fickian diffusion coefficient; additionally, the system exhibited loss of mass, indicating a significant vulnerability to moisture-based degradation [Maggana

1999]. From these overall results systems A and C were chosen for the primary test program.

4.3 Primary Testing Results

4.3.1 Moisture

Figure 24 shows a typical plot of moisture uptake for System A in the primary test program, which performed very similarly to System C. Each plot trace corresponds to a different environmental treatment. The nearly flat trace is moisture uptake in a dry, ambient temperature environment and is close to zero, as expected. The negative, or weight-loss trace, is a warm dry environment and indicates a slight drying. The strongly positive traces are moisture gain from immersive environments. The three tightly grouped traces are for the three different chemical environments: de-ionized water, salt solution, and concrete leachate solution. The common parameter of these three immersive environments was temperature: 23°C. So the level of similarity between the three moisture uptake traces indicates that no significant chemical vulnerability exists to salt or concrete leachate solutions beyond that of moisture, for the time periods considered in this test program. The two steeper traces show accelerated moisture uptake with increasing temperature. This acceleration is typical of epoxy systems undergoing moisture uptake in an immersive environment. The increased temperature speeds the diffusion of moisture into the material.

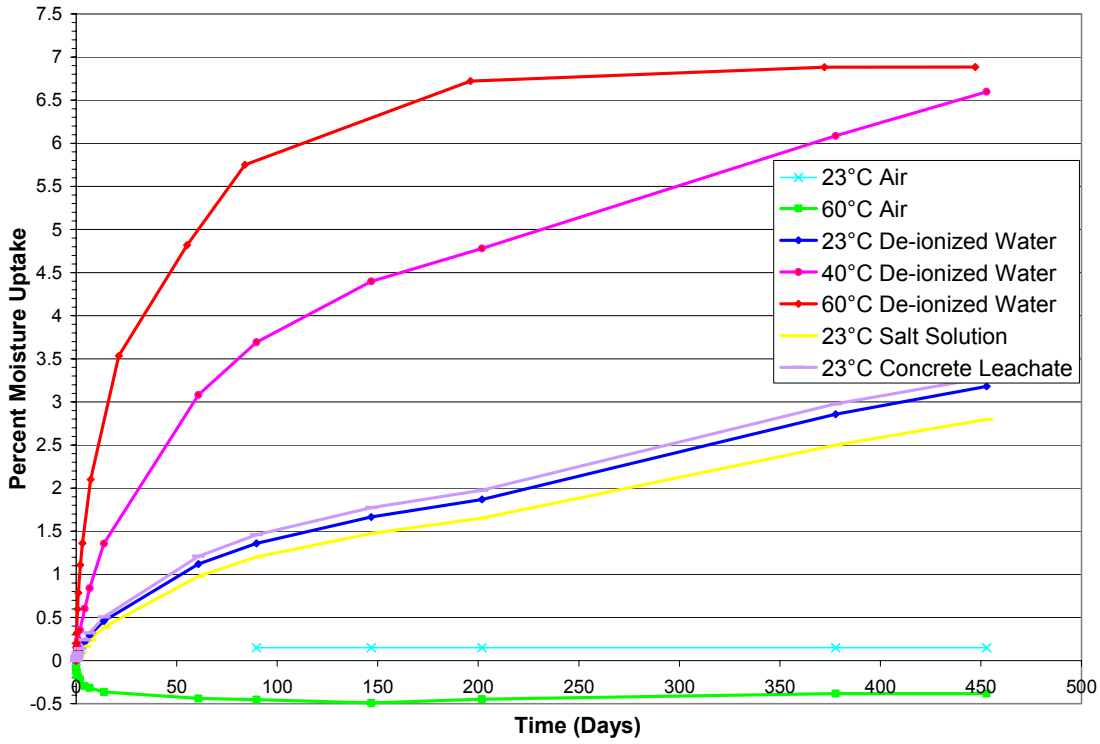

Figure 24: Typical moisture uptake results for primary test program. Each trace represents moisture uptake in a different environmental treatment. System A shown.

Figure 25 shows a plot of a Fick's Law equation curve-fit of typical moisture uptake data. From this curve fit, Fickian moisture diffusion parameters were calculated. The relevant parameters were predicted maximum moisture uptake and the diffusion coefficient. These parameters are summarized for both systems in the moisture summary table.

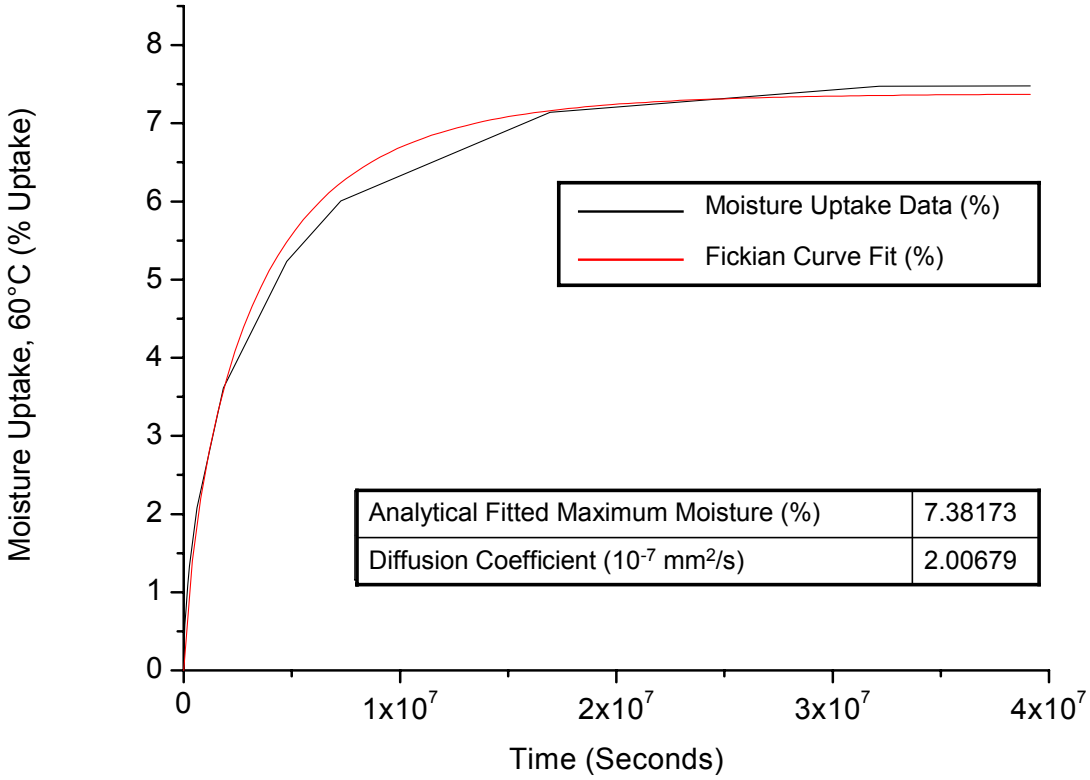

Figure 25: Typical Fickian diffusion equation curve fit to moisture uptake data. Predicted maximum moisture content, at time infinity, and Fickian diffusion coefficient are calculated. System C in 60°C environment shown.

4.3.2 Activation Energy

Figure 26 shows a plot of the natural logarithm of moisture uptake ratio, multiplied by the universal gas constant vs the inverse of absolute temperature. The slope of these two plots is equal to the activation energy for each material system. In qualitative terms the activation energy of a material system describes the amount of energy necessary for the diffusion process to occur. A higher activation energy is associated with a material system whose diffusion process is less sensitive to changes in temperature [Phani and Bose 1987].

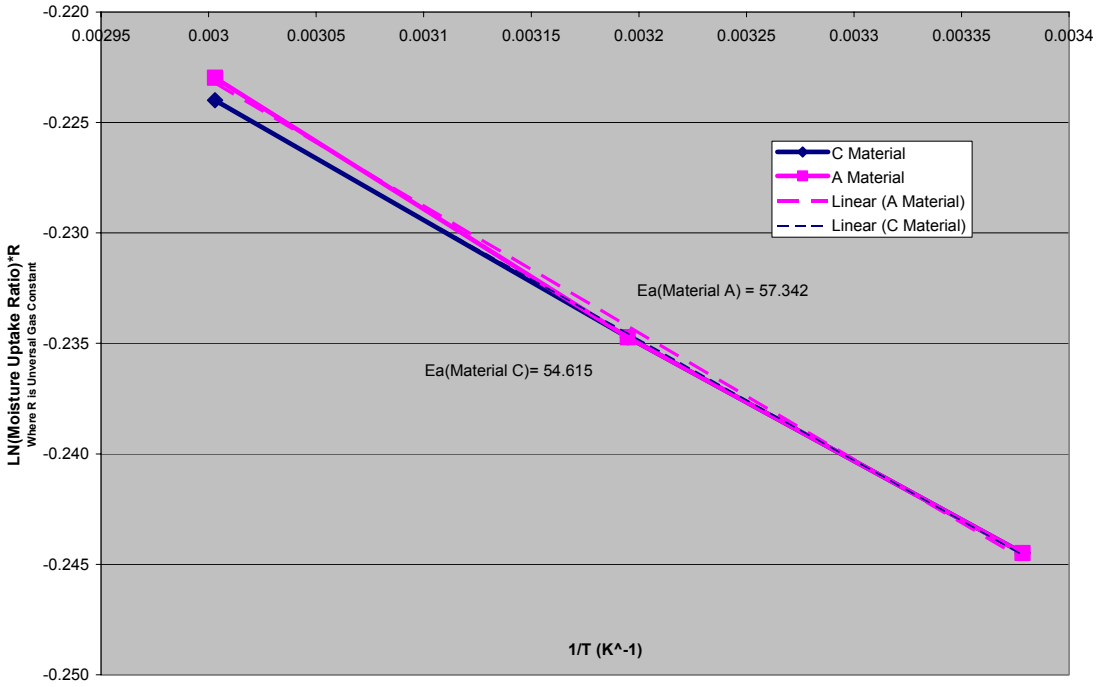

Figure 26: Typical curve fit of natural logarithm of moisture uptake ratio, normalized by the universal gas constant, with respect to inverse of absolute temperature. Curve fit of linear slope yields Activation Energy (E_a). Systems A and C shown.

Activation Energy, E_a is calculated from this relationship and the diffusion coefficients, D at a range of temperatures, by rearranging Equation 11:

$$D = D_o e^{\left(\frac{-E_a}{R \cdot T}\right)} \tag{11}$$

$$\ln\left(\frac{D}{D_o}\right) = \left(\frac{-E_a}{R \cdot T}\right) \tag{16}$$

$$\ln\left(\frac{D}{D_o}\right) \cdot R = -E_a\left(\frac{1}{T}\right) \tag{17}$$

which is in the form of a linear equation with slope, m

$$y = m \cdot x \tag{18}$$

where –Ea is m, the slope of the resulting linear equation fit of data plotted in the form of

$$\ln\left(\frac{D}{D_o}\right)\cdot R \quad vs. \quad \left(\frac{1}{T}\right) \tag{19}$$

4.3.3 Moisture Summary

Table 4 shows a summary of the moisture uptake behavior of the two material systems. From this table several important trends are displayed. The moisture uptake parameters for the three environments at ambient temperatures, 23°C de-ionized water, 23°C salt solution and 23°C concrete leachate, are quite similar, for both systems. Marked differences in diffusion coefficients can be seen for the two higher temperature environments, which is why these two environments, along with 23°C de-ionized water were used to calculate the activation energies, which are also very similar for the two material systems.

Table 4: Summary of results for moisture uptake. Systems A and C shown.

System A Plates

Environment	Moisture Uptake % at 14.5 Months	Projected Moisture Uptake %, time(∞)	Diffusion Coefficient 10^{-7} mm^2/s	Activation Energy kJ/mol
23°C De-Ionized Water	3.2	4.8	0.17	From 23°C, 40°C, and
40°C De-Ionized Water	6.6	6.9	0.55	60°C Deionized Water
60°C De-Ionized Water	6.9	6.8	2.26	57.3
23°C Salt Solution	2.8	4.2	0.17	
23°C Concrete Leachate	3.3	4.6	0.21	

System C Plates

Environment	Moisture Uptake % at 14.5 Months	Projected Moisture Uptake %, time(∞)	Diffusion Coefficient 10^{-7} mm^2/s	Activation Energy kJ/mol
23°C De-Ionized Water	4.2	6.3	0.17	From 23°C, 40°C, and
40°C De-Ionized Water	7.7	8.1	0.55	60°C Deionized Water
60°C De-Ionized Water	7.5	7.4	2.00	54.6
23°C Salt Solution	3.9	5.6	0.18	
23°C Concrete Leachate	4.4	6.2	0.21	

4.3.4 Material Tension

Figure 27 shows typical stress vs. strain plot for system in the primary testing program, showing changes in response at various times of exposure. General trends are similar to those observed during the preliminary de-selection test: ultimate tensile stress and tensile modulus decrease with increasing exposure time and with increasing exposure temperature. These results were typical for both systems, and all environments.

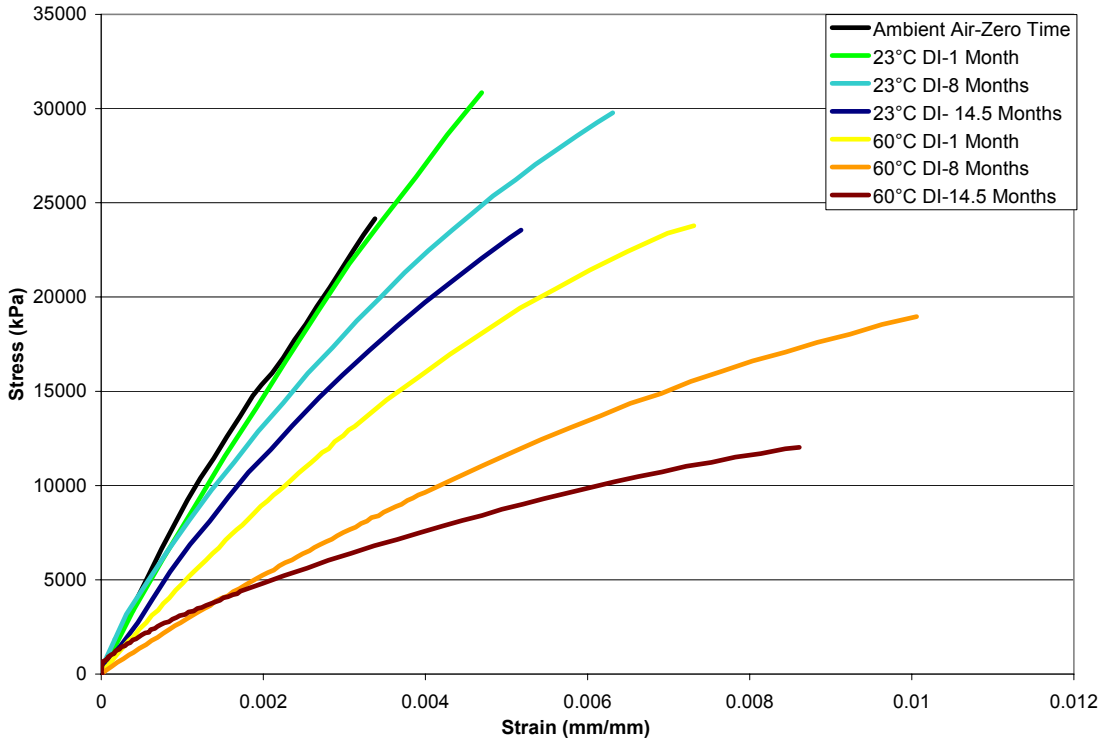

Figure 27: Typical tensile test results showing changes in epoxy material performance over exposure time. System A shown.

Figure 28 and Figure 29 show typical bar charts of retention of tensile secant modulus, after increasing exposure time in various environments, for System A and C, respectively. These charts give an idea of the level of scatter which was present in the

tensile testing, by observing the spread of tensile secant modulus values for the 23°C Air environment, since the mechanical properties of the materials should not be changing appreciable in this benign environment. No loss of tensile secant modulus is observable in the data for the 60°C air environments; the conclusion from this data is that the decline of tensile secant modulus only occurs in the immersive environments, not the hot, dry air environment.

For the three immersive environments at 23°C: de-ionized water, salt solution and concrete leachate solution, the tensile secant modulus retention trends appear similar, especially for System C. The conclusion from this data is that the important characteristics of these environments are that they are immersive, and they share a common temperature. It does not appear that the addition of ions to the immersive solution has a large impact on the retention of tensile secant modulus, so that no particular chemical vulnerability of the materials' tensile secant modulus exists to the 23°C salt solution and concrete leachate solution. Interestingly, System A seemed to maintain more of its tensile secant modulus in the 23°C salt solution and concrete leachate solution environments than in the 23°C de-ionized water environment. While this difference could be due to experimental variables, it does indicate that no vulnerability exists.

The clearest trend from these charts is the ongoing decrease in tensile secant modulus retention with increasing time and significant decrease in properties with increasing environmental temperature. The most serious decreases in property retention are for 60°C, the second largest decreases are for 40°C.

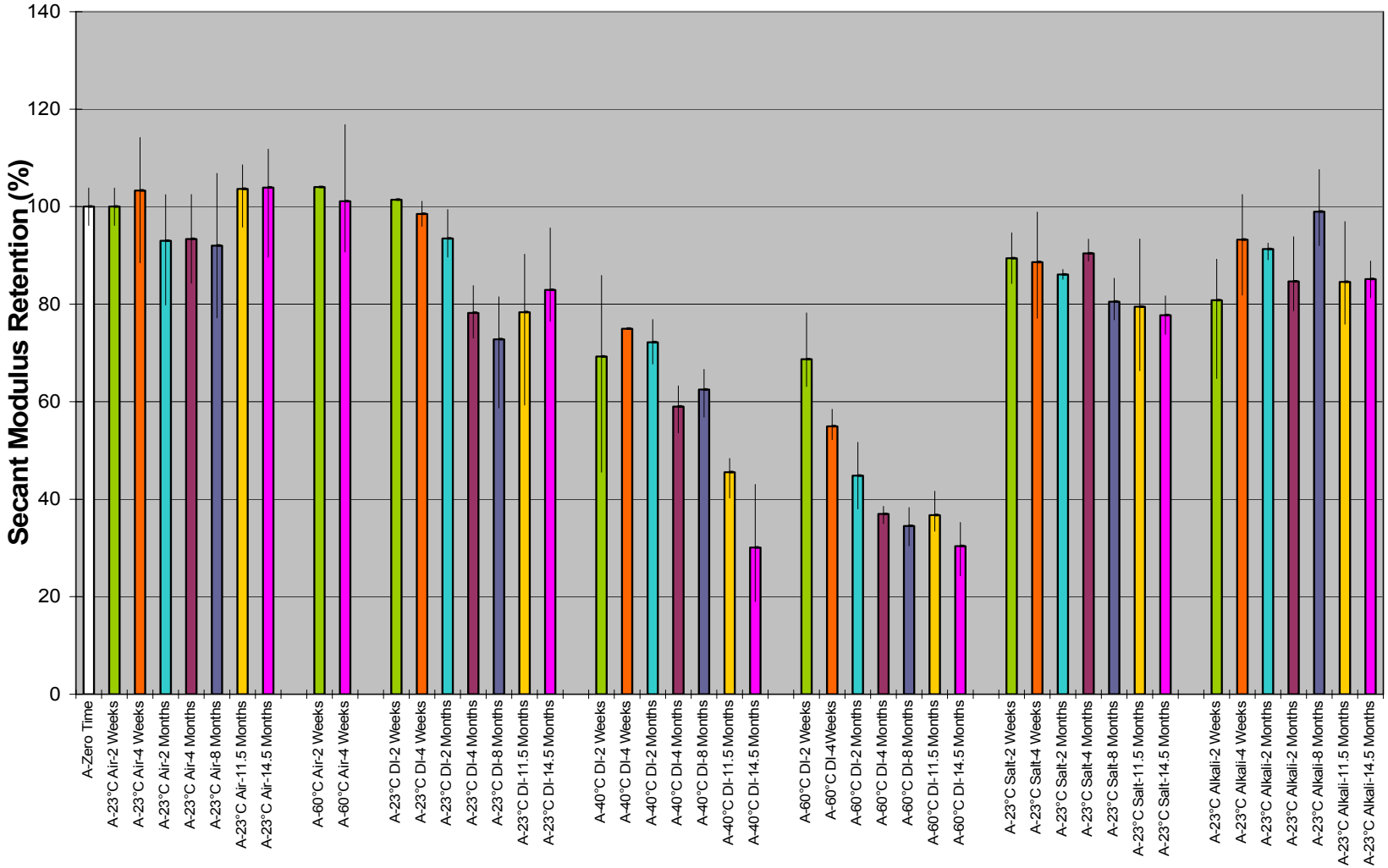

Figure 28: Typical % retention of tensile secant modulus results. System A shown. Original value of 6.8 GPa.

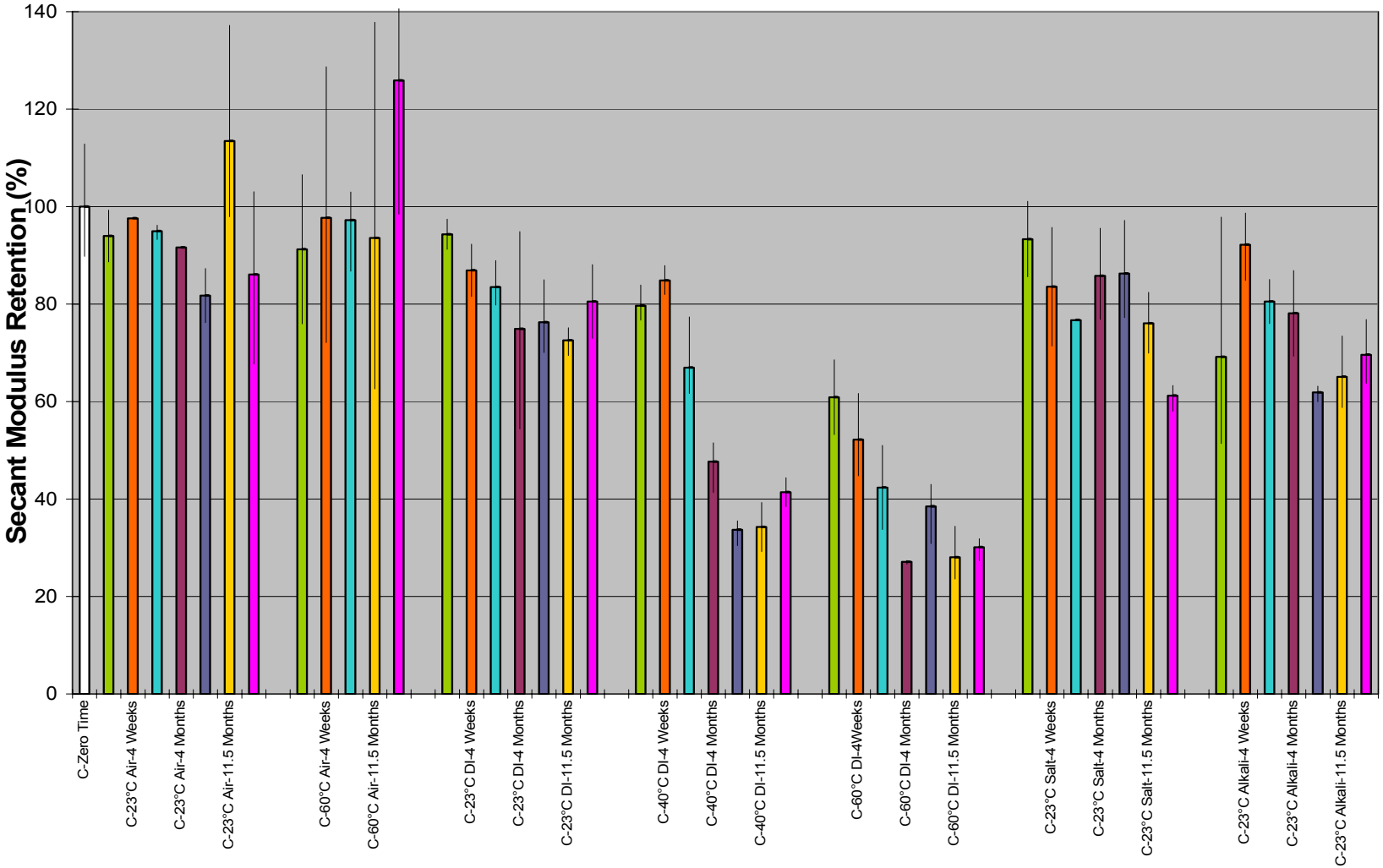

Figure 29: Typical % retention of tensile secant modulus results. System C shown. Original value of 7.1 GPa.

Table 5 summarizes the results of the tension testing for both systems and displays both actual material property values, and percent retention at 14.5 months values, for tensile secant modulus and tensile ultimate strength. The impressions from the comparison of Figure 28 and Figure 29 is corroborated by the percentage retention values for tensile secant modulus in Table 5. System A does retain significantly more of its tensile secant modulus, at 14.5 months, in the 23°C salt solution and concrete leachate solution environments. So, either System A is somehow stiffened by the ions in the 23°C salt solution and concrete leachate solution environments or System C does have a slight chemical vulnerability that does cause it to lose more of tensile secant modulus in the 23°C salt solution and concrete leachate solution environments than it does in the 23°C de-ionized water environment.

Table 5: Summary for tension test results for Systems A and C.

System A

	Elastic Modulus, GPa		Ultimate Strength, MPa	
Environment	Value at 14.5 Months	Percent Retention at 14.5 Months	Value at 14.5 Months	Percent Retention at 14.5 Months
Untreated, Original Value	7.1		31	
23°C De-ionized Water	6.3	88	26	84
40°C De-ionized Water	3.8	53	15	47
60°C De-ionized Water	3.4	47	13	41
23 Salt Solution	6.3	88	25	79
23 Concrete Leachate	6.9	97	27	85

System C

	Elastic Modulus, GPa		Ultimate Strength, MPa	
Environment	Value at 14.5 Months	Percent Retention at 14.5 Months	Value at 14.5 Months	Percent Retention at 14.5 Months
Untreated, Original Value	7.7		32	
23°C De-ionized Water	7.6	100	27	87
40°C De-ionized Water	3.8	50	12	39
60°C De-ionized Water	2.7	36	16	50
23 Salt Solution	5.1	67	25	79
23 Concrete Leachate	5.9	77	22	71

Figure 30 shows a typical plot of a material tensile parameter decreasing with the natural logarithm of time, at a range of exposure temperatures. The slope values of linear curve fits to these parameters are then plotted vs the inverse of the absolute value of temperature to produce Figure 31.

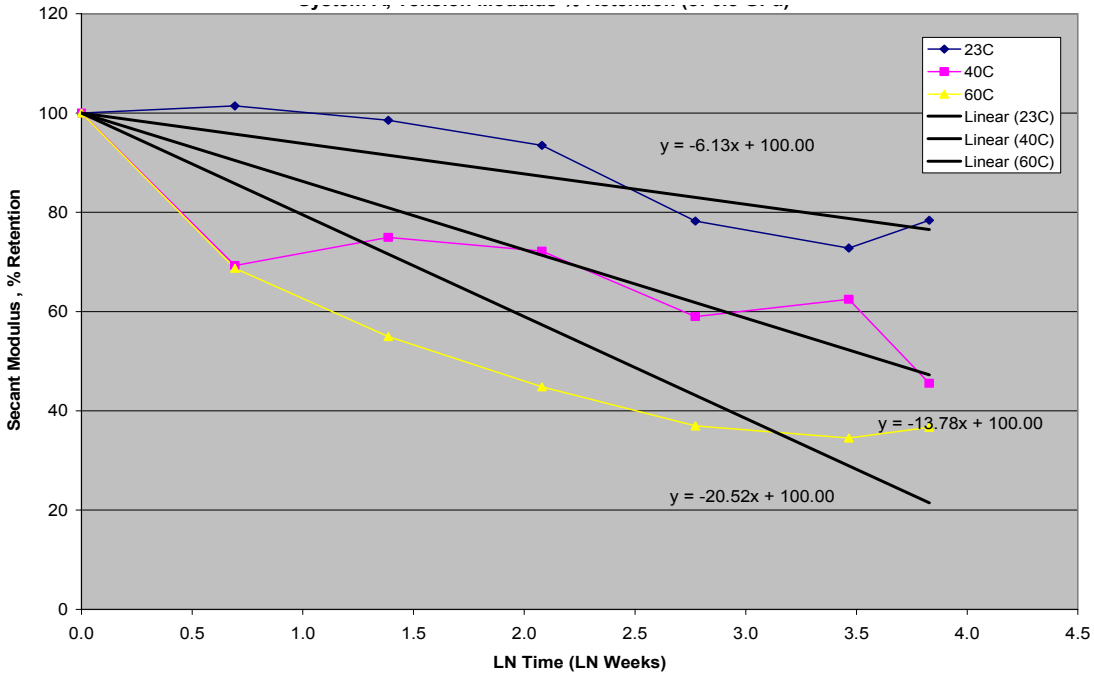

Figure 30: Percent retention of tensile modulus with respect to natural logarithm of time. Original value of 6.8 GPa. Linear curve fit yields Arrhenius degradation coefficient. System A shown.

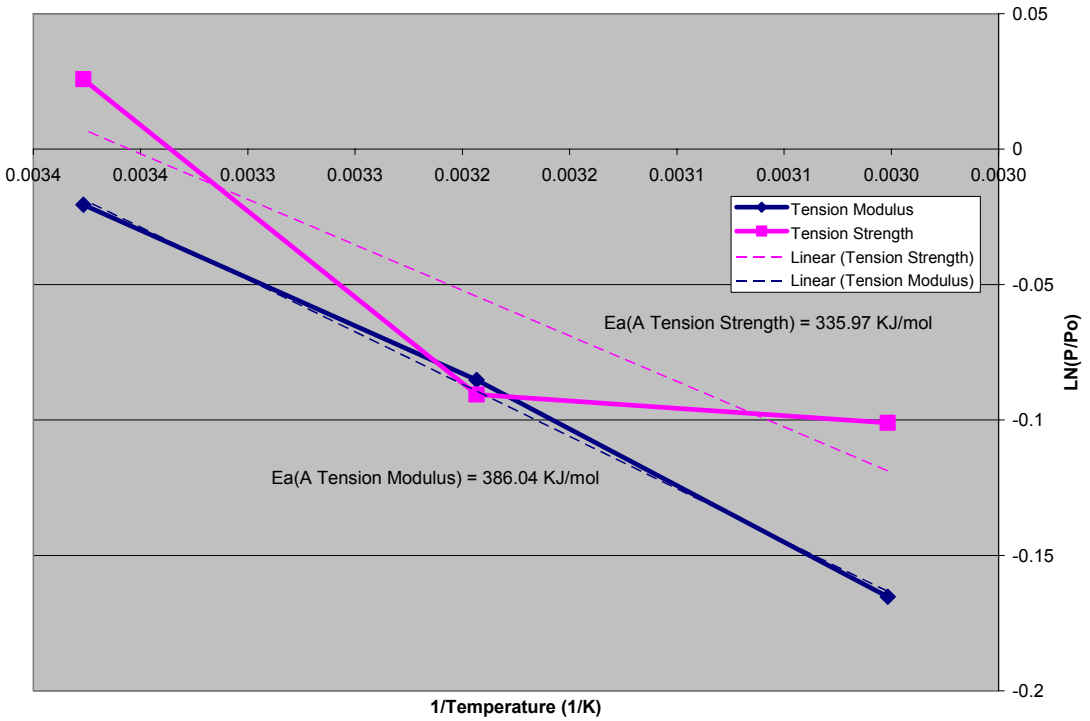

Figure 31: Typical plot of tensile Arrhenius degradation coefficients with respect to inverse of temperature. Linear curve fit yields Activation Energy (E_a). System A Shown.

The slopes taken from this typical graph are equal to the activation energy of the material for tension. This graph shows that the tensile secant modulus results from this material fit the Arrhenius assumption better than the ultimate strength results, but as mentioned previously, tensile strength results were highly sensitive to specimen imperfections and stress concentrations, such as air bubble inclusions shown in Figure 32. The resulting activation energies yielded from the linear curve fitting of these plots are summarized in Table 6.

Figure 32: Photograph of fracture surface, including air void, of tensile test specimen. Voids can contribute to variability of tensile test results.

Table 6: Summary of Activation Energies (Ea's), from tensile properties, of Systems A and C.

	System A	System C
Activation Energy, by Tension Secant Modulus	309 KJ/mol	306 KJ/mol
Activation Energy, by Tension Strength	304 KJ/mol	275 KJ/mol
Average	307 KJ/mol	291 KJ/mol

4.3.5 Material Compression

Figure 33 shows a typical compressive stress vs. strain plot for System A in the primary testing program, showing changes in response at various times of exposure. The material behavior is approximately elastic-plastic. Generally, elastic modulus, yield strength, maximum compressive strength, and strain-to-failure all decrease with increasing exposure time and temperature. However, maximum compressive strength did not decrease, with increasing temperature of exposure, in proportion to the other values. This behavior can be seen in Figure 33 as steeper, thus stiffer, post-yield behavior between the zero-time specimen and the specimens treated in 60°C de-

ionized water. This effect is likely due to some post-cure which occurs in the material at higher exposure temperatures, which offsets some of the plasticization effects of moisture uptake. These results were typical for both systems.

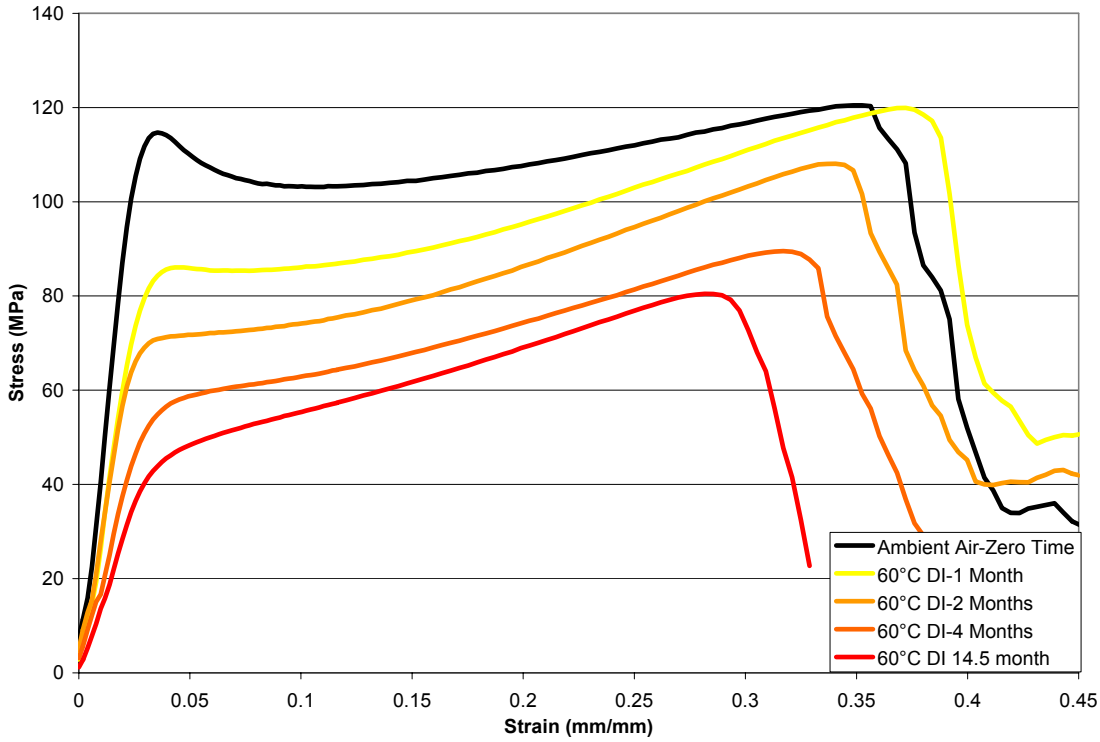

Figure 33: Typical compressive test results showing changes in epoxy material performance over exposure time. System A shown.

Figure 34 and Figure 35 show typical bar charts of retention of compressive yield strength, after increasing exposure time in various environments, for System A and C, respectively. These charts give an idea of the kind of scatter which was present in the tensile testing, by observing the spread of compressive yield strength values for the 23°C Air environment, since the mechanical properties of the materials should not be changing appreciable in this benign environment. No loss of compressive yield strength is observable in the data for the 60°C air environments, and an increase is even evident for System C. The conclusion from this data is that the decline of

compressive yield strength only occurs in the immersive environments, not the hot, dry air environment, which may actually improve the compressive yield strength of the material. The probably explanation for this improvement is that the elevated temperature, in sufficiently dry conditions, furthered the cure of (post-cured) the epoxy system.

For the three immersive environments at 23°C: de-ionized water, salt solution and concrete leachate solution, the compressive yield strength retention trends appear similar. The conclusion from this data is that the important characteristics of these environments are that they are immersive, and they share a common temperature. It does not appear that the addition of ions to the immersive solution has a large impact on the retention of compressive yield strength, so that no particular chemical vulnerability of the materials' tensile secant modulus exists to the 23°C salt solution and concrete leachate solution.

The clearest trend from these charts is the ongoing decrease in compressive yield strength retention with increasing time and significant decrease in properties with increasing environmental temperature. The most serious decreases in property retention are for 60°C, the second largest decreases are for 40°C.

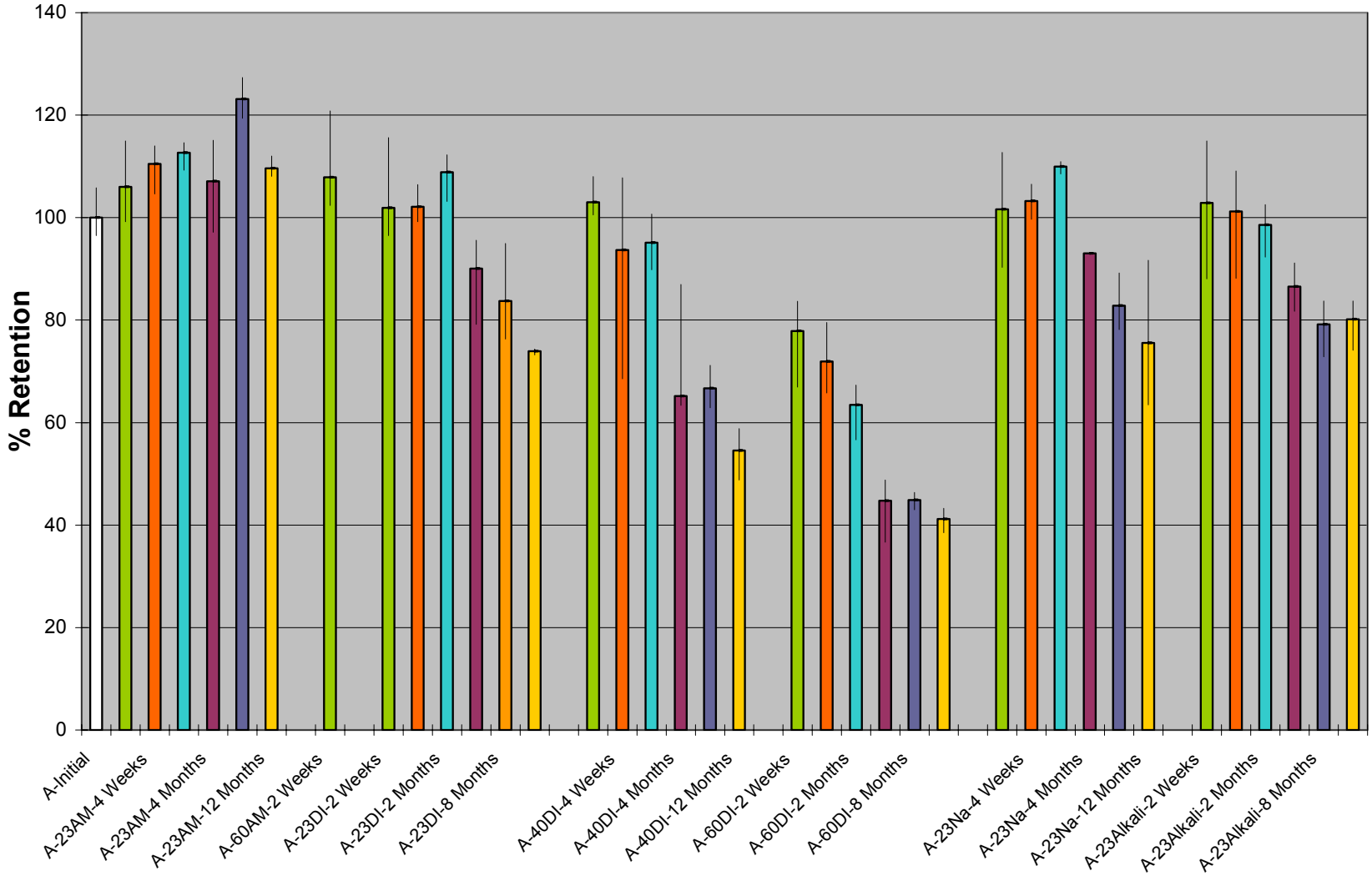

Figure 34: Typical % retention compressive yield strength results. System A shown. Original value of 77 MPa.

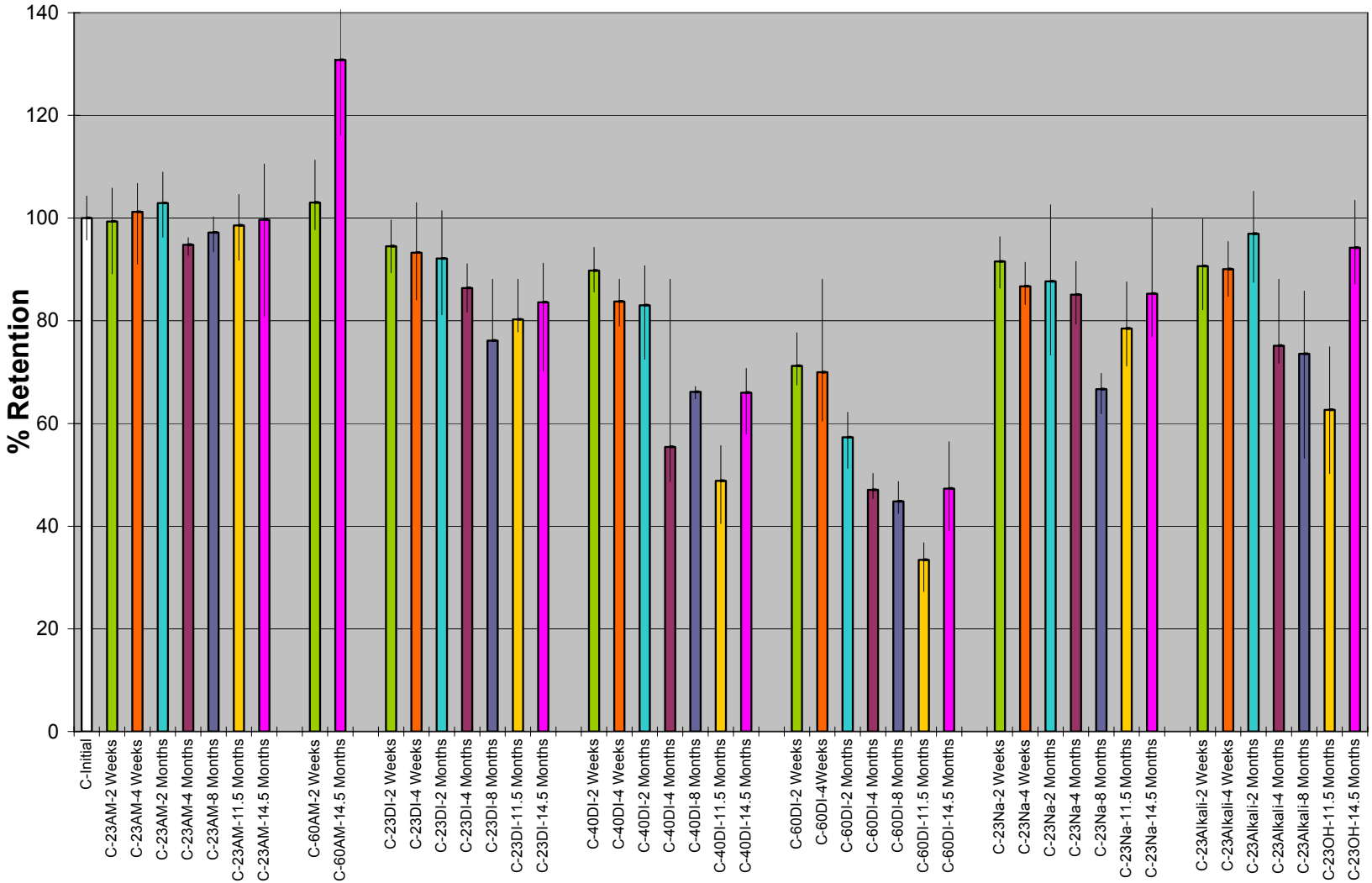

Figure 35: Typical % retention compressive yield strength results. System C shown. Original value of 85 MPa.

Table 7 summarizes the results of the compression testing for both systems and displays both actual material property values, and percent retention at 14.5 months values, for compressive elastic modulus, compressive yield strength and tensile ultimate strength. Comparing the results of Table 4 and Table 5 reveals some anomalies: System C retains more compressive yield and ultimate strength but System A retains more of its tensile secant modulus and compressive elastic modulus. The tensile ultimate strengths of the two Systems are similar. It appears that System A is stiffer than System C and that this stiffness hurts the compressive strength performance of the System. This relationship may be related to the failure mode of the compression tests; the specimens either crushed or cracked before failure, and shown in Figure 36. The higher stiffness of System A may have caused it to crack earlier.

Table 7: Summary for compression test results for Systems A and C.

System A

Environment	Elastic Modulus, GPa		Yield Strength, MPa		Maximum Strength, MPa	
	Value at 14.5 Months	Percent Retention at 14.5 Months	Value at 14.5 Months	Percent Retention at 14.5 Months	Value at 14.5 Months	Percent Retention at 14.5 Months
Untreated, Original Value	4.0		85		112	
23°C De-ionized Water	2.4	61	70	82	87	77
40°C De-ionized Water	1.7	41	43	51	72	64
60°C De-ionized Water	1.4	34	34	41	75	66
23 Salt Solution	2.3	58	69	82	88	78
23 Concrete Leachate	2.2	55	63	74	78	70

System C

Environment	Elastic Modulus, GPa		Yield Strength, MPa		Maximum Strength, MPa	
	Value at 14.5 Months	Percent Retention at 14.5 Months	Value at 14.5 Months	Percent Retention at 14.5 Months	Value at 14.5 Months	Percent Retention at 14.5 Months
Untreated, Original Value	4.2		83		121	
23°C De-ionized Water	2.2	53	70	84	112	92
40°C De-ionized Water	1.9	44	55	67	124	102
60°C De-ionized Water	0.8	20	40	48	99	82
23 Salt Solution	2.4	56	72	86	129	107
23 Concrete Leachate	2.1	50	79	95	122	101

Figure 36: Photograph of cracking and crushing failure behavior of compressive test specimen.

Figure 37 shows a typical plot of a material compressive parameter decreasing with the natural logarithm of time. Each trace corresponds to a different exposure temperature. Clearly shown in Figure 37 is the increasing slope, corresponding to increasing degradation rate, with increasing exposure temperature. The slope values of linear curve fits to these parameters are then plotted vs the inverse of the absolute value of temperature, yielding Figure 38. Each trace of the figure corresponds to a different test type, and each data point is the is the slope of an Arrhenius curve fit to a data set, of that test type, for a single exposure temperature. A linear curve fit of a trace of Figure 38 yields the Activation Energy, Ea, as calculated from the results of test results: modulus, yield strength and maximum strength. The activation energies

from Figure 38, for compressive testing of Systems A and C, are summarized in Table 8.

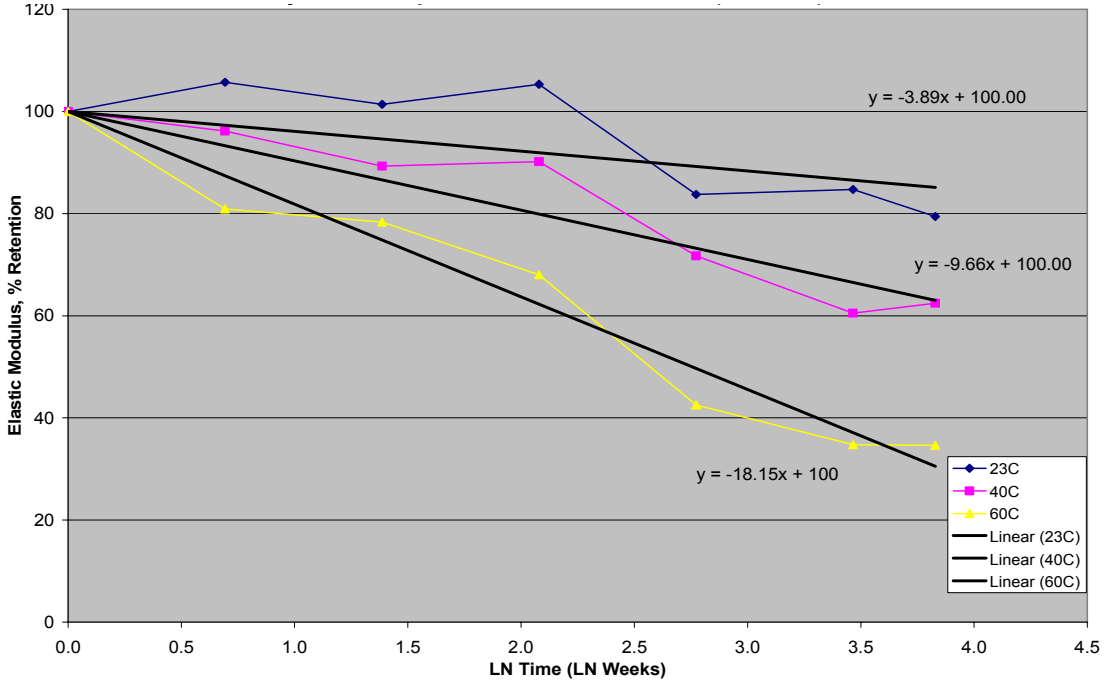

Figure 37: Percent retention of compressive modulus with respect to natural logarithm of time. Original value of 4.0 GPa. Linear curve fit yields Arrhenius degradation coefficient. System A shown.

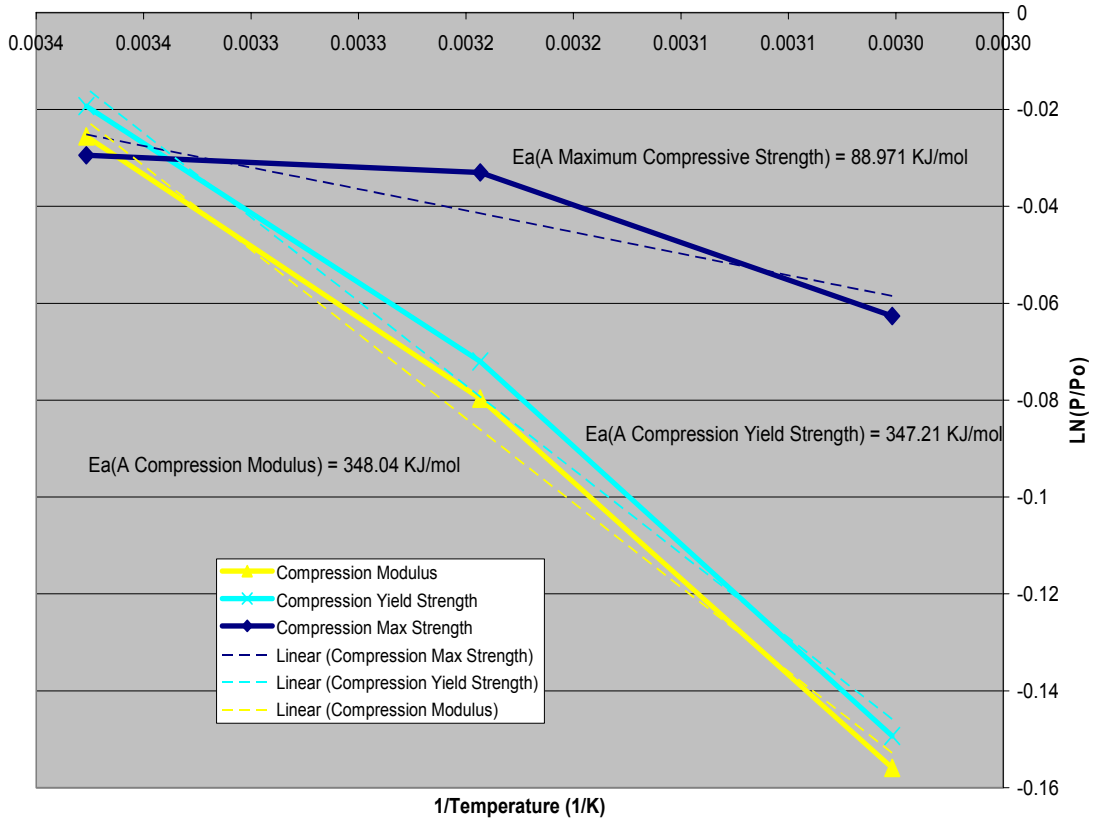

Figure 38: Typical plot of compressive Arrhenius degradation coefficients with respect to inverse of temperature. Linear curve fit yields Activation Energy (E_a). System A shown.

Table 8: Summary of Activation Energies (E_a's), from compressive properties, of Systems A and C.

	System A	System C
Ea, by Compression Modulus	348 KJ/mol	256 KJ/mol
Ea, by Compression Yield Strength	279 KJ/mol	299 KJ/mol
Ea, by Compression Maximum Strength	81 KJ/mol	82 KJ/mol
Average	236 KJ/mol	212 KJ/mol
(without Compression Max Strength) Average	314 KJ/mol	278 KJ/mol

4.3.6 Dynamic Mechanical Thermal Analysis (DMTA)

Figure 39 and Figure 40 show bar charts of the glass transition temperature, T_g, of Systems A and B, at varying times of exposure, in different environments. The two materials display very similar overall trends. One of the clear trends displayed by

these charts are that T_g increases in the 60°C air environment, presumably due to post-cure of the material. In both materials, in all three 23°C immersive environments, T_g appears to decline at a slow rate. For System A, in the 40°C de-ionized water environment, the rate of decline is higher, but the initial value is elevated above the ambiently-cured levels; so in elevated temperature immersions the initial temperature increase raised the T_g through post-cure, but then the elevated temperature and moisture lowered the T_g at a higher rate, in an instance of competing effects. Interestingly, for System A at a higher temperature, 60°C de-ionized water, environment, the initial gain due to post cure is not a high, and the subsequent decline of T_g is not as pronounced. In contrast, System C shows almost no initial gain or subsequent decline in T_g in the 40°C and 60°C de-ionized water environments.

These DMTA test results provide additional confirmation of the general stability of both Systems, A and B, when exposed to moisture. Had a precipitous drop in T_g been observed, it would have indicated that more complex, and potentially critical, degradation mechanisms were at work. Instead, rate of decline of Tg is shown to increase with increasing exposure temperature, so that the DMTA results see to match the trends observed from the simpler tensile and compressive testing. Additionally, these results show little difference between the three 23°C immersive environments, providing additional assurance that these materials have no particular chemical vulnerability to salt or concrete-leachate solutions.

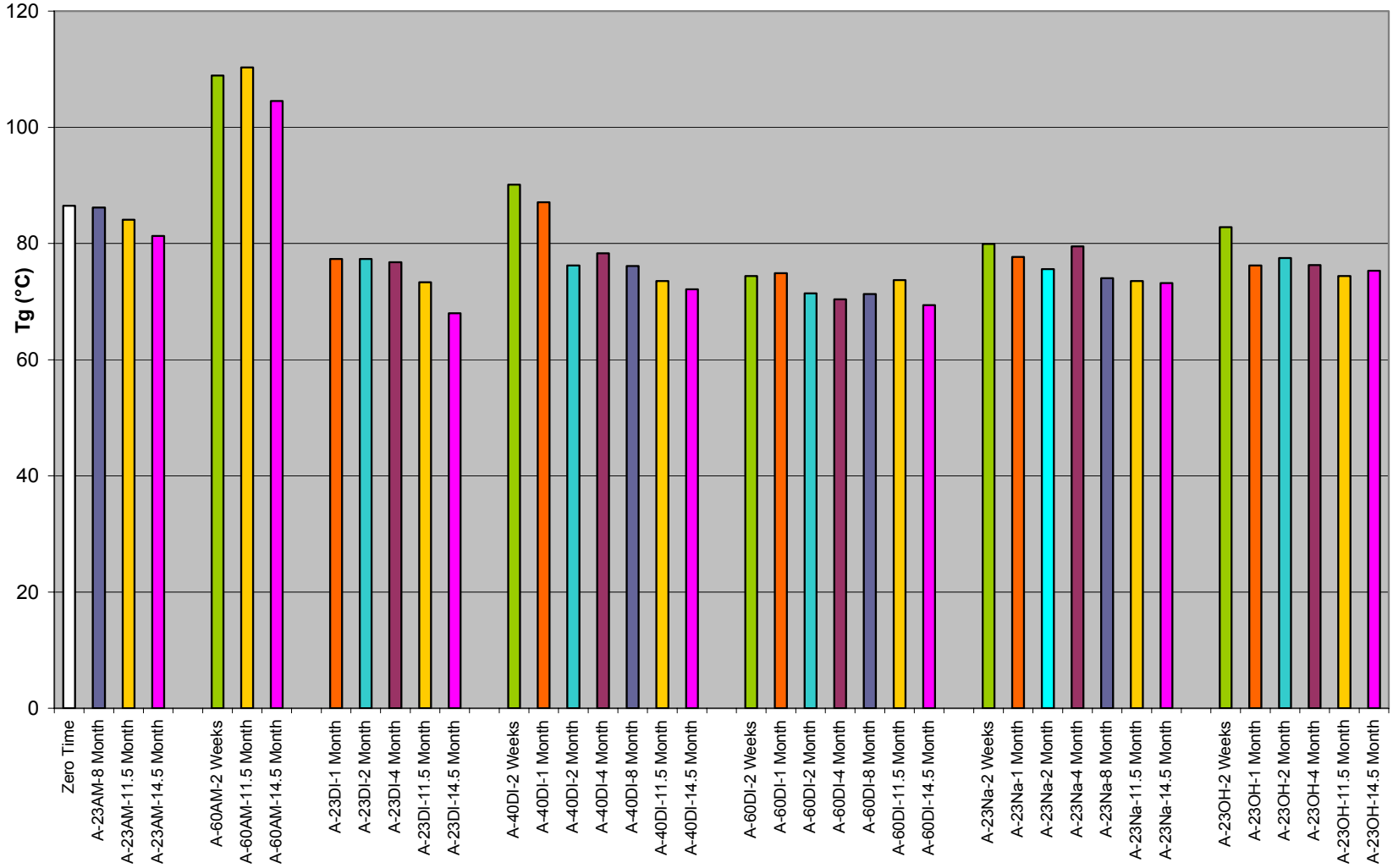

Figure 39: Glass Transition temperatures (T_g) at 1 hz, after varying time periods of different environmental conditions, System A.

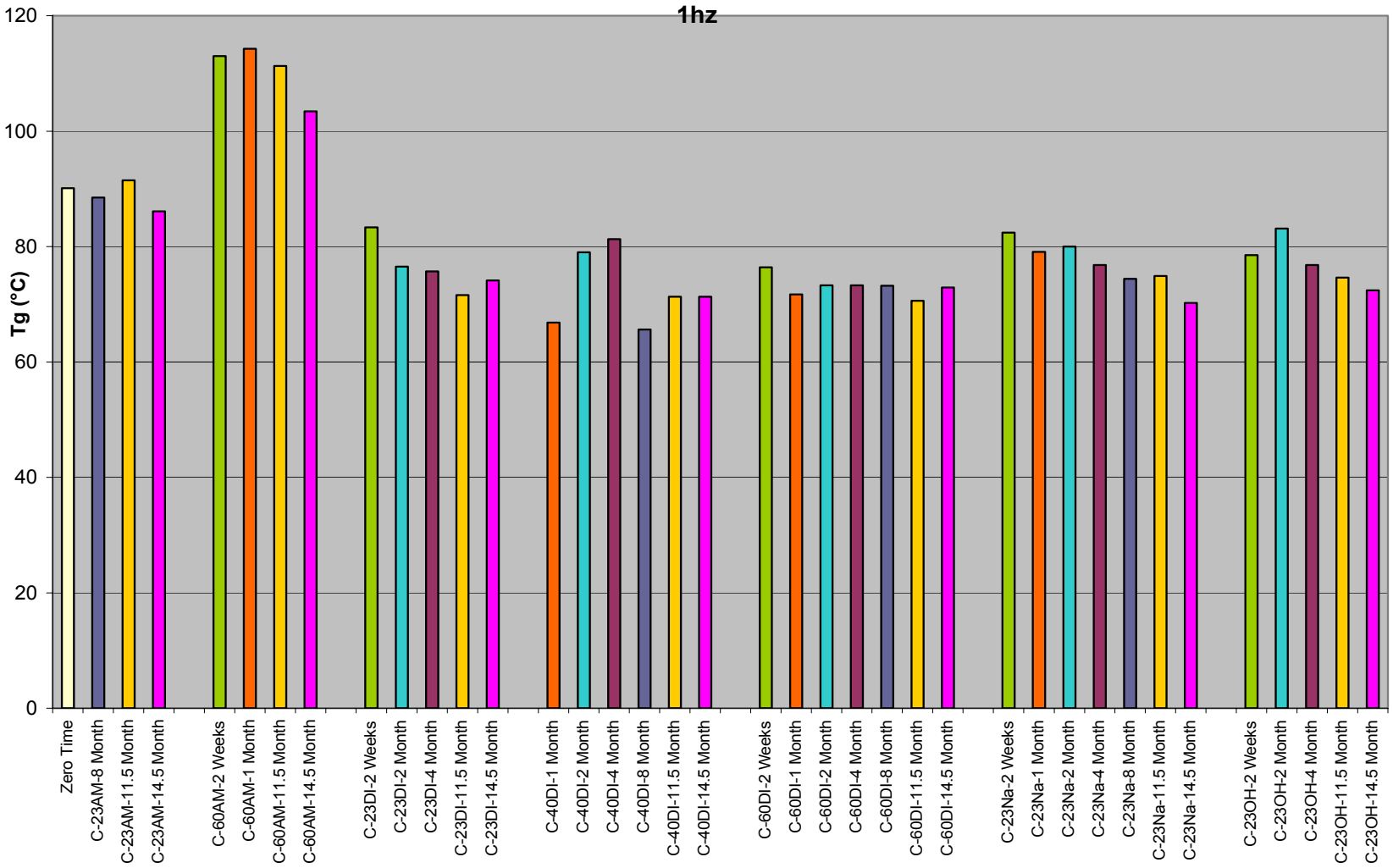

Figure 40: Glass Transition temperatures (T_g) at 1 hz, after varying time periods of different environmental conditions, System C.

4.3.7 Coupler System

All rebar-coupler tensile tests resulted in the fracture of the reinforcing bar before the failure mode of the splice was reached. Due to the consistency of these results, few valuable results were produced, since the majority of the data collected during these tests measured the tensile behavior of reinforcing bars, not the rebar-couplers themselves.

Figure 40 shows a typical set of load vs displacement plots for rebar tensile tests. These plots show that the variance in load vs displacement response of the rebar overshadows any changes of the rebar coupler system due to environmental ageing of the epoxy. The load vs displacement traces for three identical rebar couplers, which were assembled and stored in 23°C air conditions, are shown in Figure 33. Together these three traces give an indication of an envelope of rebar-coupler system behavior. This envelope is due to the variation in performance of the reinforcing bars.

The load vs displacement traces of several rebar-coupler specimens, which underwent a variety of treatments prior to testing, are also plotted in Figure 40. One of the specimens was tested after 11.5 months of treatment in the 60°C de-ionized water environment. Another was preloaded to half of the rebar yield stress, to potentially introduce cracking or seating movement in the bulk of epoxy in the coupler, and then treated for 14.5 months in the 60°C de-ionized water environment. A third coupler was fatigue-tested, as per California Test 670, and then tensile-tested to failure. Although these rebar-couplers were pretreated and environmentally treated in a variety of ways prior to tensile testing, their results still fall within the envelope for 23°C air conditioned rebar-couplers.

The most salient observable trend from Figure 41 is the difference, in load vs displacement response of a bare rebar, in comparison to the rebar couplers. The bare rebar had an identical gauge length as the coupler specimens, and the higher overall extension of the bare rebar indicates that the coupler is behaving stiffer than the equivalent length of bare rebar. This stiffness is not surprising since the rebar coupler sleeve does not yield, in tension, along its length as the rebar does. Although the relative stiffness of a rebar coupler, compared to a bare rebar, may have significance to the design of reinforced concrete structures, it does not give any indication of the vulnerability of the epoxy-bonded rebar-coupler system to moisture-based degradation of its epoxy.

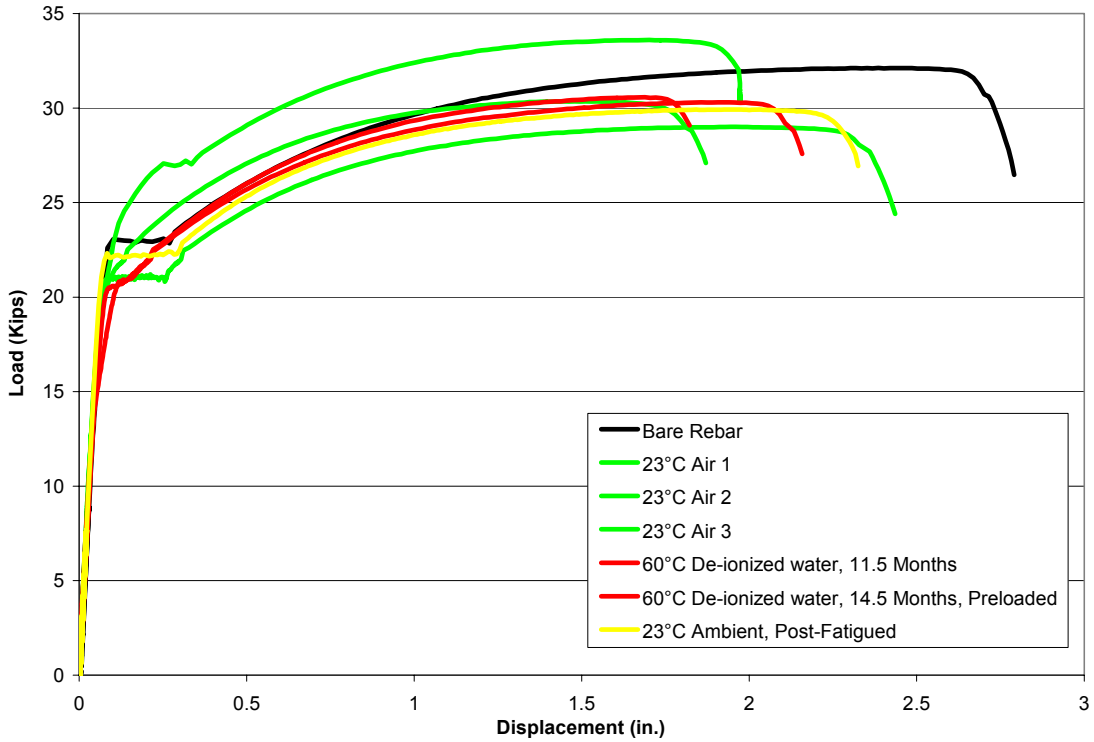

Figure 41: Typical rebar-coupler system, and bare rebar, tensile test results of load, with respect to crosshead displacement. System C shown.

4.3.7.1 Slip Tests

Figure 42 shows a bar chart of slip measurements of rebar coupler tensile tests after varying times and environmental exposures. No clear trends are visible which could explain the variation of results. The slip of the rebar-coupler does not appear to be linked to exposure environment or length of exposure. Instead, the system appears to have an inherent variability of slip performance, and any changes due to environmental exposure are small enough that they are indistinguishable when measured in this way.

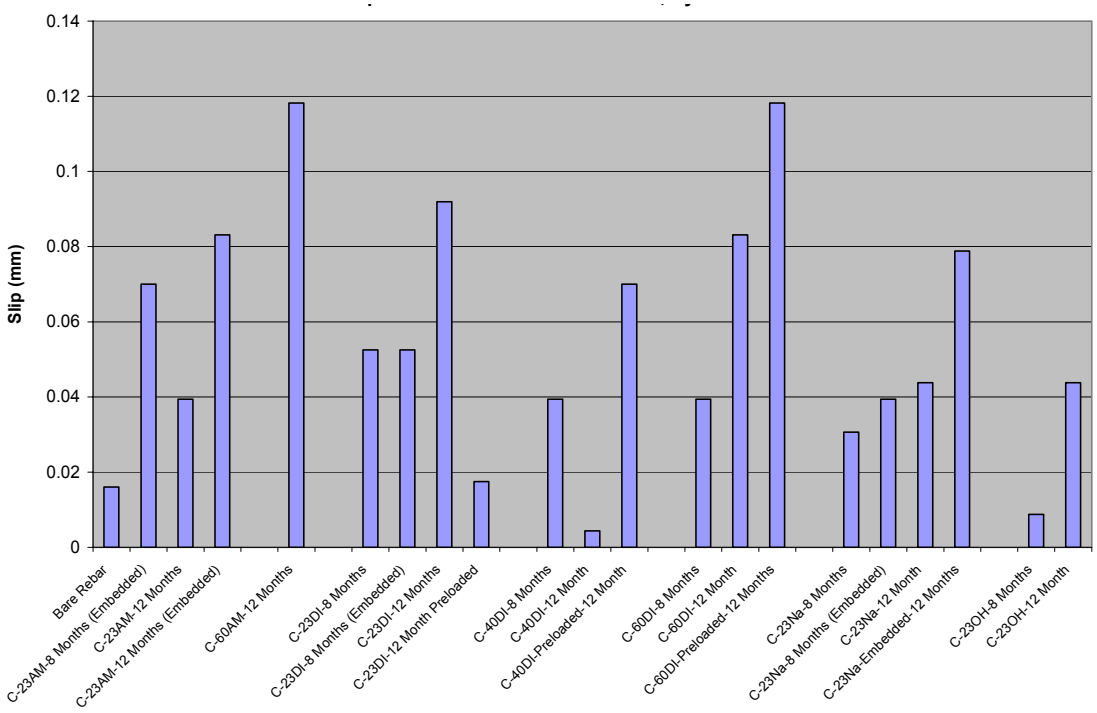

Figure 42: Typical rebar-coupler system, and bare rebar, tensile test results of slip, across coupler length. System C shown.

4.3.7.2 Cyclical Tests

All specimens passed the cyclical test regime, and subsequently developed rebar ultimate strength and produced rebar fracture in a standard tensile test. The

results of this testing program indicated that epoxy-bonded rebar-couplers have no unusual vulnerability to cyclical loading.

4.3.7.3 Fatigue Tests

All specimens passed the fatigue test regime, and subsequently developed rebar ultimate strength and produced rebar fracture in a standard tensile test.

To examine the rebar coupler's vulnerability to fatigue, above and beyond the requirements of California Test 670, specimens were fatigue-tested to failure. All specimens survived 23,200+ cycles of the higher, cyclical testing level load, and fractured at the welded base of the coupler sleeve. A photograph of a fatigue-fracture is shown in Figure 43.

Figure 43: Photograph of an epoxy-bonded rebar-coupler, assembled with System C, which has been fatigue tested to failure. The fatigue-fracture occurred at the location of the factory rebar-to-sleeve weld at the closed end of the coupler, not adjacent to the epoxy-system.

The results of this testing program indicated that epoxy-bonded rebar-couplers have no unusual vulnerability to fatigue loading. These results are expected, since the couplers do not rely on threads, or other small features, which create stress concentrations. The development-length transfer mechanism of the system is effect at smoothly transferring forces across a long length, avoiding concentrations. Although

the weld of the coupler was produced in a factory environment, which generally leads to a more consistent and reproducible weld than would be created in a field environment, it still proved more vulnerable to fatigue than coupler connection through the epoxy system.

4.3.7.4 Elevated Temperature Tests

4.4 Modified Rebar Couplers

Few useful results were generated from the rebar-coupler test program, because the controlling structural element of the rebar-coupler system was always the rebar itself. In an effort to gain insight into the other potential failure modes of the rebar-coupler system a series of tests was undertaken to intentionally change the failure-mode of the system and observe system behavior.

4.4.1 Thin Walled

Figure 44 and Figure 45 show the coupler specimen, which was fabricated with proportionally thinner sleeve wall thickness, tested to failure in tension. The sleeve walls near the mouth of the coupler have yielded and dilated outwards, in the radial direction. This dilation indicates a strong expansive stress from the epoxy in this region. Figure 44 does show some possible fracture surfaces in the bulk of epoxy near the dilated region, which would seem to corroborate with this indication. Also, as can be seen on the right side of Figure 45, a gap has opened between the end of the rebar, and the epoxy attached to it, and the bottom of the coupler cavity. This gap

indicates either significant yielding of the coupler sleeve in the axial direction, or a movement of the rebar, and with it the surrounding epoxy, towards the mouth of the coupler. This later explanation is corroborated by the expansion of the coupler cavity near the mouth of the coupler, where the thickness of the epoxy layer can be seen to be larger than its original dimension. If additional epoxy accumulated near the mouth of the coupler, the movement of the epoxy, and with it the rebar, at the bottom of the coupler is explained.

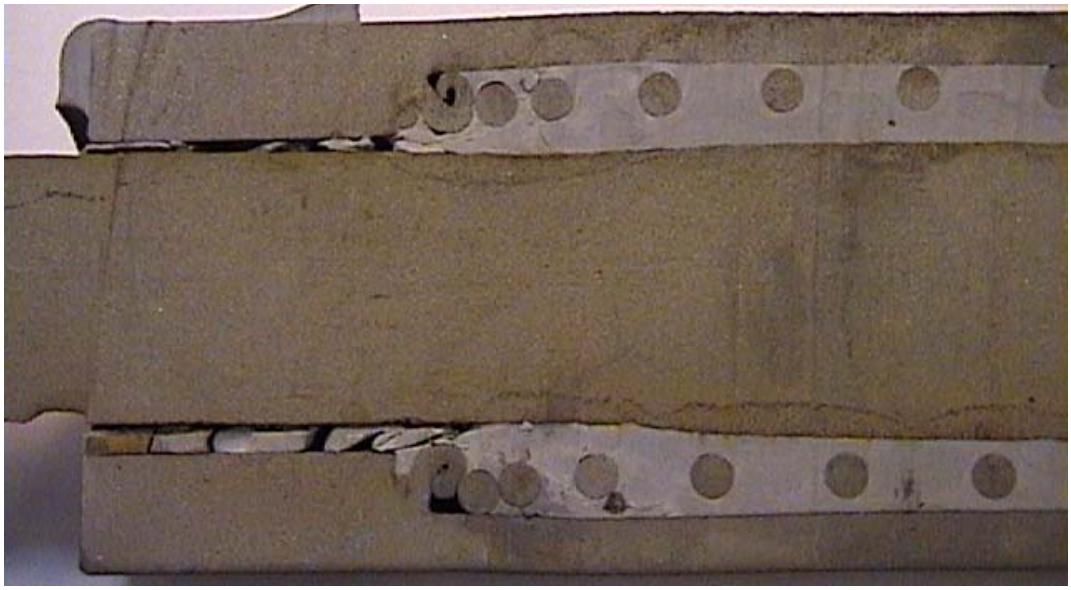

Figure 44: Photograph of a modified epoxy-bonded rebar-coupler, assembled with System C, which has been tested to failure. The thinner walls of this coupler yielded outward and created a permanent, visible bulge.

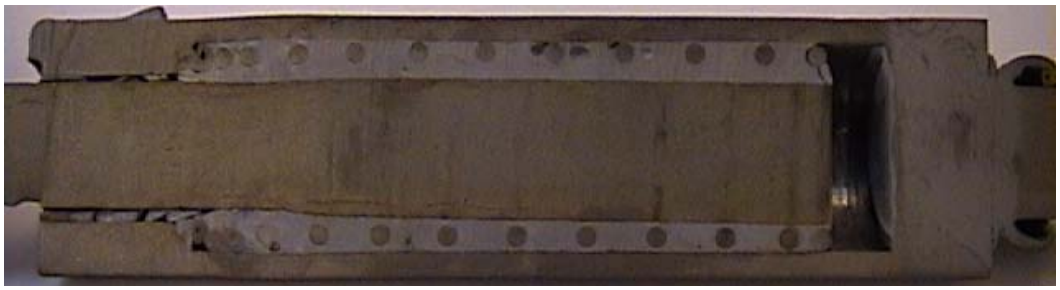

Figure 45: Photograph of a modified epoxy-bonded rebar-coupler, assembled with System C, which has been tested to failure. The thinner walls of this coupler yielded outward and created a permanent, visible bulge. Also, the bulk of epoxy, and embedded rebar, moved visibly towards the mouth of the coupler.

4.4.2 No Choked Mouth

Figure 46 shows the failed specimen which was constructed without a choked mouth. Testing on the no-choked-mouth coupler specimen was performed May 29th, 2007 by Christian Dahl, at HRC Facility. Rebar and block of epoxy pulled out of coupler at approximately 10% of ultimate load: 9 kN. These results indicate that the adhesive bond between the epoxy and the inside of the coupler sleeve is inadequate to transfer ultimate rebar loads. Therefore, the existence of the chocked mouth of the rebar coupler is necessary to develop force transfer from the epoxy to the coupler sleeve.

Figure 46: Photograph of a modified epoxy-bonded rebar-coupler, assembled with System C, which has been tested to failure. The lack of a choked-mouth on this coupler allowed the bulk of epoxy and embedded rebar to pull out of the coupler intact.

4.4.3 No Choked Mouth, Ribbed Inner Sleeve Wall

The test of the rebar coupler specimen without a chocked entrance, with a ribbed insider sleeve surface was performed May 29th, 2007 by Christian Dahl, at HRC Facility. This coupler was able to transfer load between the epoxy and the inside of the sleeve and rebar fracture was attained. The stark contrast between the results of this coupler specimen test and a similar specimen, without the sleeve ribbing, suggests that mechanical interlock between the epoxy and the ribbed sleeve is, and adhesive bond to a smooth sleeve is not, sufficient to transfer rebar ultimate forces. The epoxy material appears to be more effective, in this mechanical system, as a compressive

grout than as an adhesive. Figure 47 shows a cross-section of the coupler, Figure 48 is a detail of the base of the coupler, and Figure 49 is a detail of the entrance of the coupler.

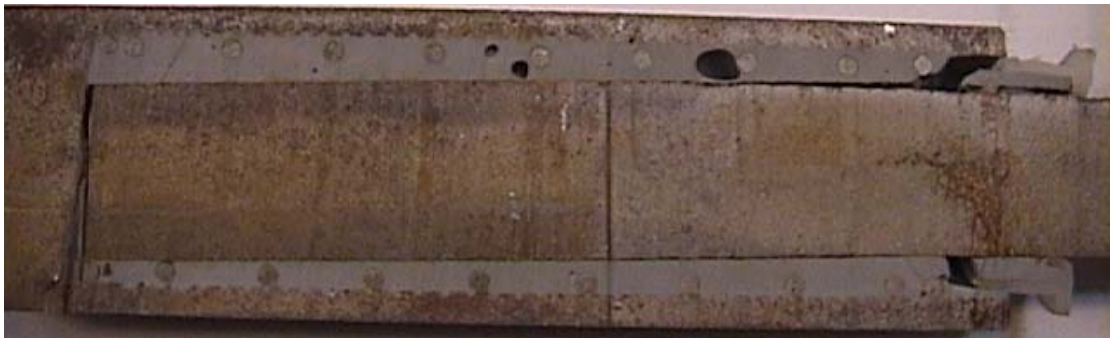

Figure 47: Photograph of a modified epoxy-bonded rebar-coupler, assembled with System C, which has been tested to failure. Some displacement at the entrance of the coupler is evinced by the movement of the plastic alignment cap. However, the movement of the embedded rebar at the back of the coupler is orders of magnitude less than that shown by the thin-walled coupler.

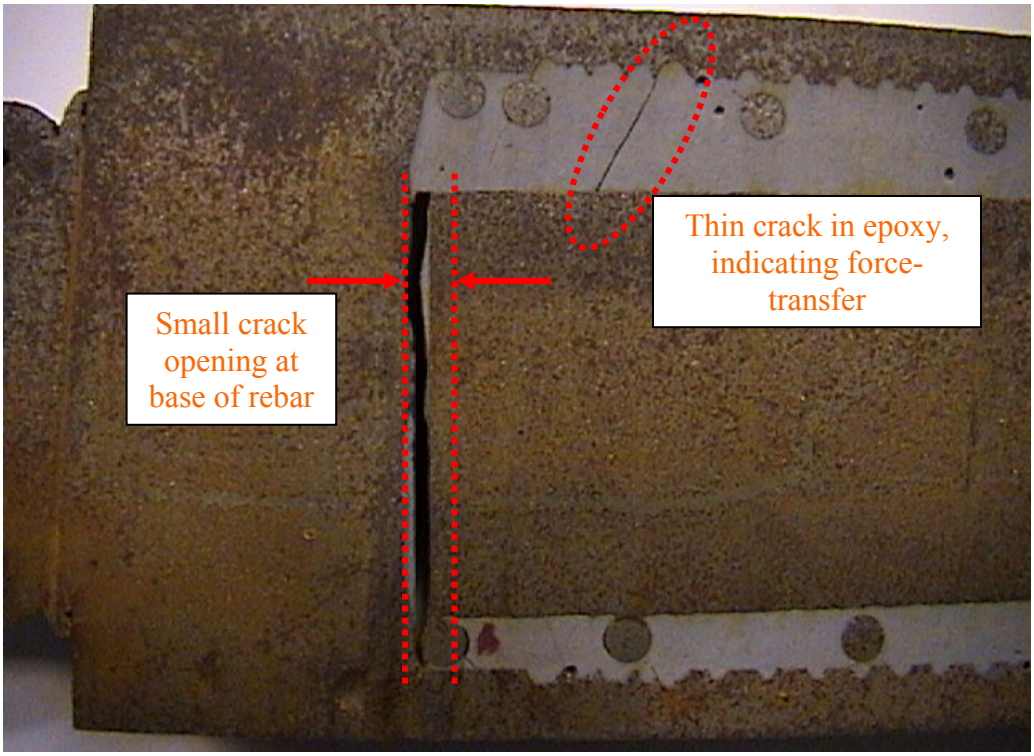

Figure 48: Photograph of a modified epoxy-bonded rebar-coupler, assembled with System C, which has been tested to failure. A small crack opening is visible at the base of the embedded rebar. Another, thinner crack is visible in the upper cross

section of epoxy in this photograph. The direction of this crack is consistent with the expected direction of tensile forces in the material due to shear loading between the embedded rebar and threaded sleeve.

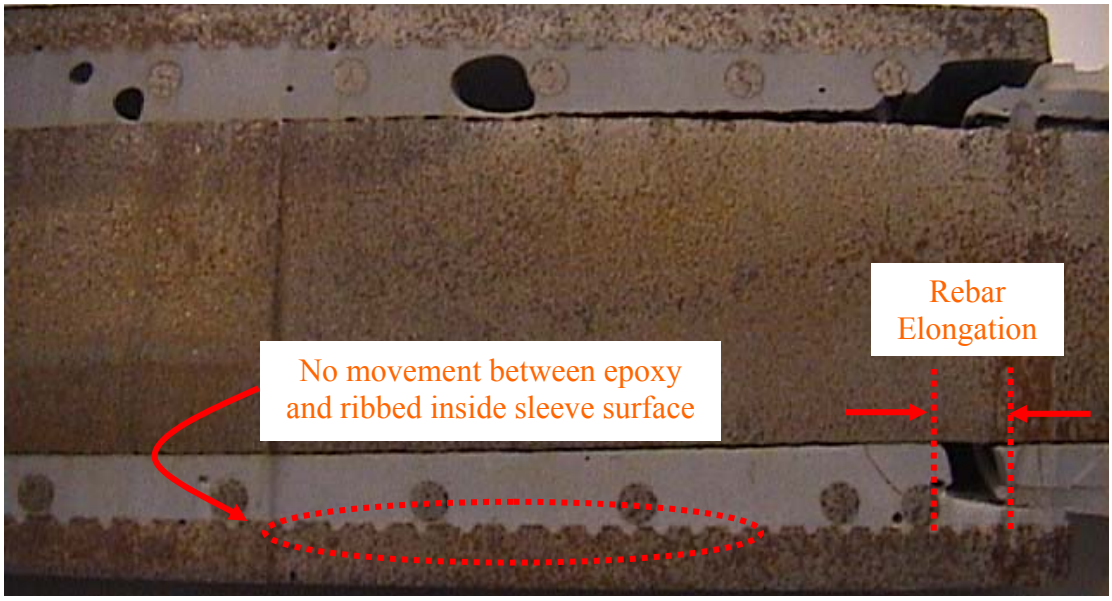

Figure 49: Photograph of a modified epoxy-bonded rebar-coupler, assembled with System C, which has been tested to failure. Elongation of the rebar is visible near the entrance of the coupler.

4.4.4 Non-Optimal Epoxy System

To examine the failure mechanisms which would occur if the epoxy weakened, due to moisture uptake, a coupler was assembled using a less-optimal epoxy system. The system used was System F from the Preliminary De-Selection test. The coupler was loaded to failure and even the less-optimal epoxy system was sufficient to bring the rebar to the point of incipient fracture. However, with the load held at that level, the rebar slowly pulled out of the epoxy. Figures 50, 51 and 52 show cross-sections of both couplers after testing.

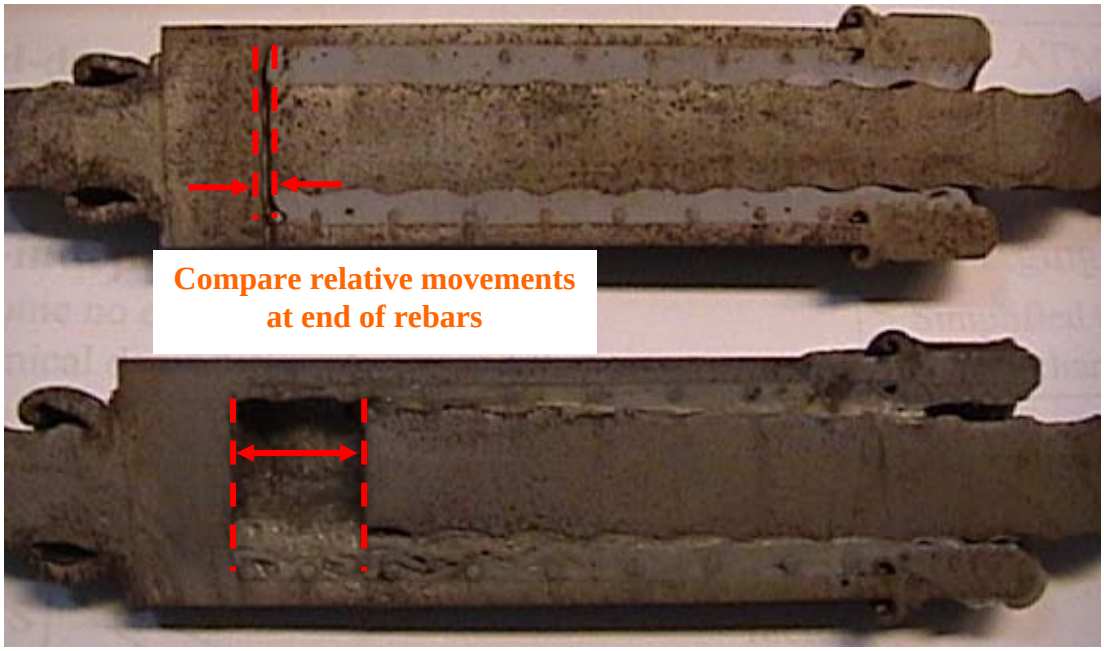

Figure 50: Photograph comparing a standard epoxy-bonded rebar coupler, assembled with System C(top), to one assembled with a non-optimal epoxy system(bottom); both have been tested to failure. The embedded rebar pulled a significant distance out of the non-optimal epoxy.

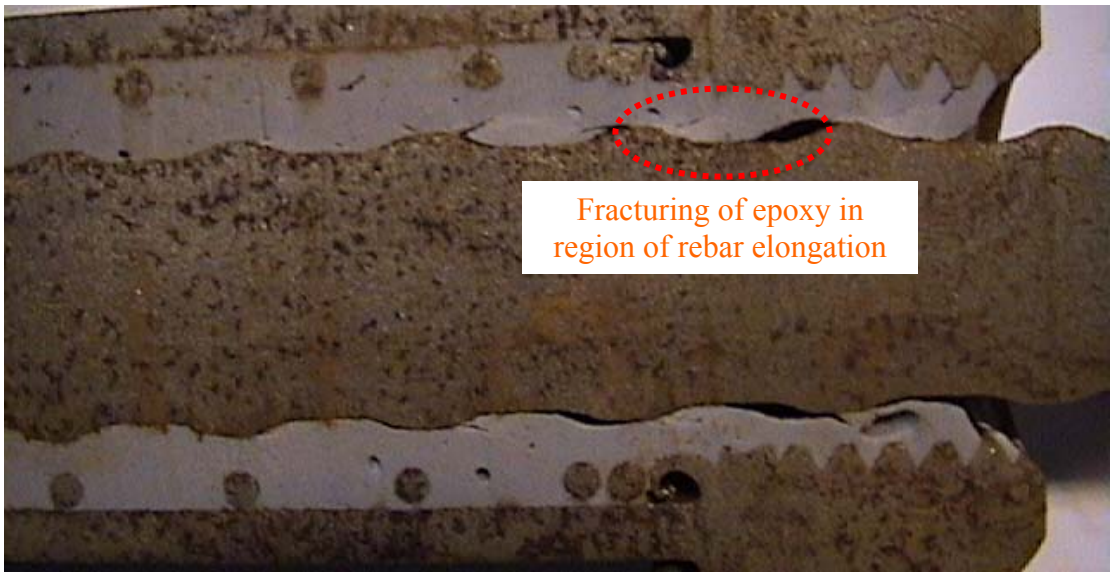

Figure 51: Photograph showing a standard epoxy-bonded rebar coupler, assembled with System C, tested to failure.

Figure 52: Photograph showing an epoxy-bonded rebar coupler, assembled with a non-optimal epoxy system, tested to failure.

Comparing Figure 51 to Figure 52 reveals important differences between normal coupler behavior and the behavior of a coupler assembled with a non-optimal epoxy system. The comparison also gives potential insight into what a failure of the normal coupler system, due to extreme degradation of its epoxy system, might look like. Figure 50 shows that the rebar has elongated and necked near the coupler entrance and cracking is evident in the bulk of epoxy, but no striations suggesting movement planes are visible. In Figure 52 fracture and movement planes are visible in the bulk of epoxy, at the outer edges of the embedded rebar deformations. These failure planes appear as striations and were the location of movement which allowed the embedded rebar to measurably pull out of the coupler, when tested. The locations of the intra-epoxy fracture surfaces, along the outside edges of the rebar deformations, indicates where failure can be expected when the epoxy becomes the weak link in the structural system.

4.5 Destructive Testing of Moisture Sleeves

Moisture content, as determined by gravimetric drying tests, for System C material, in the coupler geometry, was measured to be 4.5%. Although lower than the maximum predicted moisture content, at time infinity, from the moisture uptake modeling, this result does confirm that the confining geometry of the coupler does not prevent significant moisture uptake.

4.6 Creep Testing

Figure 53 shows the creep test data, and associated curve fits, for both Systems. Data was recorded for 42 days and fitted to Equation 20.

$$y = c \cdot \ln(x) + b \tag{20}$$

Where y is displacement, and c and b are constants. The resulting curves were extrapolated to a time of 600 days, as per ASTM E 1512. The extrapolated creep displacements at 600 days are 0.75mm and 3.3mm, for Systems C and F, respectively. ASTM E 1512 recommends comparing creep displacement to ultimate displacement during a tensile test; However, AC 58 is more explicit in its creep displacement limits. AC 58 specifies displacement, at 600 days, to be below the lesser of displacement at ultimate load, or 3mm. Taking 3mm as the limit, we can see that System C meets the requirements of AC58, but that System F does not. These results provide another example of the large disparities in long-term performance of different ASTM C 881 systems. Figure 54 shows a comparison of the permanent, post-creep-test, displacement at the entrances of the rebar-couplers with each system.

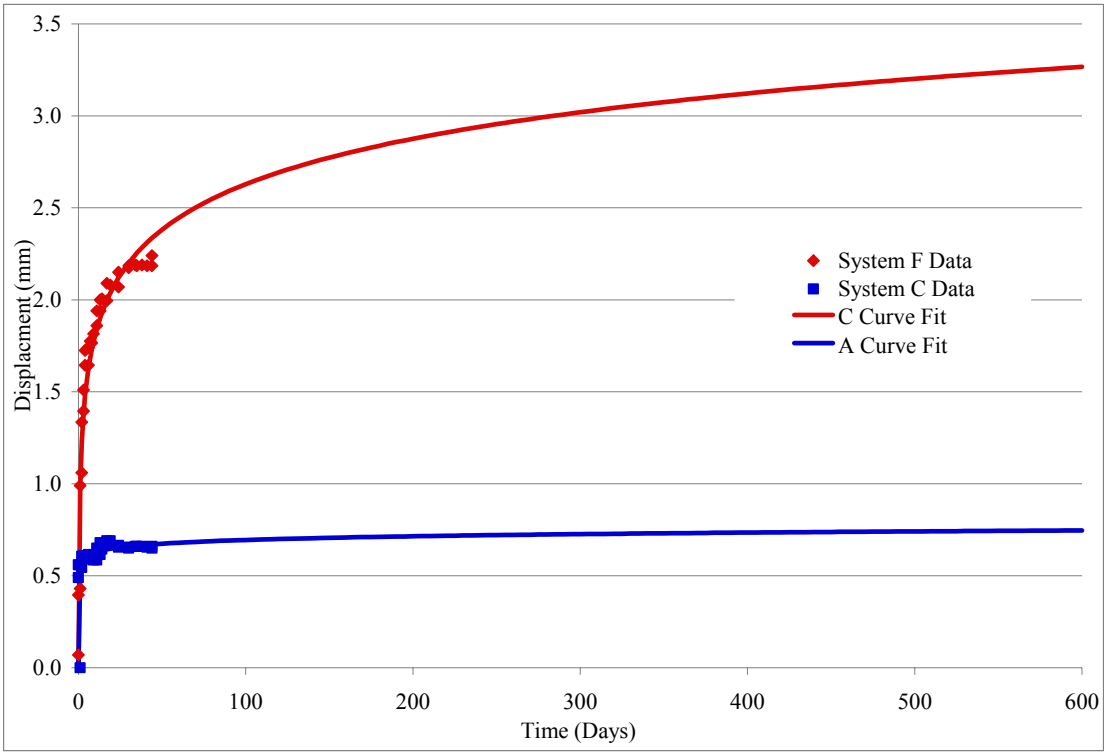

Figure 53: Figure of Creep Testing Results Summary

These creep test results are significantly higher than those found for a similar type of rebar-coupler, evaluated in a similar way. Cementitious-grouted rebar-couplers were found to have creep displacements, extrapolated to 600 days, of around 0.75mm [Jansson, 2008]. So the results for System C indicate that epoxy-bonded rebar-couplers, if used with a well-suited epoxy system, do not have any significant vulnerability to excessive creep displacement, compared to other types of rebar-couplers.

Figure 54: Photograph comparing permanent creep displacements, System C on the left, System F on the right.

5 Analysis

A FEA model was developed to simulate the failure of an epoxy-bonded rebar-coupler. The model combines the epoxy system material properties from the test program with the phenomenological coupler testing, as well as the moisture-based degradation models to predict long-term behavior.

5.1 Finite Element Analysis (FEA)

The model, in its basic form, simulates an epoxy-bonded rebar-coupler tensile test. The model accurately predicts the behavior of the system, which fails by rebar fracture in its untreated state. By changing the properties of all the epoxy from untreated to heavily treated values, the failure mechanism changed from rebar fracture to epoxy pull-out. The epoxy material property values used for this trial were 14.5 month values from the 60°C de-ionized water environment; the lowest, worst-case measured values. By establishing that the failure mode of the system could be changed by lowering epoxy material property values to actual measured values, more FEA simulations were justified. If these lowest *measured* values had not induced a change in simulated failure mode, then the lowest *projected* values would have been used in the model. If even the lowest projected epoxy material property values could not induce a change in failure mode, then no further FEA simulation would have been necessary.

To account for the effects of moisture-based degradation the results of the diffusion modeling and the results of the degradation modeling were integrated into

the FEA simulation to not only investigate the effects of moisture progressively degrading the epoxy material, but also to investigate the effects of longer moisture exposure times on system failure mode. Figure 55 shows a flowchart, diagramming the flow of information through the FEA model.

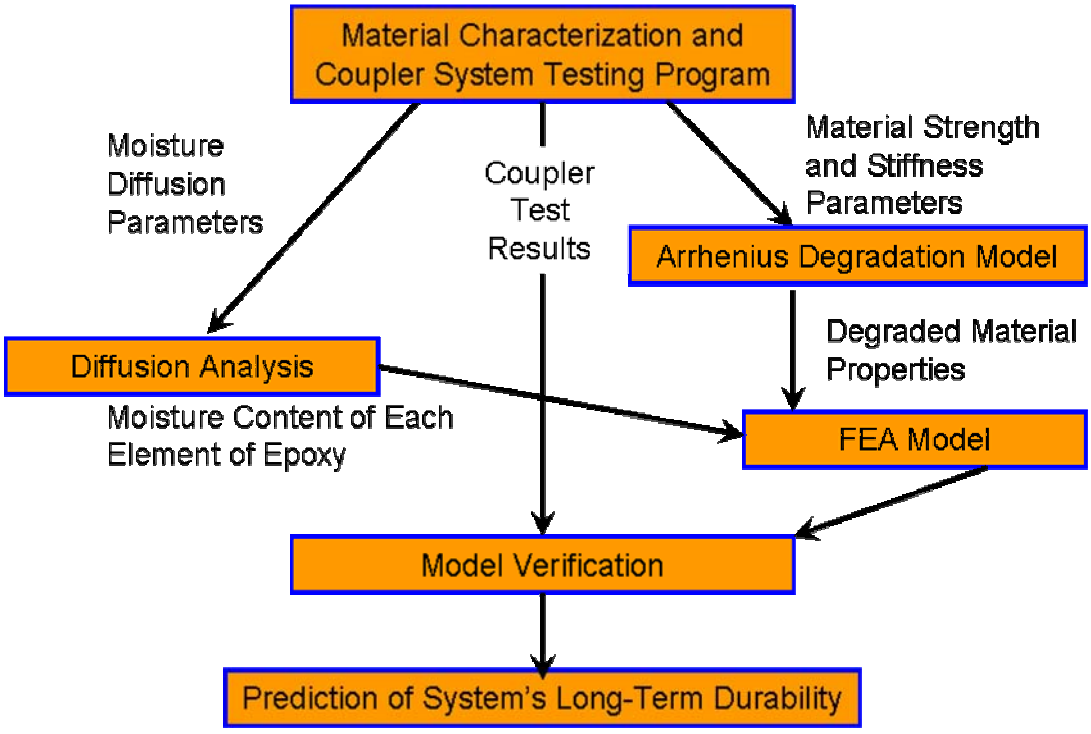

Figure 55: Photograph comparing permanent creep displacements, System C on the left, System F on the right.

5.1.1 Assumptions/Geometry

Although the ribbed deformations on the rebar are not regular and do not form continuous, circumferential rings, a geometric assumption was made to model them axisymetrically.

Due to its observed ineffectiveness at controlling the movement of the bulk of epoxy sliding against the inner surface of the sleeve an assumption was made to ignore

the spring on the inside sleeve of the coupler. This geometric simplification also improved computational and modeling expediency.

5.1.2 Moisture Diffusion Analysis

Although ABAQUS software is able to model mass-diffusion processes, it does not yet allow for coupled stress and mass diffusion analyses. However, the software does allow for both sequentially-coupled and fully-coupled thermal-stress analyses. The governing equations for heat transfer and mass diffusion are proportional and analogies for using thermal analyses to model diffusion phenomena are known [Yoon 2007]. To ensure the compatibility of thermal and moisture parameters the results of a heat-transfer analysis were correlated to the results of the moisture diffusion model. The primary drawback to employing such an analogy is that thermal effects can no longer be modeled concurrently. However, the service thermal cycles are orders of magnitude shorter than moisture diffusion processes; daily heating and cooling cycles compared to months and years of moisture uptake. So the epoxy was assumed to be isothermal for all FEA simulations. This assumption did necessitate that all diffusion parameters, being entered into the ABAQUS model as thermal parameters, were from a single temperature environment. In-field service temperatures would actually vary widely on daily and seasonal cycles. The correlation of cyclic temperatures to system degradation is beyond the scope of this research, but would need to be assessed for each bridge site, and for the location of each rebar-coupler in the structure, for true accuracy. For this model, 23°C was chosen as the temperature to use for both the diffusion model and degradation model.

Several assumptions were made about the start of the diffusion path. Although the choked mouth of the coupler theoretically limits the area of the initiating diffusion surface, the process was assumed to occur evenly from the top of the epoxy bulk, across the larger, inside diameter of the coupler sleeve. Figure 56 shows the location of the assumed moisture diffusion starting surfaces, compared to the actual moisture diffusion paths. This assumption is a worst-case scenario of a gap allowing moisture to enter the entire top of the epoxy bulk at once. Such a gap could be the result of epoxy shrinkage, air voids from the assembly process, or differential thermal expansion of the epoxy and steel. Another advantage of performing this diffusion analysis in the FEA program is that the undulations of the inner epoxy surface, around the ribbed deformations of the rebar, are taken into account.

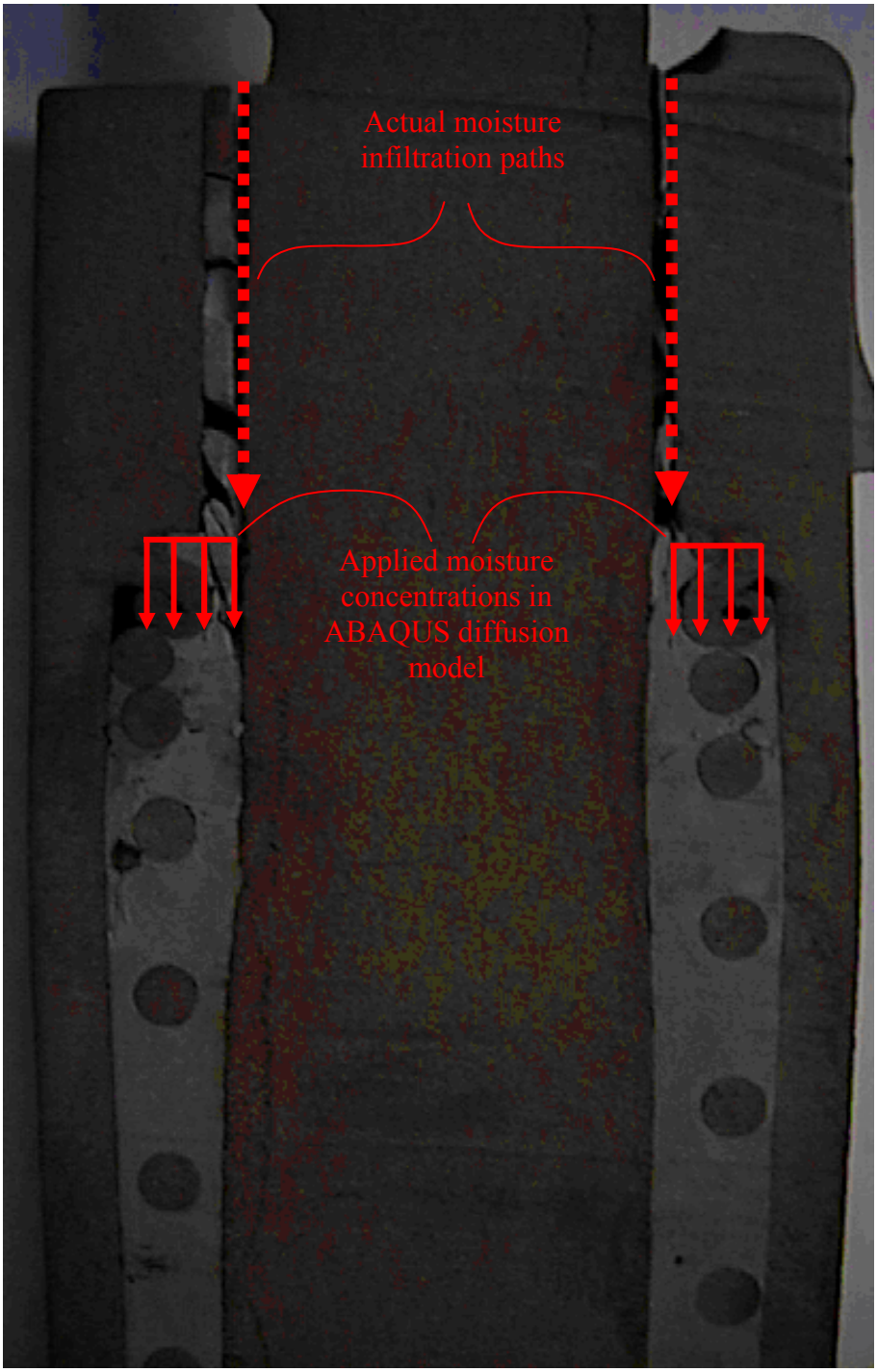

Figure 56: Comparison of actual vs. idealized(modeled) moisture diffusion paths.

Shown in Figures 57-60 are a the moisture diffusion profiles, calculated from Equation 8, for System C at 23°C de-ionized water environment, at a number of time steps in the assumed service life of the coupler. Together the plots show the progression of

moisture into the bulk of epoxy material from the top, the open end of the coupler. The color scale represents percent moisture concentration and the times represented are 0.5, 1, 2, 4, 8, 11.5, 14.5, 24, 60, 120, 240, 480, 600, and 900 months.

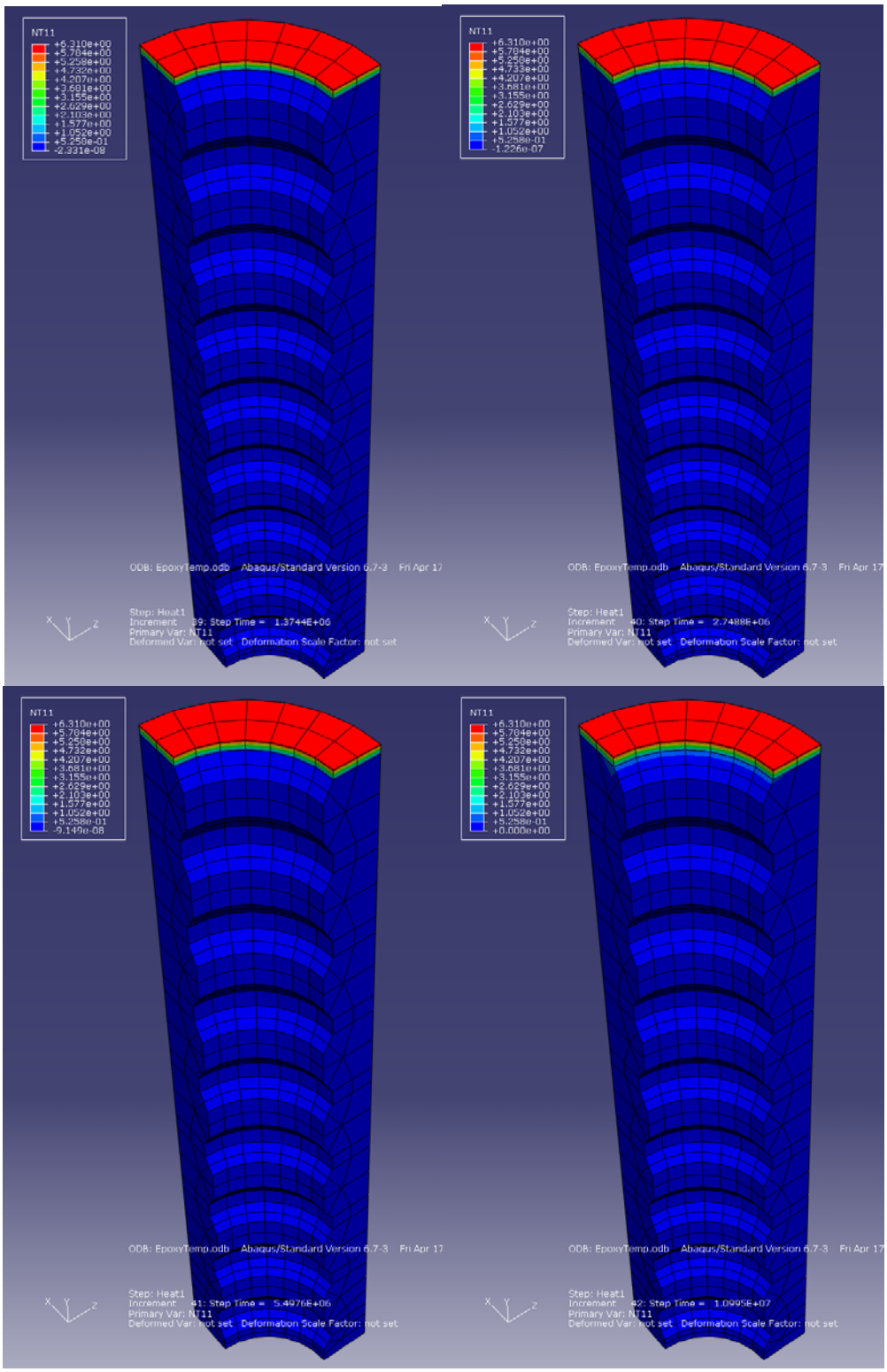

Figure 57: Results of ABAQUS FEA diffusion analysis. Red color is high moisture content; blue is low or zero moisture content. Top-left shows moisture content at 0.5 Months, top-right at 1 month, bottom-left at 2 months and bottom-right at 4 months.

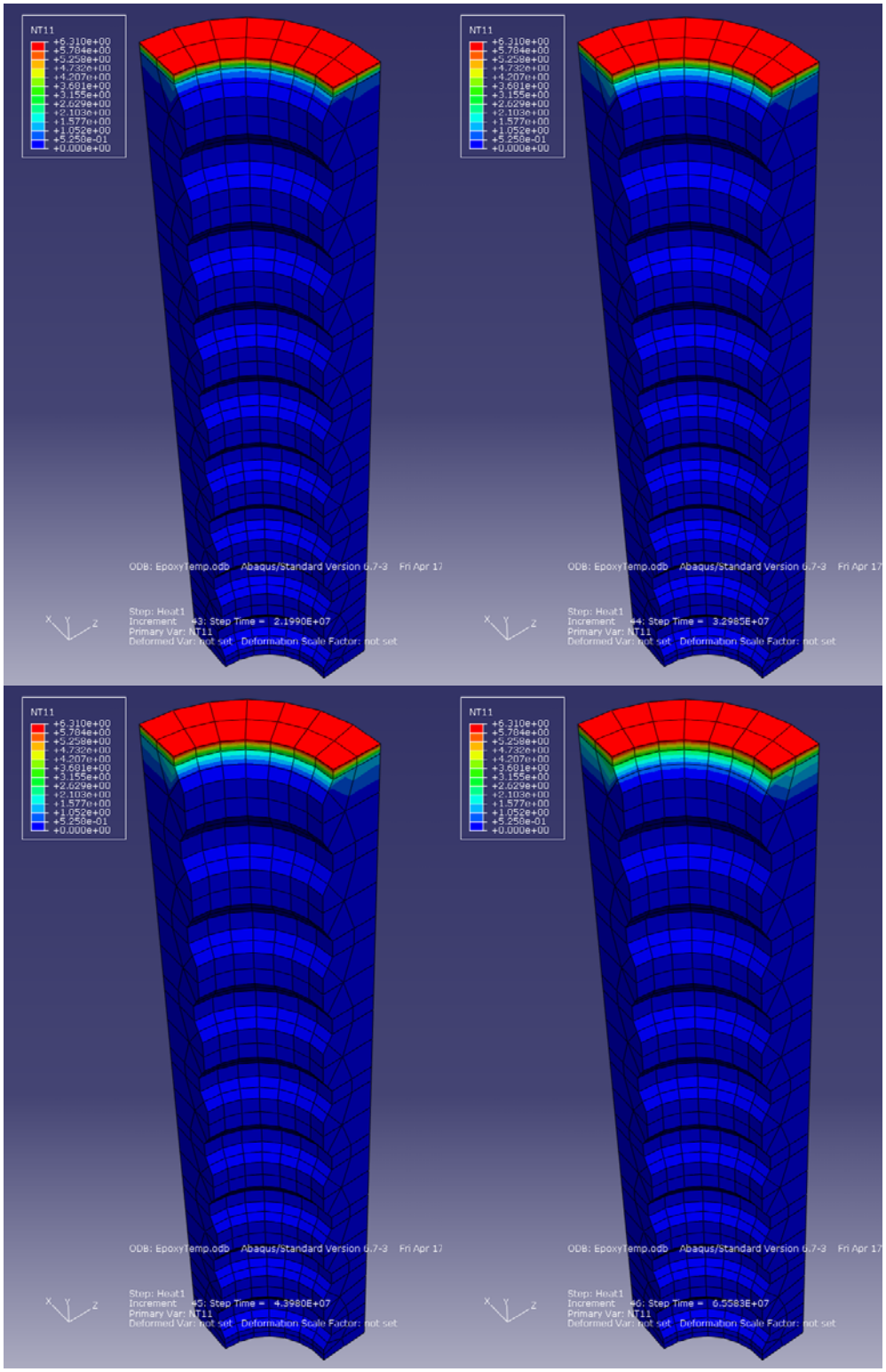

Figure 58: Results of ABAQUS FEA diffusion analysis. Red color is high moisture content; blue is low or zero moisture content. Top-left shows moisture content at 8 Months, top-right at 11.5 month, bottom-left at 14.5 months and bottom-right at 24 months.

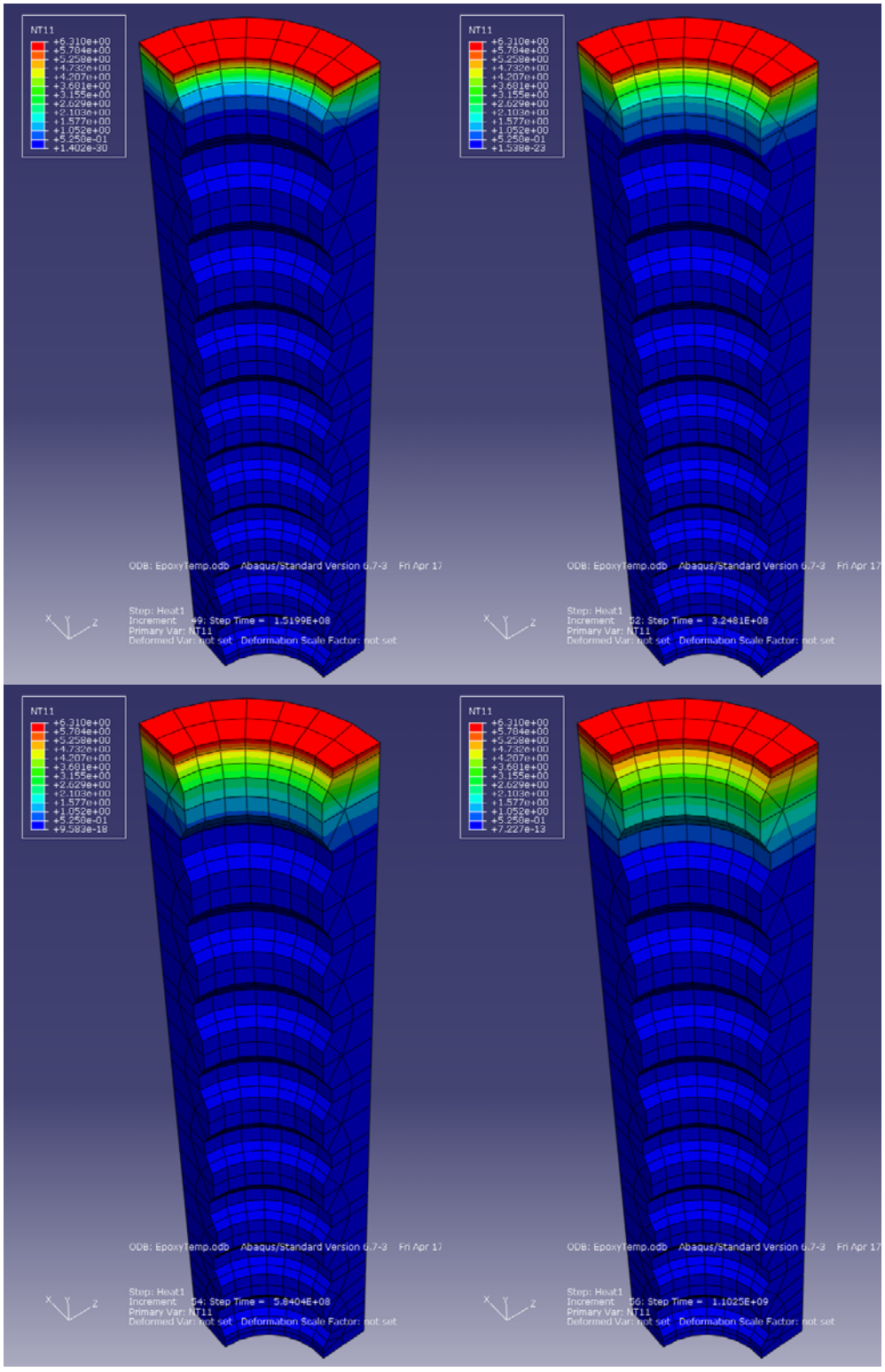

Figure 59: Results of ABAQUS FEA diffusion analysis. Red color is high moisture content; blue is low or zero moisture content. Top-left shows moisture content at 60 Months, top-right at 120 month, bottom-left at 240 months and bottom-right at 420 months.

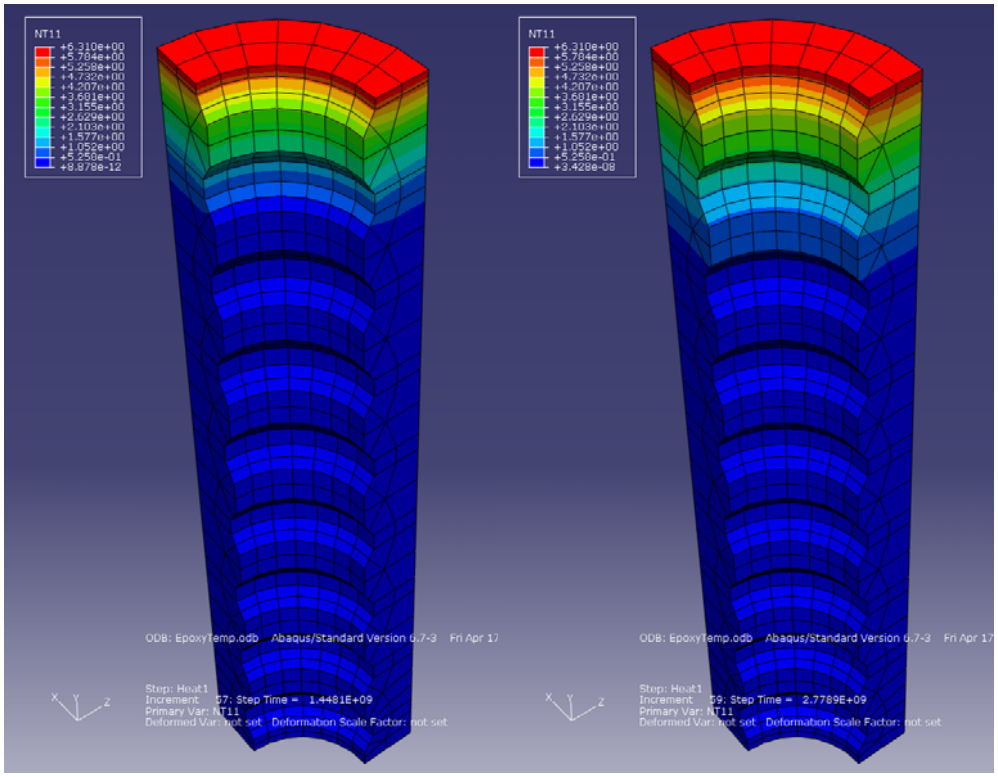

Figure 60: Results of ABAQUS FEA diffusion analysis. Red color is high moisture content; blue is low or zero moisture content. Left shows moisture content at 600 Months and right at 900 months.

5.1.3 Material Properties

5.1.3.1 Tension vs. Compression

To simplify the epoxy material property model for the FEA, the compressive elastic modulus, from the results of the primary material testing program, was used instead of the tensile elastic modulus. A material model using different moduli for tension and compression, from the different material tests, respectively, would have been possible. However, the tensile modulus, which in all cases was higher than the compressive modulus, was assumed to be less critical and less applicable than the compressive modulus. From the phenomenological test results, the primary force transfer mechanism through the epoxy appears to be compression, not tension.

Relying again on the phenomenological test results, epoxy fracture and failure appear to follow the compressive crushing mechanism instead of brittle, tensile fracture.

5.1.3.2 Engineering Stress vs True Stress

Although all data presented in this work has been in units of engineering stress, the ABAQUS FEA software uses true stress.

The conversion from engineering stress to true stress:

$$\sigma_T = \sigma_E \cdot (1 + \varepsilon) \tag{21}$$

where σ_T is true stress, σ_E is engineering stress and ε is strain. A tensile test direction corresponds to a positive ε and thus a true stress greater than engineering stress. A compressive test direction corresponds to a negative ε and thus a true stress less than engineering stress. The relative difference between true and engineering stress increases with increasing strain, so the differences are much more significant for the compressive behavior of the epoxy than for its tensile behavior.

5.1.3.3 Epoxy System

The purpose of the FEA simulation is not to comparatively examine the relative merits of two commercially available epoxy systems, but rather to predict the behavior of the rebar-coupler system with epoxy in various states of moisture treatment. To this end, the test results of System C are used in the FEA model. In

most cases, the properties of the two systems are within 10% of each other, which would make them nearly equal for their use in the model, since their differences are small enough that they approach the accuracy of several of the model inputs.

The degradation behavior, with respect to time, of the epoxy material properties is captured by the Arrhenius model. It would have been possible to input the Arrhenius degradation relationship into the ABAQUS material model and allow the program to modify the epoxy system material properties with respect to time. However, such a model would consider that not all of the epoxy material comes into contact with moisture at the start of the analysis. The variable of the model which allows for the spatially coherency of the onset of degradation for each epoxy material element is moisture content. Both the Arrhenius equation, Equation 13, modeling material property degradation, and the Fickian diffusion equation, Equation 8, modeling moisture uptake, are functions of time. Both Equation 8 and Equation 13 are shown again below.

$$M_t \approx M_\infty \left(1 - e^{-7.3\frac{D \cdot t}{h^2}}\right) \tag{8}$$

$$P_{(t)} = F\left(1 - A \cdot \ln(t)\right) \tag{13}$$

By solving Equation 9 for *t* and substituting into Equation 13 yields:

$$P_{(M)} = F\left[1 - A \cdot \ln\left(\frac{h^2}{d}\left(\frac{-\ln\left(1 - \frac{M}{M_{Max}}\right)}{7.3}\right)^{\frac{4}{3}}\right)\right] \tag{22}$$

Using this equation, material data inputs could be generated which relate the Arrhenius degradation of the epoxy material properties, as a function of moisture content of a given element. While this approach resolves the issue of varying degradation initiation time for different elements, it does have a limitation. The Fickian diffusion equation explains a moisture content which starts from zero and quickly, relative to the considered service life, reaches a maximum. Arrhenius degradation continues indefinitely, albeit at a continually decreasing rate, as shown in Figures 61 and 62. Therefore, for the area of the epoxy material close to the mouth of the coupler, and all the epoxy material to a depth which reaches maximum moisture content within the service life of the coupler, material property degradation occurring past the time for the material to reach maximum moisture is not considered by this approach. However, the proportion of material property degradation occurring during this time period, which would go unconsidered, is small compared to the degradation which is captured by this method. To ensure that this post-peak-moisture degradation is considered two versions of the material model will be run. Both versions of the model are shown in Figure 63. The first version will relate epoxy material mechanical properties to moisture content; these properties will cease to degrade once the material has reached maximum moisture content. The second version of the model will, as the material reaches maximum moisture content, degrade the material properties to the lowest level reached during the considered service lifespan of the rebar-coupler. The Arrhenius model will be used to extrapolate the material properties at a time of 75 years, and these properties will be used once the material reaches maximum moisture

content. This second version of the model should be overly-conservative, so true behavior should be captured by the envelope of results between the two models.

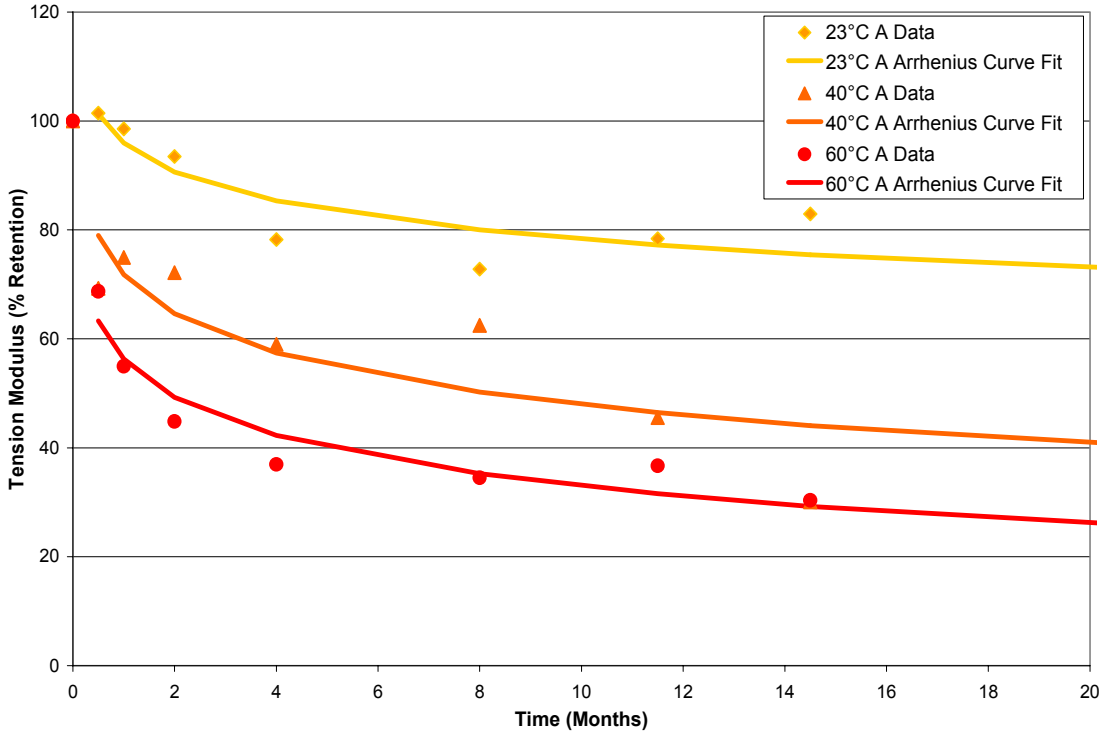

Figure 61: Typical comparison plot of material property data vs. Equation 13 curve-fits, both with respect to time. Tension modulus, System C shown.

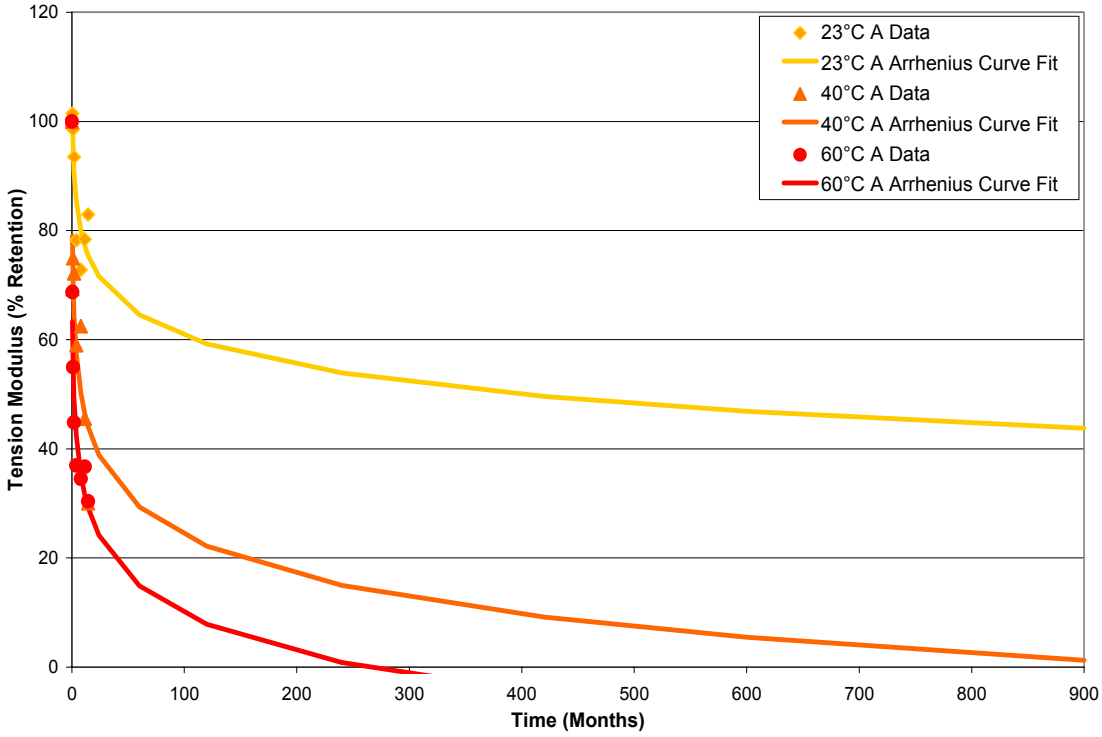

Figure 62: Typical comparison plot of Equation 13 curve-fits, extrapolated out to 75 year service life. Tension modulus, System C shown.

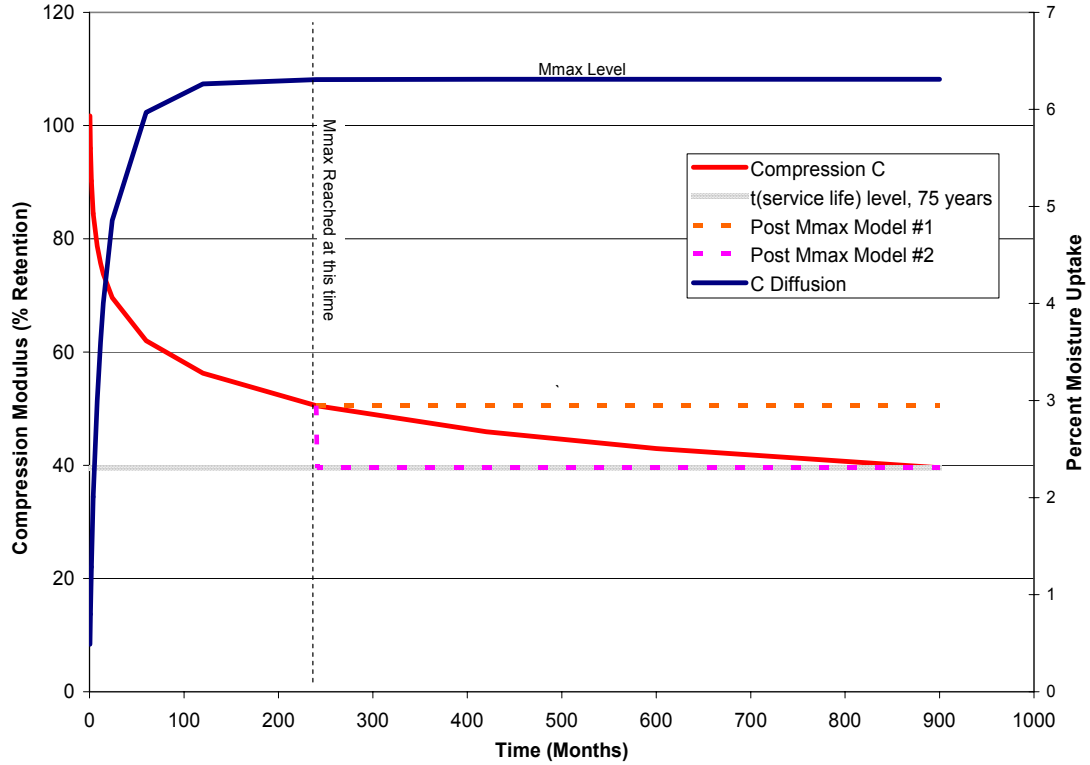

Figure 63: Typical plot of moisture uptake and its associated material degradation curve, along with the two versions of material models which are generated from the

combination. Moisture uptake curve is by Equation 8. Material property curve is by Equation 13, and can be reproduced, in terms of moisture content, using Equation 22.

5.1.4 Finite Element Analysis Results

5.1.4.1 Phenomenological Correlations

Figure 64 shows a view of contact pressures in the model, undergoing pullout load, with untreated epoxy. Elevated contact pressure can be seen on the upper faces of all rebar deformations, indicating that mechanical interlock is transferring force between the rebar and the epoxy. The highest contact pressures are seen at the choked region of the sleeve, where the bulk of epoxy is prevented from pulling out of the sleeve. These results are consistent with the phenomena observed in the phenomenological coupler testing and modeling assumptions.

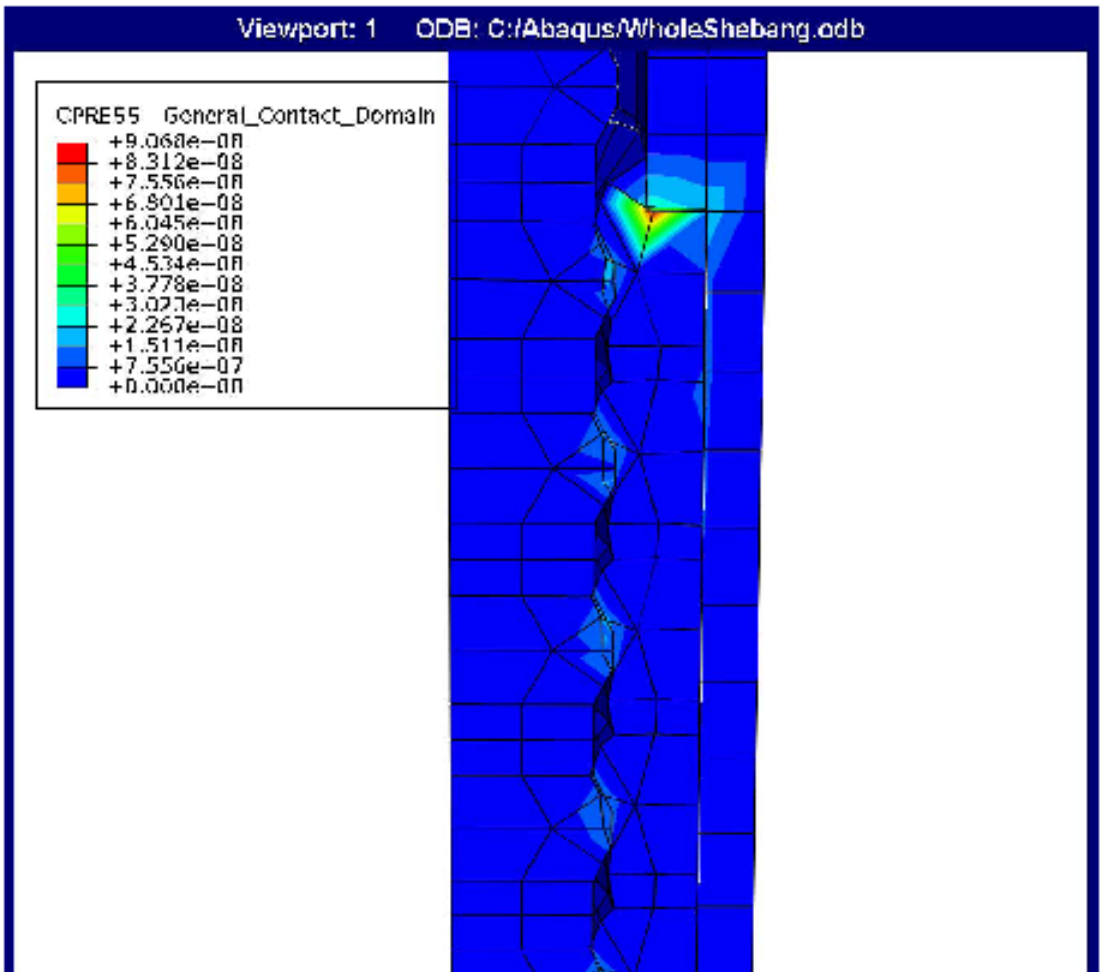

Figure 64: Contact pressures during a pullout load. Epoxy properties at zero time (un-degraded) values.

Figure 65 shows maximum principle stresses in the model during a pull-out load. Several phenomena are illustrated and assumptions about model behavior verified. Notice the light blue color in the epoxy near the mouth of the coupler. From the scale on the figure, these colors represent strongly negative, compressive, stresses. Also, the concentration of stresses in the coupler wall bordering this region is consistent with the results of the phenomenological testing.

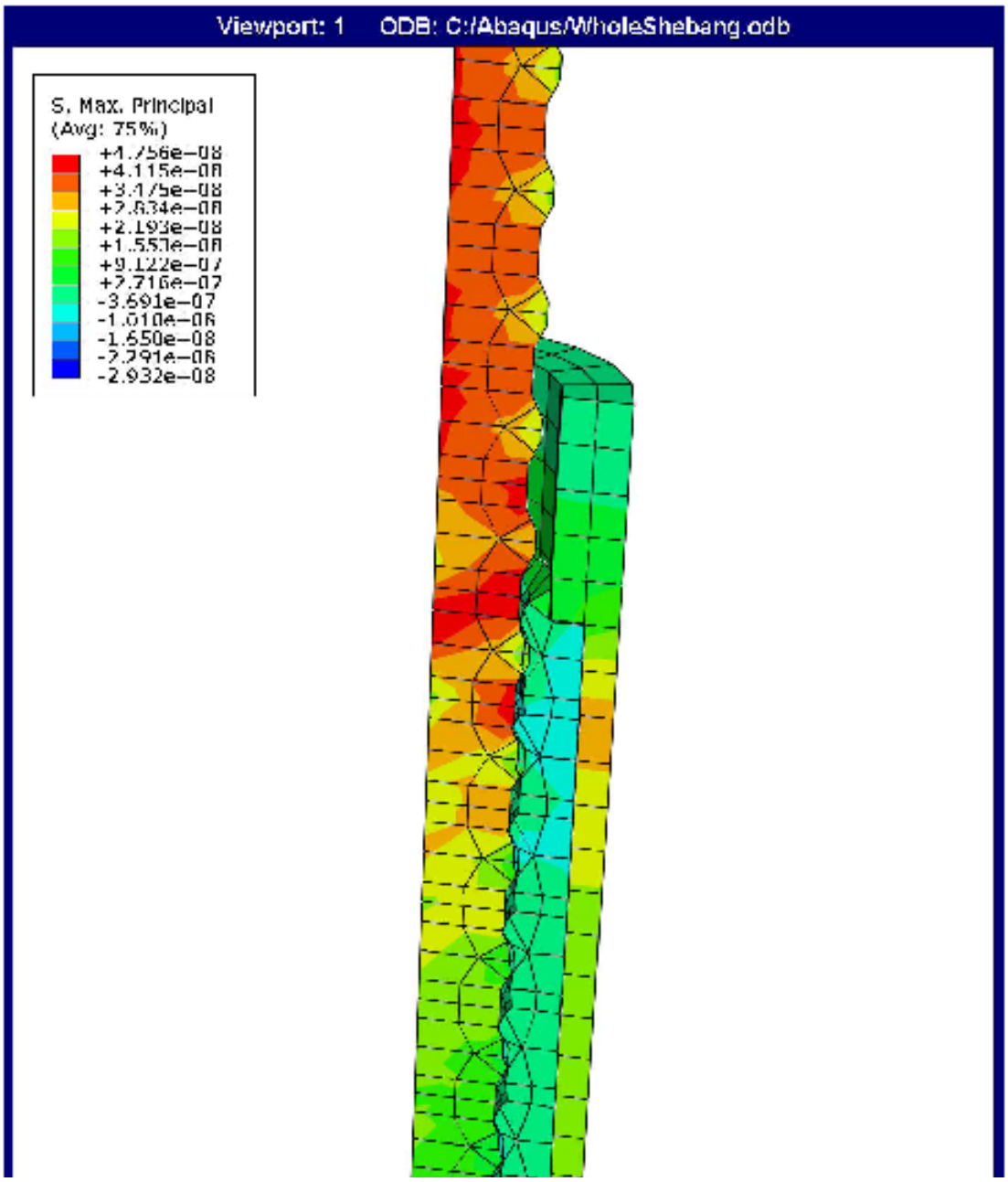

Figure 65: Maximum principle stresses during a pullout load. Epoxy properties at zero time (un-degraded) values.

Figure 66 shows the displacement of the rebar, during a pull-out simulation, with three different moisture distributions; and thus three different sets of epoxy mechanical properties. The three moisture distributions are zero-time, 75 years of

diffusion, and maximum diffusion throughout. The last case should correspond to an infinite diffusion time. The model passes the simulation in all cases, and only small differences are evident in the displacement levels in each case.

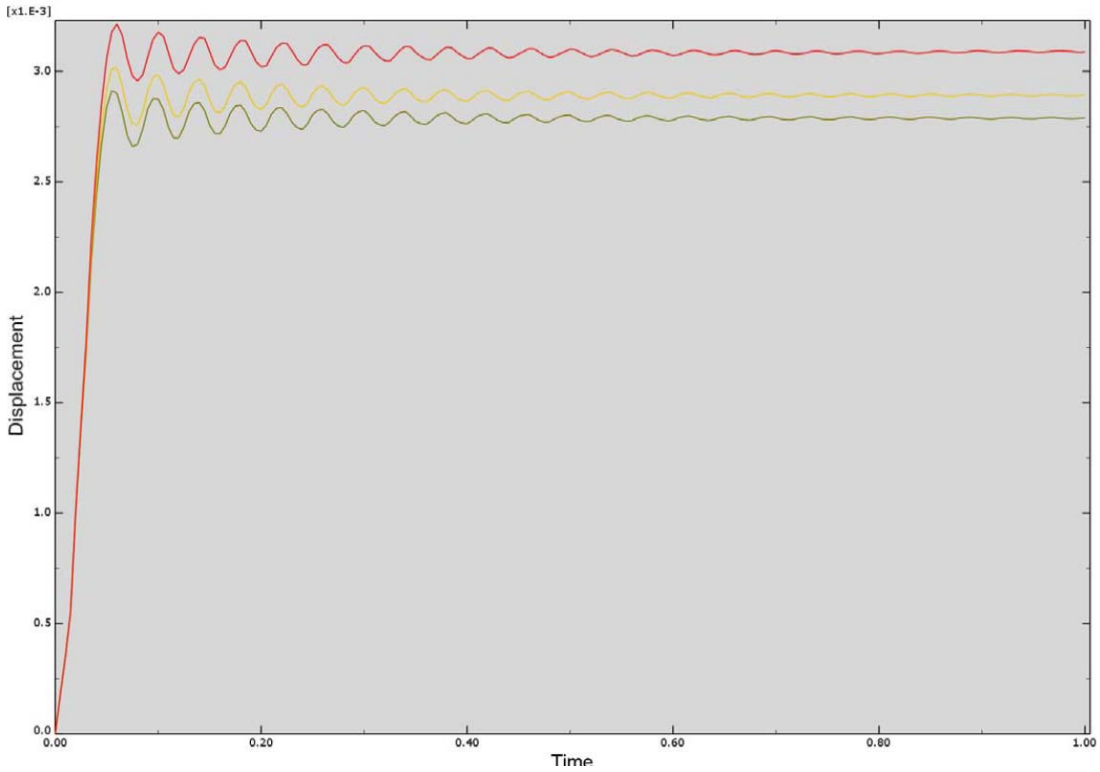

Figure 66: Rebar displacement from three different versions of the model. Top trace is with all epoxy at maximum moisture content. Middle trace is with epoxy at 75 year diffusion profile. Bottom trace is with untreated epoxy. Oscillations are due to dynamic model seeking equilibrium.

5.1.4.2 Service Life Implications

From the results of this FEA simulation predictions can be made about the long-term performance of the epoxy-bonded rebar-coupler system, in relation to service lifetimes. The system passed a pull-test with the epoxy diffused to a state equal to 75 years of treatment. So if the service life of the coupler consists of being embedded in a 23°C, moist environment for its assumed service life, then being tested

to failure, a single time in tension, the original failure mode of the system should remain unchanged. That is, the rebar should still fracture before pulling out of the epoxy.

The results of this analysis predict that in a 23°C immersive environment, unless modes of epoxy failure changed, the mechanical properties of the epoxy would not be severely degraded, to levels which would change the behavior of the epoxy-bonded rebar-coupler. However, as shown in Figure 60, at elevated temperatures, the epoxy properties could be degraded to essentially zero within the assumed service life of 75 years. At elevated temperatures, the problem is compounded since, not only can the epoxy properties go to zero within the assumed life span of the system, but the moisture would diffuse into the epoxy much faster. In this way, the level of degradation would penetrate deeper into the epoxy sooner.

6 Conclusions

6.1 Summary

The long-term performance of epoxy-bonded rebar-couplers has been investigated. This investigation has focused primarily on the moisture-based degradation of the epoxy and its effect on the performance of the rebar-coupler system. A preliminary de-selection test was undertaken to select several epoxy systems, from the many commercially available systems, for further study to characterize the moisture-based degradation of the materials. Based on the results from this material characterization test program, the moisture uptake behavior and moisture-based degradation behavior of the epoxy systems were modeled and used to build a Finite Element Analysis (FEA) model of the rebar-coupler system. This FEA model was used to simulate the tensile, pull-out behavior of the rebar-coupler with epoxy properties corresponding to different times in the system's service life. Using the FEA model with appropriate degradation parameters, predictions of service life in varying environmental conditions can be made.

6.2 Service Life Considerations

The results of the FEA indicate that the long-term performance, and failure mode, of the epoxy-bonded rebar-coupler system is unchanged due to immersion in a 23°C de-ionized water environment, even after an extended period of time, assuming self-similar mechanisms of damage through the time period under consideration, and at the considered rebar size of #5. However, not all rebar-couplers can be expected to

stay below that temperature for their entire service lives. The results of the material testing program indicate that these material systems would not perform well over the assumed service life of the system if exposed to a 60°C de-ionized water environment, or to degradation levels indicated by that exposure. Although the effects of relative humidity were not investigated in this research, it may be that the service environment of warmer concrete, which is occasionally wetted, is more critical than immersed concrete, which stays at or below 23°C.

6.3 Recommendations

6.3.1 Proposed Modification of California Test 670 Specification

The California Department of Transportation Method of Tests for Mechanical and Welded Reinforcing Steel Splices is included as Appendix A. A version of the test protocol with recommended additions, highlighted in grey, is included as Appendix B. These recommendations are included for review by the California Department of Transportation, who has been the sponsor of this research. One of the additions is to allow the use of a long-gauge extensometer as an option to measure slip, the other is the addition of an adhesive material pre-screening test. The pre-screening test would apply only to epoxy-bonded rebar-couplers and would help to ensure the adhesive system used in the coupler would not be highly vulnerable to moisture-based degradation.

6.3.2 Recommended Material Rapid-Assessment Protocol

This research has shown that not all adhesive systems, designed for adhesive anchorage to concrete, and certified by ASTM C881, have equal resistance to moisture-driven degradation. However, the extensive studies on, and analysis based upon, Systems A and C indicate that an epoxy-bonded rebar-coupler should be able to achieve its service-life goals. However, System F proved inadequate based on the results of coupler testing. The question then becomes how to effectively and efficiently determine the relative resistance, to moisture-driven degradation, of epoxy adhesive systems.

All ASTM C881 certified systems must meet standard requirements in their non-degraded state; several additional tests should allow their long-term performance, and resistance to moisture-driven degradation, to be roughly assessed. Based on the results of this research it is recommended that an ASTM C 881 epoxy system not be used if any of the following test results are found:

- The tension or compression, strength and modulus of the material maintains at least 50% of its initial level, after 1 week immersed in 60°C de-ionized water
- The glass transition temperature of the material, after 1 week immersed in 60°C de-ionized water, is at least equal to the expected maximum environmental service temperature + 30°C
- The Fickian diffusion coefficient is lower than 10-6 mm^2/s, measured by moisture uptake due to immersion in 60°C de-ionized water

6.4 Areas for Future Research

This research has investigated the long-term performance of epoxy-bonded rebar-couplers from the perspective of moisture-based epoxy degradation. However many factors on the long-term behavior of the couplers remain to be understood. Although this research included some preliminary work on creep at the rebar-coupler level and testing of the rebar coupler at elevated temperature, investigations of coupler creep at elevated temperature and creep during environmental conditioning remain to be studied. Additionally, this research made the simplification of simple immersion for its environmental treatment, though in reality the epoxy would be contained inside the coupler, embedded in a reinforced concrete component, and would be exposed to humidity, not true immersion.

The natural extension of this research, and ultimately the direction which may be more important for the advancing the state of the art in engineering, is the transfer of the principles of this research into the area of the long-term performance of adhesive anchors to concrete. Not only are adhesive anchors much more common in contemporary construction than epoxy-bonded rebar-couplers, but a long-term failure has already been recorded and significant potential vulnerabilities exist if the moisture-based degradation of the epoxy is not accounted for first in research, and eventually in design codes.

All coupler testing in this research was performed at ambient temperature conditions of 23°C. Because the epoxy systems were shown to be so sensitive to increased temperature, the coupler level testing, especially the creep testing, should be

repeated at a range of increased temperature to investigate the effect of temperature on the rebar-coupler behavior.

This research has shown the force transfer mechanisms of epoxy-bonded rebar-couplers to be different than those occurring in adhesive anchorage to concrete. In the former, the forces are transferred by compression struts through the epoxy in the area around the mouth of the coupler; in the later they are distributed along the length of embedment. These differences in force transfer have implications for scaling the system to larger rebar sizes. As the rebar size increases, the force in the rebar increases proportionally to the diameter squared. The region of the force transfer zone through the epoxy increases proportionally to the circumference, and thus the diameter of the rebar. Unlike adhesive anchorage to concrete, the region of force transfer through the epoxy cannot simply be increased by increasing embedment length. Further research into the effects of increasing rebar size is recommended.

6.5 Afterword

Since the initiation of this research, and partly as a result of this research, the design of commercially produced epoxy-bonded rebar-couplers has been modified. The spring has been omitted from current production and the inside of the coupler sleeve is now ribbed, much like the phenomenological test specimen, in an effort to generate mechanical interlock force transfer between epoxy and the sleeve. However, the choked mouth of the coupler remains intact, so that although the geometry of the coupler has changed slightly, the analyses in this research still appear valid and appropriate. Mechanical interlock of the epoxy in the sleeve should distribute the

forces better through the depth of the epoxy embedment, and make the uniform bond stress model more applicable to the design. Also, since the presence of the spring has been largely ignored in the course of this research, its omission from future production of couplers should only make these analyses more applicable.

REFERENCES

Abeysinghe, H.P., W. Edwards, G. Pritchard, and G.J. Swampillai. "Degradation of crosslinked resins in water and electrolyte solutions." *Polymer*. Vol. 23 (1982) 1785-1790.

Acceptance Criteria for Adhesive Anchors in Concrete and Masonry Elements, International Code Committee – Evaluation Service (ICC-ES), Acceptance Criteria 58. Whittier, CA. 2006.

Acceptance Criteria for Mechanical Connector Systems for Steel Reinforcing Bars, International Code Committee – Evaluation Service (ICC-ES), Acceptance Criteria 133. Whittier, CA. 2008.

Acceptance Criteria for Post-Installed Adhesive Anchors in Concrete Elements, International Code Committee – Evaluation Service (ICC-ES), Acceptance Criteria 308. Whittier, CA. 2008.

Antoon, M.K. and J.L. Koenig. "The structure and moisture stability of the matrix phase in glass-reinforced epoxy composites." *Journal of Macromolecular Science – Reviews in Macromolecular Chemistry and Physics*. Vol. C19, No. 1 (1980) 135-173.

Best, J.F., and J.E. McDonald, "Evaluation of polyester resin, epoxy, and cement grouts for embedding reinforcing steel bars in hardened concrete," Technical Report REMR-CS-23, U.S. Army Engineer Waterways Experiment Station, Vicksburg, MS, 1990.

Calfornia Test 670, 2004. State of California, Department of Transportation.

Carslaw, H.S. and J.C. Jaeger. *Conduction of Heat in Solids*. 2nd ed. Oxford University Press: New York, 1959.

"Ceiling Collapse in the Interstate 90 Connector Tunnel, Boston, Massachusetts, July 10, 2006", Highway Accident Report NTSB/HAR-07/02, National Transportation Safety Board, Washington, DC, July 2007.

Chamis, C.C. "Simplified Composite Micromechanics Equations for Strength, Fracture Toughness, Impact Resistance and Environmental Effects." *NASA Technical Memorandum* Number 83696 (1984).

Cook, R. A., and Konz, R. C., Factors Influencing Bond Strength of Adhesive Anchors, *ACI Structural Journal*, Vol. 98, No. 1, (2001) 76-86.
Cook, R.A., G.T. Doerr and R.E. Klingner, Bond Stress Model for Design of Adhesive Anchors, *ACI Structural Journal*, V. 90, No. 5, (1993) 514-524.

Cook, R. A., Kunz, J., Fuchs, W., and Konz, R. C. Behavior and Design of Single Adhesive Anchors under Tensile Load in Uncracked Concrete, *ACI Structural Journal*, Vol. 95, No. 1, (1998) 9-26.

Cotugno, S., D. Larobina, G. Mesitieri, P. Musto, and G. Ragosta. "A novel spectroscopic approach to investigate transport processes in polymers: the case of water-epoxy interaction." *Polymer*. Vol. 42 (2001) 6431-6438.

Crank, J., *Diffusion in Polymers*, Academic Press Inc., London, 1968, pp. 42.

Crank, J. *The Mathematics of Diffusion*. Oxford University Press: New York (1970).

Eligehausen, R., Cook, R.A.,and Appl, J. "Behavior and Design of Adhesive Bonded Anchors." *ACI Structural Journal*. Vol. 103, No. 6, (2006) 822-831.

Florida Department of Transportation (FDOT) (2000), Florida Method of Test for Anchor
System Tests for Adhesive-Bonded Anchors and Dowels, Florida Department of Transportation, FM 5-568. Tallahassee, Florida.

Fuchs, W., Eligehausen, R., and Breen, J. E. (1995), Concrete Capacity Design (CCD) Approach for Fastening to Concrete, *ACI Structural Journal*, Vol. 92, No. 1, pp. 73-94.

Higgins, C.C., and R.E. Klingner. "Effects of Environmental Exposure on the Performance of Cast-in-Place and Retrofit Anchors in Concrete", *ACI Structural Journal*, V. 95, No. 5, September-October 1998.

James, R. W., De la Guardia, C., and McCreary, Jr., C. R. "Strength of Epoxy-Grouted Anchor Bolts in Concrete", *Journal of Structural Engineering*, American Society of Civil Engineers, Vol. 113, No. 12 (1987) 2365-2381.

Jansson, Peter O. "Evaluation of Grout-Filled Mechanical Splices for Precast Concrete Construction", Report Number TI-2094, Michigan Department of Transportation, Construction and Technology Division, Lansing, MI. 2008.

Jost, W. *Diffusion in solids liquids, gases*. Academic Press Inc.: New York (1960).

Karbhari, V.M. "Dynamic Mechanical Analysis of the Effect of Water on EGlass/ Vinylester Composites." *Journal of Reinforced Plastics and Composites*. Vol. 25, No. 6 (1996) 631-644.

Kaw, A. K. *Mechanics of Composite Materials*. CRC Press LLC: Boca Raton, Florida (1997).

Kornreich, B. (2001), "Grouted and Adhesive Anchor Tests: Chemrex Products 1090, Thoroc 10-60", 648 CP+, 928, Masters Report, University of Florida, Gainesville, Florida.

Kwei, T.K. "Strength of Epoxy Polymers. I. Effect of Chemical Structure and Environmental Conditions." *J. of Applied Polymer Science*. Vol. 10 (1966) 1647-1655.

Lee, M.C. and N.A. Peppas. "Water transport in epoxy resins." *Prog. Polymer Science.*
Vol. 18 (1993) 947-961.

Lee, S.-B., T.J. Rockett, and R.D. Hoffman. "Interactions of water with unsaturated polyester, vinyl ester and acrylic resins." *Polymer*. Vol. 33, No. 17 (1992) 3691-3697.

Litherland, K.L., D.R. Oakley, and B.A. Proctor. "The use of accelerated ageing procedures to predict the long term strength of GRC composites." *Cement and Concrete Research*. Vol. 11 (1981) 455-466.

Manning, David G. "Fatigue Behavior of Welded and Mechanical Splices in Reinforcing Steel." *National Comparative Highway Research Program Research Results Digest.* Number 197 (1994)

Mather, Bryant. "Concrete Need Not Deteriorate", *Concrete International,* September (1979) 32-37.

McVay, M., Cook, R. A., and Krishnamurthy, K. (1996), "Pullout Simulation of Postinstalled Chemically Bonded Anchors", *Journal of Structural Engineering*, American Society of Civil Engineers, Vol. 122, No. 9, pp. 1016-1024.

Menard, Kevin P. *Dynamic Mechanical Analysis: A Practical Introduction*. CRC Press LLC: Boca Raton, Florida (1999).

Nakada, M., Y. Miyano, M. Kinoshita, R. Koga, T. Okuya, and R. Muki. "Time-Temperature Dependence of Tensile Strength of Unidirectional CRFP." *Journal of Composite Materials*. Vol. 36, No. 22 (2002) 2567-2581.

Nissan, A.H. "H-Bond Dissociation in Hydrogen Bond Dominated Solids." *Macromolecules*. Vol. 9, No. 5 (1976) 840-850.

Phani, K.K., and N.R. Bose. "Temperature Dependence of Hydrothermal Ageing of CSM-Laminate During Water Immersion." *Composites Science and Technology*. Vol. 29 (1987) 79-87.

Priestley, M. J. N. "Linear Heat-Flow Analysis of Concrete Bridge Decks," University of Canterbury, Department of Civil Engineering. 1976.

Shen, C.H. and G.S. Springer. "Moisture Absorption and Desorption of Composite Materials." *Journal of Composite Materials*. Vol. 10 (1976) 2-20.

Starkweather, H.W. "Clustering of water in polymers." *Journal of Polymer Science Part B – Polymer Letters*. Vol. 1, No. 3 (1963) 133-138.

Stark et al. "Eliminating or Minimizing Alkali-Silica Reactivity". SHRP-C-343, National Research Council, Washington, DC. 1993.

Standard Specification for Epoxy-Resin-Base Bonding Systems for Concrete, C881C/C881M-02, American Society for Testing and Materials (ASTM), West Conshohocken, PA. 2005.

Standard Test Methods for Testing Bond Performance of Bonded Anchors, E 1512, American Society for Testing and Materials (ASTM), West Conshohocken, PA. 2001.

Standard Test Method for Water Absorption of Plastics, D570-98, American Society for Testing and Materials (ASTM), West Conshohocken, PA. 2005.

Standard Test Method for Tensile Properties of Plastics, D638-03, American Society for Testing and Materials (ASTM), West Conshohocken, PA. 2005.

Standard Test Method for Compressive Properties of Rigid Plastics, D695-02a, American Society for Testing and Materials (ASTM), West Conshohocken, PA. 2005.

Tolson, B. "The Growing Use of Rebar Couplers". *Concrete*, 35, 2001.

van Amerongen, G.J. "Diffusion in Elastomers." *Rubber Chemistry and Technology*. Vol. 37, No. 5 (1964) 1065-1152.

Whitney, J.M. and C.E. Browning. "Some Anomalies Associated with Moisture Diffusion in Epoxy Matrix Composite Materials." *Advanced Composite Materials – Environmental Effects, ASTM STP 658*. J.R. Vinson, Ed., American Society for Testing and Materials (1978) 43-60.

Williams, M.L., R.F. Landel, and J.D. Ferry. "The Temperature Dependence of Relaxation Mechanisms in Amorphous Polymers and Other Glass-forming Liquids." *Journal of the American Chemical Society*. Vol. 77 (1955) 3701-3707.

Xian, G., and Karbhari, V. “Segmental Relaxation of Water-Aged Ambient Cured Epoxy.” *Polymer Degradation and Stability*. 92 (2007) 1650-1659.

Yoon, S., B. Han, and Z. Wang. “On Moisture Diffusion Modeling Using Thermal-Moisture Analogy.” *Journal of Electronic Packaging*. Vol. 129, No. 12 (2007) 421-426

Zamora, N. A., Cook, R. A., Konz, R. C., and Consolazio, G. R. (2003), “Behavior and
Design of Headed and Unheaded Grouted Anchors Loaded in Tension”, *ACI Structural Journal*, Vol. 100, No. 2, pp. 222-230.

Zhou, J. and J.P. Lucas. “Hygrothermal effects of epoxy resin. Part I: the nature of water in epoxy.” *Polymer*. Vol. 40, No. 20 (1999) 5505-5512.

Zhou, J. and J.P. Lucas. “Hygrothermal effects of epoxy resin. Part II: variations of glass transition temperature.” *Polymer*. Vol. 40, No. 20 (1999) 5513-5522.

TE OF CALIFORNIA—BUSINESS, TRANSPORTATION AND HOUSING AGENCY

California Test 670
September 2004

PARTMENT OF TRANSPORTATION
ISION OF ENGINEERING SERVICES
nsportation Laboratory
0 Folsom Boulevard
ramento, California 95819 - 4612

METHOD OF TESTS FOR MECHANICAL AND WELDED REINFORCING STEEL SPLICES

AUTION: Prior to handling test materials, performing equipment setups, and/or conducting this method, testers are required to read "**SAFETY AND HEALTH**" in Section G of this method. It is the responsibility of the user of this method to consult and use departmental safety and health practices and determine the applicability of regulatory limitations before any testing is performed.

SCOPE

This method presents the testing procedures for determining mechanical properties of spliced reinforcing steel.

DEFINITIONS

Coupler – mechanical device that physically connects two reinforcing bars.

Lot – quantity of spliced reinforcing steel, as defined in Caltrans *Standard Specifications* Section 52.

Necking – localized reduction in cross-section that may occur in material under tensile stress. For this California Test, a sample has necking if the reduction in cross-section is visible, or if the sample has sufficient ductility, as determined by the strain measurement in Section D below.

Sample – spliced reinforcing steel bar that has the physical properties required in Section D below.

Sample No. – unique tracking number assigned to the sample(s) or set of samples being tested.

Slip test – procedure for determining inherent axial displacement within the mechanical coupler.

Splice – physical device or mechanism for joining reinforcing steel, as defined in Caltrans *Standard Specifications* Section 52. Mechanical non-lap splices and resistance welded splices are the most common types encountered.

C. TESTING APPARATUS AND ACCESSORIES

1. Tensile test machine able to apply a tensile force greater than the ultimate tensile strength of the sample. Tensile test machine must be accurate in accordance with ASTM A 370.
2. Slip measurement device consisting of two dial indicators that measure displacement across the splice to the nearest 0.025 mm. See Figure 1. A dial indicator may have an analog dial or be digital. Alternatively, an extensometer accurate to within 0.025 mm.
3. Caliper accurate to 0.025 mm.

D. TEST PROCEDURES FOR PRODUCTION TESTING AND QUALITY ASSURANCE TESTING

PHYSICAL PROPERTIES AND PREPARATION

Before accepting samples, ensure each sample has these physical parameters:

1. Sample length. A minimum sample length is required for the submitted samples. Depending on a lab's specific testing equipment, the lab may shorten, machine, or otherwise alter the submitted samples to meet the configuration of its testing equipment. This alteration is allowable under this Test Method and *Standard Specifications* Section 52.
   For rebar sizes #25 and smaller, sample length must be at least 1.5 m. For rebar sizes #29 and larger, sample length must be at least 2 m.
2. Coupler diameter. For mechanical couplers, length of the coupler must be less than 10 times the nominal bar diameter.
3. Alignment. With the exception of spliced hoops, the alignment across the splice must be straight to within 7 mm in 0.9 m of length.

Record results on the Test Form (Figure 2).

SLIP TEST

The slip test is required for all splices except mechanical lap splices, welded splices, or splices on hoops. There are two acceptable options for measuring slip.

Slip Test (Option I)

Option I uses two dial indicators that measure displacement across the splice. Steps:

1. Mount the sample in the tensile test machine.
2. Preload the sample to 4 MPa to set the jaws on the bar ends. Attach the slip measurement device so that the dial indicators are 180° apart. Zero them out.
3. Apply an axial stress of 200 MPa. Maintain load until obtaining a steady reading on both dial indicators.
4. Reduce the stress to 20 MPa and measure the two readings. Sum the value of the two readings and divide the resultant sum by two. This is the total slip. Record the total slip on the Test Form (Figure 2).
5. Remove the two dial indicators.

Slip Test (Option II)

The second option for measuring slip (Option II) uses punch marks. Steps:

1. Place one set of punch marks that span the splice. The distance between the punch marks should be approximately equal to the coupler length plus four bar diameters. Place a second set of punch marks 180° apart from the first set.
2. Preload the sample to 4 MPa to set the jaws on the bar ends.
3. Measure distance between the punch marks to the nearest 0.025 mm.
4. Apply an axial stress of 200 MPa. Maintain the load for 60 seconds.
5. Reduce the stress to 20 MPa and measure the distance between each set of punch marks. For each set, calculate the slip (measured length – original length) and average the results. This is the total slip. Record result on the Test Form.

TENSILE TEST

Tensile testing must be done in general accordance with ASTM A 370 Sections 13 and A9.

1. Apply an axial tensile load to the sample sufficient to cause failure.
2. Document the maximum load obtained.
3. Calculate the ultimate tensile strength by dividing the maximum load by the sample's nominal cross-sectional area. ASTM A 706, Table 1, provides the nominal cross-sectional areas for A 706 reinforcing steel. Record the ultimate tensile strength on the Test Form.
4. Check for necking. This can be done visually (Option I) or by measuring strain (Option II). Also, it does not matter which option was used for the slip test when choosing an option to assess necking.

Necking (Option I)

Examine the fractured area. If there is a visible decrease in the sample's cross-sectional area at the point of fracture, there is visible necking. Record result on the Test Form.

Necking (Option II)

Alternatively, assess necking by measuring the sample's strain. Follow this procedure for measuring strain:

a. For straight samples, place punch marks along the sample to create three gauge lengths with a nominal length of 200 mm. For hoops, place punch marks along the sides of the hoop rebar samples (not the concave or convex sides of the bar) to create a total of three gauge lengths, each 200 mm in length. For both straight samples and hoops, leave a gap of at least 25 mm between any two 200 mm gauge lengths to separate the gauge marks. Splices, if any, shall be centered in the middle 200 mm gauge length. See figure below:

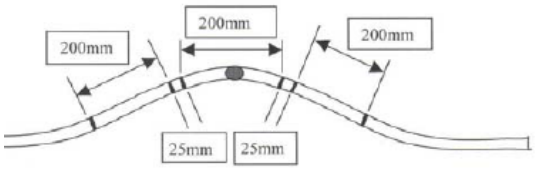

b. Do not confuse these punch marks with the punch marks that may have been placed for the slip test.
c. Straight samples are tested as received. For hoops, straighten the ends of hoop samples to fit sample into the testing grips. This straightening should be outside of the gauge marks, in accordance with the Concrete Reinforcing Steel Institute's *Manual of Standard Practice MSP-1-90*.
d. Mark each one of the 200 mm nominal gauge lengths sequentially as A, B, C. B designates the middle segment and it contains the splice, if any.
e. Individually, measure and record the initial three 200 mm gauge lengths A, B, and C to the nearest 0.025 mm.
f. Tensile test each sample following the instructions in "Tensile Test" above.
g. Measure the two gauge lengths not encompassing the location of failure. For hoop samples, correct the final gauge length values for curvature by multiplying the final readings by this factor:

corrected gauge (L_n) = *measured gauge * factor*

$$factor = \frac{L_c}{D * ArcSin\left(\frac{L_c}{D}\right)}$$

where:

L_c = length of chord (200 mm nominal)
D = diameter of the hoop (rebar center to rebar center in mm)
L_n = corrected gauge length (in mm)
ArcSin is in radians

h. Calculate the percent strain for each one of the gauge lengths measured in step g. For straight samples:

$$\% strain = (L_f - L_o)/L_o * 100$$

where:

L_f = final gauge length
L_o = original gauge length

For hoop samples:

$$\% strain = (L_n - L_o)/L_o * 100$$

where:

L_n = corrected gauge length
L_o = original gauge length

i. If the largest measured strain is $\geq$ 6% for #36 and larger bars, or $\geq$ 9% for #32 and smaller bars, then

the sample is considered to have necking. If the largest measured strain is < 6% for #36 and larger bars, or < 9% for #32 and smaller bars, then the sample is considered to have no necking.

j. Record the largest measured strain on the Test Form.

CYCLICAL TESTING

This section applies only to mechanical splices on straight reinforcing steel:

1. Cyclically load the sample from 5% σ_y to 90% σ_y for 100 cycles. Use a haversine waveform at 0.5 cps for #36, #43, and #57 bars, and a haversine waveform at 0.7 cps for smaller bars.
2. If sample has not failed, increase axial tensile load to cause failure.
3. On the Test Form, record whether or not the sample passed the cyclical testing and, if applicable, the ultimate tensile strength, location of failure, and any necking.

FATIGUE TESTING

This section applies only to mechanical splices on straight reinforcing steel:

1. Fatigue load the sample from + 173 MPa to - 173 MPa for 10,000 cycles. Use a sine waveform at 0.083 cps for #36, #43, and #57 bars, and a sine waveform at 0.35 cps for smaller bars.
2. If sample has not failed, increase axial tensile load to cause failure in the sample.
3. Record whether or not the sample passed the fatigue testing and, if applicable, the ultimate tensile strength, location of failure, and any necking.

CONTROL BARS

Control bars must comply with the requirements in Caltrans *Standard Specifications* Section 52.

1. Apply an axial tensile load to the sample sufficient to cause failure.
2. Note the maximum load obtained and record on the Test Form.
3. Calculate the ultimate tensile strength by dividing the maximum load by the sample's nominal cross-sectional area. Record on the Test Form.

E. REPORT

The Test Form shall report the following information, as necessary for the user:

1. Date sampled
2. Date received
3. Date tested
4. Sample no.
5. Lot no.
6. Contract no.
7. Person results reported to
8. Material
9. Bar size
10. Manufacturer
11. Splice type
12. Sampler or inspector
13. Results.

F. HAZARDS

The test samples are heavy and may contain sharp edges or burrs. Sample failure may involve brittle fractures and ejection of sample fragments. Use appropriate safety measures.

G. SAFETY AND HEALTH

Prior to handling, testing or disposing of any waste materials, testers are required to read the *Caltrans Laboratory Safety Manual*. Users of this method do so at their own risk.

REFERENCES:

ASTM Designations A 370 and A 706; Caltrans Standard Specifications Section 52; Concrete Reinforcing Steel Institute's Manual of Standard Practice MSP-1-90.

End of Text
(California Test 670 contains 7 pages)

Figure 1. Example of dial indicators used for measuring slip.

Figure 2. Test Form

Date sampled: _____ Sample No. _____

Date received: _____ TL-101 No. _____

Date tested: _____ Contract No. _____

Sampler/inspector: _____ Lot No. _____

Report to: _____ Material: _____

Lab technician: _____ Bar size: _____

Contract No. _____ Manufacturer: _____

Service or Ultimate? _____ Splice type: _____

	Sample No. 1	Control No. 1	Sample No. 2	Control No. 2	Sample No. 3	Control No. 3	Sample No. 4	Control No. 4
Sample long enough?								
Coupler not longer than 10 times the bar diameter?		n/a		n/a		n/a		n/a
Sample straight enough?								
Total slip (μm)		n/a		n/a		n/a		n/a
Passed cyclical?		n/a	n/a	n/a	n/a	n/a	n/a	n/a
Passed fatigue?	n/a	n/a		n/a	n/a	n/a	n/a	n/a
Ultimate tensile strength (MPa):								
95% of tensile strength (MPa):	n/a		n/a		n/a		n/a	
Strain (%)								
Necking?								

[] Samples pass.

[] Samples fail, because _____

_____

_____

_____

_____

_____

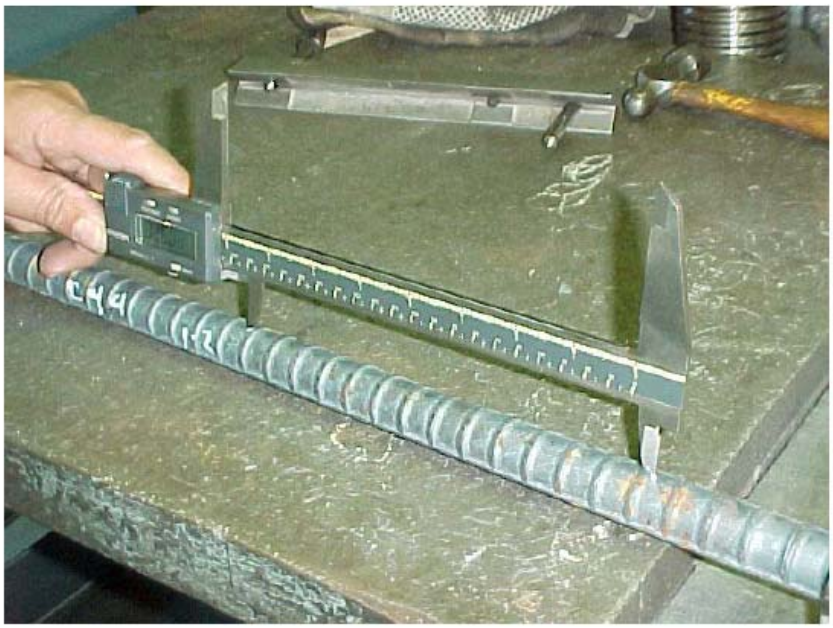

Figure 3. Digital calipers used to measure initial gauge length to the nearest 0.025 mm.

APPENDIX B: CALIFORNIA TEST 670 WITH RECOMMENDED CHANGES

California Test 670
September 2004

STATE OF CALIFORNIA—BUSINESS, TRANSPORTATION AND HOUSING AGENCY

DEPARTMENT OF TRANSPORTATION
DIVISION OF ENGINEERING SERVICES
Transportation Laboratory
5900 Folsom Boulevard
Sacramento, California 95819 - 4612

METHOD OF TESTS FOR MECHANICAL AND WELDED REINFORCING STEEL SPLICES

CAUTION: Prior to handling test materials, performing equipment setups, and/or conducting this method, testers are required to read "**SAFETY AND HEALTH**" in Section G of this method. It is the responsibility of the user of this method to consult and use departmental safety and health practices and determine the applicability of regulatory limitations before any testing is performed.

A. SCOPE

This method presents the testing procedures for determining mechanical properties of spliced reinforcing steel.

B. DEFINITIONS

Coupler – mechanical device that physically connects two reinforcing bars. Lot – quantity of spliced reinforcing steel, as defined in Caltrans *Standard Specifications* Section 52. Necking – localized reduction in crosssection that may occur in material under tensile stress. For this California Test, a sample has necking if the reduction in cross-section is visible, or if the sample has sufficient ductility, as determined by the strain measurement in Section D below. Sample – spliced reinforcing steel bar that has the physical properties required in Section D below. Sample No. – unique tracking number assigned to the sample(s) or set of samples being tested. Slip test – procedure for determining inherent axial displacement within the mechanical coupler. Splice – physical device or mechanism for joining reinforcing steel, as defined in Caltrans *Standard Specifications* Section 52. Mechanical non-lap splices and resistance welded splices are the most common types encountered.

C. TESTING APPARATUS AND ACCESSORIES

1. Tensile test machine able to apply a tensile force greater than the ultimate tensile strength of the sample. Tensile test machine must be accurate in accordance with ASTM A 370.
2. Slip measurement device consisting of two dial indicators that measure displacement across the splice to the nearest 0.025 mm. See Figure 1. A dial indicator may have an analog dial or be digital. Alternatively, an extensometer accurate to within 0.025 mm.
3. Caliper accurate to 0.025 mm.

Alternatively, an extensometer accurate to within 0.025 mm, with a 200 mm gauge length and enough clearance to be installed over the coupler section, could be used.

D. TEST PROCEDURES FOR PRODUCTION TESTING AND QUALITY ASSURANCE TESTING PHYSICAL PROPERTIES AND PREPARATION

Before accepting samples, ensure each sample has these physical parameters:

1. Sample length. A minimum sample length is required for the submitted samples. Depending on a lab's specific testing equipment, the lab may shorten, machine, or otherwise alter the submitted samples to meet the configuration of its testing equipment. This alteration is allowable under this Test Method and *Standard Specifications* Section 52. For rebar sizes #25 and smaller, sample length must be at least 1.5 m. For rebar sizes #29 and larger, sample length must be at least 2 m.
2. Coupler diameter. For technical couplers, length of the coupler must be less than 10 times the nominal bar diameter.
3. Alignment. With the exception of spliced hoops, the alignment across the splice must be straight to within 7 mm in 0.9 m of length. Record results on the Test Form (Figure 2).

SLIP TEST

The slip test is required for all splices except mechanical lap splices, welded splices, or splices on hoops. There are two acceptable options for measuring slip.

Slip Test (Option I)

Option I uses two dial indicators that measure displacement across the splice. Steps:

1. Mount the sample in the tensile test machine.
2. Preload the sample to 4 MPa to set the jaws on the bar ends. Attach the slip measurement device so that the dial indicators are 180° apart. Zero them out.
3. Apply an axial stress of 200 MPa. Maintain load until obtaining a steady reading on both dial indicators.
4. Reduce the stress to 20 MPa and measure the two readings. Sum the value of the two readings and divide the resultant sum by two. This is the total slip. Record the total slip on the Test Form (Figure 2).
5. Remove the two dial indicators.

Slip Test (Option II)

The second option for measuring slip (Option II) uses punch marks. Steps: 1. Place one set of punch marks that span the splice. The distance between the punch marks should be approximately equal to the coupler length plus four bar diameters. Place a second set of punch marks 180° apart from the first set.

2. Preload the sample to 4 MPa to set the jaws on the bar ends.
3. Measure distance between the punch marks to the nearest 0.025 mm.
4. Apply an axial stress of 200 MPa. Maintain the load for 60 seconds.
5. Reduce the stress to 20 MPa and measure the distance between each set of punch marks. For each set, calculate the slip (measured length – original length) and average the results. This is the total slip. Record result on the Test Form.

Slip Test (Option III)

The third option for measuring slip (Option III) uses a special, long-gauge-length extensometer. The extensometer shall have a gauge length of 200mm.

Steps:

1. Mount the extensometer around the coupler, so that it is fixed to rebar above and below the coupler.
2. Proceed with slip loading with extensometer recording data.
3. Preload the sample to 4 MPa to set the jaws on the bar ends.
4. Apply an axial stress of 200 MPa. Maintain the load for 60 seconds.
5. Reduce the stress to 20 MPa. The difference across the extensometer gauge length between steps 3 and 5 is the total slip. Record results on the Test Form.

TENSILE TEST

Tensile testing must be done in general accordance with ASTM A 370 Sections 13 and A9.

1. Apply an axial tensile load to the sample sufficient to cause failure.
2. Document the maximum load obtained.
3. Calculate the ultimate tensile strength by dividing the maximum load by the sample's nominal crosssectional area. ASTM A 706, Table 1, provides the nominal cross-sectional areas for A 706 reinforcing steel. Record the ultimate tensile strength on the Test Form.
4. Check for necking. This can be done visually (Option I) or by measuring strain (Option II). Also, it does not matter which option was used for the slip test when choosing an option to assess necking.

Necking (Option I)

Examine the fractured area. If there is a visible decrease in the sample's crosssectional area at the point of fracture, there is visible necking. Record result on the Test Form.

Necking (Option II)

Alternatively, assess necking by measuring the sample's strain. Follow this procedure for measuring strain:

a. For straight samples, place punch marks along the sample to create three gauge lengths with a nominal length of 200 mm. For hoops, place punch marks along the sides of the hoop rebar samples (not the concave or convex sides of the bar) to create a total of three gauge lengths, each 200 mm in length. For both straight samples and hoops, leave a gap of at least 25 mm between any two 200 mm gauge lengths to separate the gauge marks. Splices, if any, shall be centered in the middle 200 mm gauge length. See figure below:

b. Do not confuse these punch marks with the punch marks that may have been placed for the slip test.

c. Straight samples are tested as received. For hoops, straighten the ends of hoop samples to fit sample into the testing grips. This straightening should be outside of the gauge marks, in accordance with the Concrete Reinforcing Steel Institute's *Manual of Standard Practice MSP-1-90*.

d. Mark each one of the 200 mm nominal gauge lengths sequentially as A, B, C. B designates the middle segment and it contains the splice, if any.

e. Individually, measure and record the initial three 200 mm gauge lengths A, B, and C to the nearest 0.025 mm.

f. Tensile test each sample following the instructions in "Tensile Test" above.

g. Measure the two gauge lengths not encompassing the location of failure. For hoop samples, correct the final gauge length values for curvature by multiplying the final readings by this factor:

*corrected gauge (Ln) = measured gauge * factor*

where: L*c* = length of chord (200 mm nominal), D = diameter of the hoop (rebar center to rebar center in mm), L*n* = corrected gauge length (in mm) ArcSin is in radians h. Calculate the percent strain for each one of the gauge lengths measured in step g. For straight samples: *% strain = (Lf – Lo)/Lo * 100* where: L*f* = final gauge length, L*o* = original gauge length, For hoop samples: *% strain = (Ln – Lo)/Lo * 100* where: L*n* = corrected gauge length, L*o* = original gauge length

i. If the largest measured strain is > 6% for #36 and larger bars, or > 9% for #32 and smaller bars, then the sample is considered to have necking. If the largest measured strain is < 6% for #36 and larger bars, or < 9% for #32 and smaller bars, then the sample is considered to have no necking.

j. Record the largest measured strain on the Test Form.

CYCLICAL TESTING

This section applies only to mechanical splices on straight reinforcing steel:

1. Cyclically load the sample from 5% σy to 90% σy for 100 cycles. Use a haversine waveform at 0.5 cps for #36, #43, and #57 bars, and a haversine waveform at 0.7 cps for smaller bars.
2. If sample has not failed, increase axial tensile load to cause failure.
3. On the Test Form, record whether or not the sample passed the cyclical testing and, if applicable, the ultimate tensile strength, location of failure, and any necking.

FATIGUE TESTING

This section applies only to mechanical splices on straight reinforcing steel:

1. Fatigue load the sample from + 173 MPa to - 173 MPa for 10,000 cycles. Use a sine waveform at 0.083 cps for #36, #43, and #57 bars, and a sine waveform at 0.35 cps for smaller bars.
2. If sample has not failed, increase axial tensile load to cause failure in the sample.
3. Record whether or not the sample passed the fatigue testing and, if applicable, the ultimate tensile strength, location of failure, and any necking.

MATERIAL PRE-SCREENING

This section applies only to mechanical splices which rely upon an adhesive system for force transfer; all adhesive systems shall be pre-screened to ensure resistance to moisture-based degradation:

For each considered ASTM C881 Adhesive System:

1. Fabricate 2 sets of tension(as per ASTM D638) or compression (as per ASTM D695) specimens.
2. Fabricate 1 set of dynamic mechanical thermal analysis (as per ASTM D882) specimens.
3. Fabricate 1 set of moisture uptake (as per ASTM D570) specimens.
4. Immerse 1 set of each speicimen type in 60°C de-ionized water for 1 week.
5. Test all tension or compression, and dynamic mechanical thermal analysis specimens.

Only use the considered Adhesive System if all the following requirements are met:

1. Strength and modulus, by ASTM D638 or D 695, of immersed specimens are at least 50% of un-immersed specimens.
2. Glass transition temperature, by tan-delta peak, of the material is at least equal to the expected maximum environmental service temperature + 30°C.
3. Diffusion coeffcient is lower than 10-6 mm^2/s.

CONTROL BARS

Control bars must comply with the requirements in Caltrans *Standard Specifications* Section 52.

1. Apply an axial tensile load to the sample sufficient to cause failure.
2. Note the maximum load obtained and record on the Test Form.
3. Calculate the ultimate tensile strength by dividing the maximum load by the sample's nominal crosssectional area. Record on the Test Form.

E. REPORT

The Test Form shall report the following information, as necessary for the user:

1. Date sampled
2. Date received
3. Date tested
4. Sample no.
5. Lot no.
6. Contract no.
7. Person results reported to
8. Material
9. Bar size
10. Manufacturer
11. Splice type
12. Sampler or inspector
13. Results.

F. HAZARDS

The test samples are heavy and may contain sharp edges or burrs. Sample failure may involve brittle fractures and ejection of sample fragments. Use appropriate safety measures.

G. SAFETY AND HEALTH

Prior to handling, testing or disposing of any waste materials, testers are required to read the *Caltrans Laboratory Safety Manual*. Users of this method do so at their own risk.

REFERENCES:

ASTM Designations A 370 and A 706; C881 D570, D638, D695, D882

Caltrans Standard Specifications Section 52; Concrete Reinforcing Steel Institute's